Absorber management using burnable poisons

Forskningscenter Risø, Roskilde

Publication date:
1977

Document Version
Publisher's PDF, also known as Version of record

Risø Report No. 341

Risø Report No. 341

Risø National Laboratory

Absorber Management Using Burnable Poisons

by Leif Mortensen

June 1977

Sales distributors: Jul. Gjellerup, Sølvgade 87, DK-1307 Copenhagen K, Denmark

Available on exchange from: Risø Library, Risø National Laboratory, DK-4000 Roskilde, Denmark

INIS descriptors

BORON
BURNABLE POISONS
BURNUP
BWR TYPE REACTORS
CADMIUM
GADOLINIUM
MANAGEMENT
OPTIMAL CONTROL
OPTIMIZATION
POWER DISTRIBUTION
PWR TYPE REACTORS
THREE-DIMENSIONAL CALCULATIONS
TWO-DIMENSIONAL CALCULATIONS

UDC 621.039.524.44 : 621.039.515

June 1977 Risø Report No. 341

Absorber Management Using Burnable Poisons

by

Leif Mortensen

Risø National Laboratory
Department of Reactor Technology

Abstract

An investigation of the problem of optimal control carried out by means of a two-dimensional model of a PWR reactor. A solution is found to the problem, and the possibility of achieving optimal control with burnable poisons such as boron, cadmium and gadolinium is discussed. Further, an attempt is made to solve the control problem of a BWR, but no final solution is found.

This report is submitted to the Technical University of Denmark in partiel fulfilment of the requirements for obtaining the Lic. techn. (Ph.D.) degree.

ISBN 87-550-0468-7

CONTENTS

Page

1. INTRODUCTION

Absorber management is defined as the operation of control absorbers such as control rods, soluble poison and burnable poisons. The main objective of absorber management is to reduce the energy-generating costs. This may be accomplished either by increasing the fuel burn-up or by reducing the reactor size through a better power shape. For a given initial loading and a prescribed limit for the power-peaking factor, the choice of a control absorber strategy throughout the reactor period is an optimization problem because of the contradiction of the two methods of reducing the energy-generating costs. This problem is solved in the present report.

In chapter 3 it is found by means of Pontryagin's maximum principle that the optimal control strategy, i.e. the strategy which gives maximum average discharge burn-up for minimum power-peaking factor, for a two-dimensional reactor divided into two control regions is to operate the reactor at constant power shape until the control material has burned away in one of the control regions, and then to control the reactor with the remaining control material in the other control region.

Since there are obviously several ways of running the reactor that all fulfil the above-mentioned conditions for optimal control strategy, the two-dimensional program SELMA2[1)] is used in chapter 4 to find the control strategy giving minimum energy-generating costs. With a uniform fuel distribution throughout the core, this is obtained by operating the reactor at constant power shape, i.e. the control absorbers burn away at the same time in the two control regions.

In chapter 5 it is found that it is possible to realize the optimal control strategy by means of burnable poisons lumped in cylinder geometry and that boron, cadmium and gadolinium are potential burnable poison materials.

The burnable poison is usually homogeneously distributed in the fuel in a fuel rod and a number of these poisoned rods are placed in each fuel assembly. The concentration of burnable poison in a rod and the number of poisoned rods in each assembly are calculated from formulas derived in chapter 6. In chapter 8, by means of calculations with a two-dimensional program DBU, it

is shown that it is possible to control the reactor according to the optimal strategy with the burnable poison materials.

An optimal control strategy for a three-dimensional reactor shows the same characteristics as the strategy for a two-dimensional reactor. This strategy is derived in chapter 9 from the use of Pontryagin's maximum principle on a three-dimensional reactor.

Calculations on a PWR with SELMA 2 using RZ geometry show a considerable reduction in the overall power-peaking factor, compared to the power-peaking factor achieved for a reactor controlled with soluble poison when the reactor is operated at constant power shape.

Three-dimensional calculations with NOTAM for a BWR give no definite information on the effect of using burnable poison in BWRs.

2. ABSORBER MANAGEMENT

This chapter discusses the general aspects of absorber management.

2.1. The Optimization Problem

The maximum average discharge burn-up depends within certain limits on the power shape at which the reactor is operated. The power shape is here given as a power-peaking factor that is the ratio between the maximum value of the power and the average power produced by the reactor. The power-peaking factor and the maximum average discharge burn-up are related, so an increase in the power-peaking factor gives an increase in the average discharge burn-up. Furthermore, there is an optimization problem because an increase in the average discharge burn-up gives a decrease in the energy-generating costs and an increase in the power-peaking gives an increase in the energy-generating costs. We have to find the power shape that gives minimum energy-generating costs. Power is shaped by two methods, fuel management and absorber management.

Fuel management and absorber management are to some extent equivalent since the power shape depends on the spatial distribution of the infinite multiplication factor, k-infinite, which is adjusted by means of enrichment or absorption, or both.

Light-water reactor operation is based on periodical refuelling. Fuel management is, in this case, a multistage problem and the k-infinite distribution is adjusted between two reactor periods when the reactor is closed down.

During the reactor period, the k-infinite distribution is controlled by means of control absorbers.

Fuel management and absorber management are, as indicated above, not independent of each other and an optimal strategy for reactor operation should include both management methods. A reasonable way to find the optimal strategy is to separate the two management methods, find optimal strategies for each, and then use the results from the study of the two management methods to determine an optimal strategy for the operation of the reactor. Fuel management optimization has been studied by S. Weber[1] and K.L. Thomsen[2], among others, and it is the goal of this report to study absorber management with regard to the use of burnable poisons.

2.2. Lumped Absorbers

The goal of absorber management is to optimize the distribution of control absorbers, i.e. to find a distribution that gives minimum energy-generating costs.

Control absorbers are control rods, burnable poisons or soluble poisons. For obvious reasons, soluble poison is only used to control the excess reactivity of the reactor core, and it is therefore of no interest in absorber management optimization problems, since these too involve control of the power shape. This requires lumped absorbers such as control rods or burnable poisons.

The burn-up of lumped absorbers depends on:

1) The microscopic cross section of the absorber material
2) The concentration of the absorber material
3) The geometry of the absorber lump.

The microscopic cross section of the absorber material is so large that the absorber lump is black, that is all neutrons hitting the surface of the lump are absorbed. The absorption in the lump is then proportional to the surface area and the burn-up rate depends on the absorber concentration.

For a given poison material, we can control the absorption at any time during the reactor period, either by varying the geometry of the absorber lump or by varying the concentration of the absorber, or both.

In control rods, the concentration of absorber material is so high that the burn-up of the material does not change the absorption in the rods because their surface areas are not changed significantly. So we have to adjust the absorption by varying the geometry mechanically, which means that we have to change the control rod pattern during the reactor period. The long-term reactivity changes are counteracted by slow withdrawal of the control rods and the power is shaped by a control rod pattern that gives the required k-infinite distribution. However, the withdrawal of the control rods limits the possibilities for shaping the power at the end of the reactor period.

We can use the absorber concentration as a control parameter by lumping the absorber material in concentrations so small that the burn-up changes the absorption because the surface area is changed. Absorbers lumped in this way are called burnable poisons. The long-term reactivity changes are conteracted by burn-up of the absorber and the power is shaped by placing the lumps in a suitable pattern. Since this pattern does not change during the reactor period, it is possible to control the power shape even at the end of a period.

Besides the possibility for shaping the power at the end of a period, burnable poisons seem to have other advantages over control rods.

The use of burnable poisons reduces the need for mechanical control because the inherent excess reactivity of the fuel is reduced.

Power shaping with control rods means, as mentioned above, that some of the rods are only partly inserted in the core. At the end of these partly inserted rods, power peaks might exist and impede the shaping of the power and even cause the prescribed limit to the power-peaking factor to be exceeded.

These peaks are avoided by the use of burnable poison because the adjustment in the absorption is performed by burn-up and not by removal of the absorber.

It is not possible to control a reactor by burnable poisons

alone because it is difficult - if not impossible - to change the burnable poison distribution during a reactor period. The reactor can be controlled with both burnable poisons and control rods, perhaps in connection with soluble poisons. But it is possible to mainly control the reactor with burnable poisons during operation, and to use control rods and/or soluble poisons to adjust the power.

The use of burnable poison instead of soluble poisons gives another advantage. In PWRs, a high boron content in the moderator gives a positive moderator temperature coefficient. By mainly controlling the reactor by means of burnable poisons, the boron content is reduced and positive moderator-temperature coefficients avoided. This aspect has not been studied though in this work.

2.3. Optimal Control with Burnable Poisons

The problems that are to be solved are: finding an optimal control strategy, finding useful burnable poison materials, and finding suitable lump geometries and absorber concentrations.

The control strategy at which the reactor is operated determines the concentration of the absorber material and the lump geometry. The first problem to be solved is to find an optimal control strategy.

A strategy giving maximum average discharge burn-up for minimum power peaking factor is found by means of Pontryagin's maximum principle. This principle is only useful for simple mathematical models, and therefore a two-dimensional reactor model is used in the present study. A two-dimensional model is only applicable to PWRs, and most of the present results are only valid for PWRs.

The program SELMA2 is used to find the optimal strategy for a PWR. Normally, power shaping in PWRs is performed by means of enrichment, but here absorbers are used to shape the power and the enrichment is assumed uniform all over the core. Usually, only the first core has a uniform fuel distribution and burnable poisons are generally used in the first cores, but they could be used in later cores too.

Following this, absorber materials must be found. Burnable poison materials are found among the nuclides with large absorption cross sections.

Finally, geometry and concentration must be determined.

In light-water reactors the choice of geometry is limited to cylinder, slab or spherical geometry (fuel pellets containing absorbers located far from each other are regarded as spheres). It is shown in chapter five that cylinder geometry gives the required changes in reactivity with time, but the control pattern is not fully determined yet. The number of poison cylinders has still to be determined.

By means of a very simple model where the poison cylinder is placed in a homogeneous fuel mixture, cladding and moderator equations are derived giving the concentration of the poison and the number of poison cylinders.

To obtain the small concentrations necessary, the absorber is mixed with a matrix material with a relatively small microscopic cross section. Uranium fuel has absorption cross sections that are small compared to the cross sections of the absorber material and this fuel is often used as matrix material. The absorber material is then distributed homogeneously with the fuel in fuel rods.

The spatial k-infinite distribution is controlled by dividing the reactor into control regions. The absorber concentration and the number of poisoned fuel rods, poison pins, are constant within each control region. A suitable choice of concentrations and number of poison pins for each region will then give the required power shape and changes in reactivity.

The number of control regions should be as low as possible to keep the fuel production costs as low as possible. Two control regions give satisfactory results with a two-dimensional model.

3. OPTIMAL ABSORBER STRATEGY

The power-peaking factor and the average discharge burn-up are related, as mentioned in chapter 2, so that an increase in the power-peaking factor gives an increase in the burn-up; and because an increase of the power-peaking factor gives an increase in the energy-generating costs, and an increase in the burn-up gives a decrease in the energy generating costs, the optimal mode of operation is therefore that giving maximum average discharge burn-up for minimum power-peaking factor.

In this chapter the problem of finding a control strategy giving maximum average discharge burn-up for minimum power-peaking factor is solved for a two-dimensional model of a reactor by means of Pontryagin's maximum principle.

3.1. Pontryagin's Maximum Principle

The operation of a reactor during a reactor period can be described as a controlled transfer of the reactor from one state, defined by the fuel-loading at the beginning of the period, to another state defined by that which gives maximum average discharge burn-up. The transfer between the two states is controlled by control absorbers.

In general terms, we have a controllable physical process, for which we have to find an optimal control.

Pontryagin's maximum principle is a tool to solve this problem. The principle is a general mathematical method considering control processes that can be described by a set of differential equations:

$$\frac{dx^i}{dt} = f^i\ (x^1, \ldots, x^m, u^1, \ldots, u^r)\ \ i = 1,2,\ldots m \qquad (3.1)$$

where

$f^i(x^1,\ldots, x^m, u^1,\ldots, u^r)$; $i = 1,2,\ldots m$ are given functions

$x^i(t)$ $i = 1,2\ldots m$ are variables characterizing the process

$u^j(t)$ $j = 1,2,\ldots, r$ are control parameters controlling the course of the process. The control parameters belong to a closed control region U.

t is the time

m is the number of state variables

r is the number of control parameters.

The variational problem to be solved, which is related to the control process, consists of the following: Consider the integral function,

$$I = \int_{t_o}^{t_1} f^o(x^1,\ldots, x^m, u^1,\ldots, u^r)dt \qquad (3.2)$$

where

$f^o(x^1,\ldots, x^m, u^1,\ldots, u^r)$ is a given function.

t_o is the initial time

t_1 is the terminal time.

The times t_o and t_1 are not fixed, and it is necessary to find the control $u = (u^1, \ldots, u^r)$ that transfers the controlled object from a given initial state to a prescribed final state in such a manner that I has a minimum value.

To formulate the theorem yielding the solution of the problem, we shall consider another system of equations in the auxiliary variables $\psi_o, \psi_1, \ldots, \psi_m$:

$$\frac{d\psi_i}{dt} = - \sum_{\alpha=o}^{m} \frac{\partial f^\alpha(x,u)}{\partial x^i} \qquad i = o,1,\ldots, m \tag{3.3}$$

where x^o is defined by

$$\frac{dx^o}{dt} = f^o(x,u) \tag{3.4}$$

and

$$x = (x^1, x^2,\ldots, x^m).$$

Equations (3.1), (3.4) and (3.3) are combined into one entry by defining the Hamilton function H

$$H(\bar{\psi}, x, u) = \sum_{\alpha=o}^{m} \psi_\alpha f^\alpha(x,u). \tag{3.5}$$

With the aid of H, equations (3.1), (3.3) and (3.4) can be written in the following form:

$$\frac{dx^i}{dt} = \frac{\partial H}{\partial \psi_i}$$

$$i = o,1,\ldots,m \tag{3.6}$$

$$\frac{d\psi_i}{dt} = \frac{\partial H}{\partial x_i}$$

The theorem can now be formulated[3].

"In order that u(t) and x(t) be optimal it is necessary that there exist a nonzero continuous vector function $\bar{\psi}(t) = (\psi_o(t), \bar{\psi}_1(t), \ldots \psi_m(t))$ corresponding to u(t) and $\bar{x}(t)$ such that:

1) for every t, $t_o \leq t \leq t_1$, the function $H(\bar{\psi}(t), x(t), u(t))$ of the variable $u \in U$ attains its maximum M at the point u = u(t):

$$H(\bar{\psi}, x, u) = M(\bar{\psi}, x) \tag{3.7}$$

2) at the terminal time t_1 the relations

$$\psi_o(t_1) \leq 0, \quad M(\bar{\psi}(t_1), x(t_1)) = 0 \tag{3.8}$$

are satisfied. Furthermore, it turns out that if $\bar{\psi}(t)$, $\bar{x}(t)$ and u(t) satisfy system (3.6), and condition 1), the time functions $\psi_o(t)$ and $M(\bar{\psi}(t), x(t))$ are constant. Thus (3.8) may be verified at any time t, $t_o \leq t \leq t_1$, and not just at t_1".

The vector $\bar{x}(t)$ is defined as $\bar{x}(t) = (x^o, x)$.

3.2. The Reactor Model

We may use the above theory to solve the optimization problem for a suitable model of a reactor. Ideally, the reactor core should be described in as much detail as possible, but the optimum theory can only be fully applied to mathematically tractable models. The search for an optimum control strategy will therefore be performed with a simple model of the reactor.

This model has the following characteristics:

1. The reactor is one-dimensional, cylindrical and divided into two homogenized regions.
2. The neutron distribution is described by means of a one-group diffusion equation.
3. The control absorber is distributed homogeneously in the two regions so that the reactor is just critical.
4. The initial state of the reactor is known.
5. The fuel burn-up in the two regions is calculated from a region-averaged flux and is thus assumed to be uniform in the two control regions.

6. The reactor is operated at constant power and k_∞ changes linearly with burn-up.
7. A power peaking factor limit is prescribed.
8. Reactivity changes are only due to depletion and removal of control absorbers.

3.3. The One-Group Cylindrical Diffusion Equations

The one-group cylindrical diffusion equations describing the two-region reactor are

$$\frac{d^2\phi_1(r,t)}{dr^2} + \frac{1}{r}\frac{d\phi_1(r,t)}{dr} + B_1^2(t)\phi_1(r,t) = 0 \qquad (3.9)$$

for the inner region, and

$$\frac{d^2\phi_2(r,t)}{dr^2} + \frac{1}{r}\frac{d\phi_2(r,t)}{dr} + B_2^2(t)\phi_2(r,t) = 0$$

for the outer region, where

$$B_i^2(t) = (\nu\Sigma_f(t)-\Sigma_a(t)-\Sigma_c(t))_i/D_i(t) \qquad i = 1, 2. \qquad (3.10)$$

Σ_f is the macroscopic fission cross section, Σ_a is the macroscopic absorption cross section without poison, Σ_c is the macroscopic absorption cross section for the control absorber, D is the diffusion constant, ν the number of neutrons per fission, and ϕ the flux.

The power P(t) is calculated from

$$P_i(t) = k \int_{v_i} \Sigma_{fi}(t)\phi_i(r,t)\, dv_i \qquad i = 1, 2 \qquad (3.11)$$

where v_i is the volume of region i and k is a conversion constant.

3.4. The Reactor State

The use of Pontryagin's maximum principle requires that the condition of the reactor is described by a state vector and that the time variation of this state vector is described by a set of differential equations. For a given fuel loading, the state of the reactor is described by the burn-up, e_1 and e_2, and the material bucklings, $x_1 = B_1^2$ and $x_2 = B_2^2$, for the inner and outer

control regions, respectively.

The state of the reactor is thus described by means of

$$x_i(t) = (\nu\Sigma_f(t)-\Sigma_a(t)-\Sigma_c(t))_i/D_i(t) \qquad i = 1, 2 \qquad (3.12)$$

and the burn-up in the two regions which is found from

$$\frac{de_i(t)}{dt} = P_i(t) \qquad i = 1, 2. \qquad (3.13)$$

Equations (3.12) and assumptions 4 and 6, part 3.2, give:

$$x_i(t) = y_i(o) - k_i e_i(t) - c_i(t) = y_i(t) - c_i(t)$$

$$i = 1, 2 \qquad (3.14)$$

where

$$y_i(t) = (\nu\Sigma_f(o) - \Sigma_a(o))_i/D_i(o) - k_i\, e_i(t) \qquad i = 1, 2 \qquad (3.15)$$

$$c_i(t) = \Sigma_{ci}(t)/D_i(0) \qquad i = 1, 2 \qquad (3.16)$$

and k_i is a proportionality constant.

The condition that the reactor is just critical gives a relation between x_1 and x_2

$$x_2(t) = F_c(x_1(t)) \ , \qquad (3.17)$$

which means that x_2 is known when x_1 is given and the four state variables are reduced to three. The state vector x from part 3.1 is then

$$x = (e_1, e_2, x_1) \ . \qquad (3.18)$$

3.5. The Control Parameter

The control parameter u is a parameter determining the transfer of the reactor from one state to another. At first, it might seem obvious to choose the c_i's as control parameters; but as seen from (3.14) the c_i's are determined when the buckling

and the burn-up are given. However, the rate at which the control absorber is changed, or the rate at which the buckling is changed, is useful as a control parameter. As in 4),the rate at which the buckling changes is chosen as a control parameter:

$$u = \frac{dx_1(t)}{dt} . \qquad (3.19)$$

It is demanded that u is a point in a closed region U. That this is the case is shown in part 3.9.

3.6. The State Differential Equations

The set of differential equations describing the system is derived from (3.13) and (3.19) by means of expressions for the power produced in the two regions.

The power in the two regions is a function of the state variables:

$$\begin{aligned} P_1(t) &= F_1(x_1(t), x_2(t)) \\ P_2(t) &= F_2(x_1(t), x_2(t)) , \end{aligned} \qquad (3.20)$$

which by means of the criticality condition (3.17) are transformed into:

$$\begin{aligned} P_1(t) &= F_1(x_1(t)) \\ P_2(t) &= F_2(x_1(t)) . \end{aligned} \qquad (3.21)$$

The set of differential equations describing the system is then:

$$\begin{aligned} \frac{de_1(t)}{dt} &= F_1(x_1) \\ \frac{de_2(t)}{dt} &= F_2(x_1) \\ \frac{dx_1(t)}{dt} &= u . \end{aligned} \qquad (3.22)$$

The equations (3.21) determine the state of the reactor together with the criticality condition (3.17).

We have now defined a state vector $x = (e_1, e_2, x_1)$, a control parameter $u = \frac{dx_1}{dt}$, and we have found a set of differential equations describing the state vector. It remains to prove that the control parameter is bounded, to define the integral function I, to define a terminal state and to use the above mentioned theorem.

3.7. The Cycle Conditions

The reactor period, or reactor cycle, is determined by the beginning-of-cycle condition and the end-of-cycle condition.

At the beginning of the cycle, the fuel loading is known which means that:

1. $y_i(o)$ i=1,2 is known. This means that a fuel management strategy is given.
2. $e_1(o)$ i=1,2 is zero. This is not the case for all fuel, but it is fulfilled by redefinition of $y_i(o)$, which includes the burn-up at t=o

$$y_i(o) + k_i e_i(o) \rightarrow y_i(o) \qquad i = 1, 2.$$

During operation of the reactor it is assumed that

3. $c_1(t) \geq o$ and $\frac{dc_i(t)}{dt} \leq o$ $i = 1, 2,$

which means that the control poison can only be removed. This is true for burnable poisons.

The end of cycle could be determined from one of the following conditions.

4. The prescribed limit for the power peaking is reached.
5. $c_1(T) = 0$, $c_2(T) = 0$ and $F_c(x_1(T), x_2(T)) = 0$ where T is the cycle time.
6. A maximum limit for the average burn-up is reached in one of the regions.

It is shown in part 3.8 that condition 5 gives the maximum average discharge burn-up, and this condition is used as an end-of-cycle condition to solve the optimization problem. The prescribed limits in conditions 4 and 6 define a group of admissible control strategies giving maximum average discharge burn-up for minimum power-peaking factor.

3.8. Maximum Average Burn-up Condition

The maximum average burn-up is reached when no control poison is left in the reactor. This is seen from

$$x_1(t) = y_1(o) - k_1 e_1(t) - c_1(t)$$

$$x_2(t) = y_{2(o)} - k_2 e_2(t) - c_2(t). \qquad (3.22)$$

Differentiation of equations (3.22) gives:

$$\frac{dx_1(t)}{dt} = -k_1 \frac{de_1(t)}{dt} - \frac{dc_1(t)}{dt} \qquad (3.23)$$

$$\frac{dx_2(t)}{dt} = -k_2 \frac{de_2(t)}{dt} - \frac{dc_2(t)}{dt} .$$

The problem is to find the amount of control poison that gives the maximum average burn-up at the end of the cycle. For given $x_1(T)$ and $x_2(T)$, equations (3.23) give

$$k_1 \frac{de_1(t)}{dt}\Big|_T = - \frac{dc_1(t)}{dt}\Big|_T$$

$$k_2 \frac{de_2(t)}{dt}\Big|_T = - \frac{dc_2(t)}{dt}\Big|_T \qquad (3.24)$$

which give

$$\frac{de_1(t)}{dc_1(t)}\Big|_T \leq 0$$

$$\frac{de_2(t)}{dc_2(t)}\Big|_T < 0 , \qquad (3.25)$$

which tells us that any decrease in control poison will increase the burn-up; the maximum burn-up is thus achieved for $c_1(T) = 0$ and $c_2(T) = 0$. Condition 5, part 3.7, is therefore used as an end-of-cycle condition.

3.9. Control Region Bounds

According to optimal theory, the control vector should be bounded. That this is the case can be seen from (3.14). The minimum value for u is found from:

$$x_1(t) = y_1(o) - k_1 e_1(t) \tag{3.26}$$

Differentiation of equation (3.26) gives

$$u(t) = - k_1 F_1(x_1) - \frac{dc_1(t)}{dt} . \tag{3.27}$$

The maximum negative rate will then exist for $c_1 = 0$, because $\frac{dc_1(t)}{dt} \leq 0$, that is

$$u_{min} = -k_1 F_1(x_1) . \tag{3.28}$$

The maximum value for u is found from:

$$x_2(t) = y_2(o) - k_2 e_2(t) - c_2(t) \tag{3.29}$$

Differentiation of equation (3.25) gives

$$\frac{dx_2}{dt} = \frac{dx_2}{dx_1}\frac{dx_1}{dt} = -k_2 F_2(x_1) - \frac{dc_2(t)}{dt} \Rightarrow \tag{3.30}$$

$$u = (-k_2 F_2(x_1) - \frac{dc_2}{dt}) / \frac{dF_c(x_1)}{dx_1} . \tag{3.31}$$

The maximum value for the control vector will exist for $c_2 = 0$, because an increase in x_1 leads to a decrease in x_2. $dF_c(x_1)/dx_1$ is negative, and therefore we have

$$u_{max} = -k_2 F_2(x_1) / \frac{dF_c(x_1)}{dx_1} . \tag{3.32}$$

Thus we have $u_{min}(x_1) \leq u \leq u_{max}(x_1)$, and u is a point in a closed region. The bounds depend on x_1 and the relation is taken from equations (3.28) and (3.32) and written as

$$p(x_1, u) = 0 \ . \tag{3.33}$$

3.10. Function to be Minimized

The fundamental problem of finding the optimal control is formulated as "the finding of the control which transfers the phase point $(e_1(o), e_2(o), x_1(o))$ to another phase point $(e_1(T), e_2(T), x_1(T))$ for the least possible value of the function

$$I = \int_o^T f^o(e_1(t), e_2(t), x_1(t))dt$$

where

T is the cycle time

f^o is a function of the state vector"[3].

We are looking for a control strategy giving maximum average discharge burn-up for minimum power-peaking factor, and a suitable function to be minimized is then the integral of the power peaking factor over the cycle time. The power-peaking factor F_o depends on the buckling, which means that

$$f^o(e_1(t), e_2(t), x_1(t)) = F_o(x_1(t)) \tag{3.34}$$

3.11. Solution of the Control Problem

The reactor is now described by a state vector. The control parameter, the bounds on the control region, the integral function that has to take a minimum value, and the set of differential equations have been defined. We are now ready to use the theorem from part 3.1.

The auxiliary function, the Hamilton function, H corresponding to this problem, is defined as

$$H = - F_o(x_1) + \psi_1 F_1(x_1) + \psi_2 F_2(x_1) + \psi_3 u \tag{3.35}$$

where ψ_o, the factor on $F_o(x_1)$, has been arbitrarily put equal to -1. It is known from the theorem from part 3.1 that ψ_o is a

constant and that $\psi_o \leq 0$. Furthermore, H is homogeneous in $\bar{\psi}$, and one of the components is therefore redundant and can be chosen arbitrarily.

In the theorem quoted in part 1 it is required that $\bar{\psi}$ is a non-zero vector. We find $\bar{\psi}$ equal to zero if ψ_o is chosen equal to zero, and therefore ψ_o is less than zero.

The variation of the other components is determined from equations (3.6) and differentiation of H with respect to e_1, e_2 and x_1 gives

$$\frac{d\psi_1}{dt} = -\frac{\partial H}{\partial e_1} = 0$$

$$\frac{d\psi_1}{dt} = -\frac{\partial H}{\partial e_2} = 0 \qquad (3.36)$$

$$\frac{d\psi_3}{dt} = -\frac{\partial H}{\partial x_1} = \frac{dF_o(x_1)}{dx_1} - \psi_1 \frac{dF_1(x_1)}{dx_1} - \psi_2 \frac{dF_2(x_1)}{dx_1} - \psi_3 \frac{\partial u}{\partial x_1}$$

The first two equations in (3.36) give ψ_1 and ψ_2 as constants.

If u has not reached its maximum or minimum value, it is independent of x_1 and we have

$$\frac{\partial u}{\partial x_1} = C \, . \qquad (3.37)$$

Expression (3.37) in (3.36) gives

$$\frac{d\psi_3}{dt} = \frac{dF_o(x_1)}{dx_1} - \psi_1 \frac{dF_1(x_1)}{dx_1} - \psi_2 \frac{dF_2(x_1)}{dx_1} \, . \qquad (3.38)$$

The first condition in the theorem from part 3.1 is when no constraints on u are fulfilled for

$$\frac{\partial H}{\partial u} = 0 \, , \qquad (3.39)$$

and this means that ψ_3 = constant = 0, i.e.

$$\psi_3 = \frac{d\psi_3}{dt} = \frac{dF_o(x_1)}{dx_1} - \psi_1 \frac{dF_1(x_1)}{dx_1} - \psi_2 \frac{dF_2(x_1)}{dx_1} = 0 \qquad (3.40)$$

This means that x_1 should remain constant as long as there is control absorber in both control regions, because

$$\frac{dx_1}{dt} = - \frac{\partial H}{\partial \psi_3} = 0 \qquad (3.41)$$

The second condition is fulfilled if it is possible to find ψ_1 and ψ_2 so that

$$H = - F_o(x_1) + \psi_1 F_1(x_1) + \psi_2 F_2(x_1) = 0 \qquad (3.42)$$

Condition 6, part 3.2, gives

$$F_1(x_1) + F_2(x_1) = \text{constant} = \text{the power produced} \qquad (3.43)$$

and this means that the determinant of the inhomogeneous system of equations (3.40) and (3.42) is

$$- F_1(x_1) \cdot \frac{dF_1(x_1)}{dx_1} + \text{constant} \cdot \frac{dF_1(x_1)}{dx_1} + F_1(x_1) \cdot \frac{dF_1(x_1)}{dx_1}$$

$$= \text{constant} \cdot \frac{dF_1(x_1)}{dx_1} \qquad (3.44)$$

This determinant differs from zero when the power produced differs from zero, because $\frac{dF_1(x_1)}{dx_1}$ is different from zero, and it is possible to find a ψ_1 and a ψ_2 for each x_1.

It has been found that there is a non-zero vector $\bar{\psi}$, which fulfils the two conditions in the theorem for $x_1(t)$ constant for u free.

Physically, this means that the bucklings in the two regions should remain constant, and therefore the power shape should remain constant, as long as both c_1 and c_2 differ from zero, i.e. as long as there is control poison in both regions. If either c_1 or c_2 becomes zero, i.e. the poison has burned away in one of the control regions, the reactor must be kept critical with the

remaining control poison. This should be the control strategy if there is no jump in $\bar{\psi}$ when going from the situation with u free to the situations where u has a minimum or a maximum value.

When u takes its minimum or maximum value, equation (3.33) is valid and equations (3.36) are transformed into

$$\frac{d\psi_1}{dt} = 0$$

$$\frac{d\psi_2}{dt} = 0 \qquad (3.45)$$

$$\frac{d\psi_3}{dt} = - \psi_o \frac{\partial F_o(x_1)}{\partial x_1} - \psi_1 \frac{\partial F_1(x_1)}{\partial x_1} - \psi_2 \frac{\partial F_2(x_1)}{\partial x_1} - \psi_3 \frac{\partial p(x_1,u)}{\partial u}.$$

$$\frac{\partial p(x_1,u)}{\partial x_1}$$

The first condition that is a maximum condition determines a Lagrange multiplier λ

$$\lambda = \frac{\partial H}{\partial u} \Big/ \frac{\partial p}{\partial u} \qquad (3.46)$$

Because

$$\frac{\partial p}{\partial u} = 1 \qquad (3.47)$$

and

$$\psi_3 = \frac{\partial H}{\partial u} \qquad (3.48)$$

the expression for the Lagrange multiplier is transformed into

$$\psi_3 = \lambda \ , \tag{3.49}$$

which means that any value of ψ_3 satisfies the maximum condition.

The second condition, that the maximum M is equal to zero, gives for the time at which u reaches its maximum or minimum value u_m

$$M(\bar{\psi}(\tau),\ x(\tau)) = \psi_o F_o(x_1(\tau)) + \psi_1 F_1(x_1(\tau)) + \psi_2 F_2(x_1(\tau))$$

$$+ \psi_3\ u_m(x_1(\tau)) = 0 \tag{3.50}$$

ψ_o, ψ_1 and ψ_2 are constants, and we find that $\bar{\psi} = (-1,\ \psi_1,\ \psi_2,\ 0)$ fulfils the two conditions for $t = \tau$ when ψ_1 and ψ_2 are equal to the ψ_1 and ψ_2 calculated for u free.

For $t > \tau$, ψ_3 is calculated from

$$M(\bar{\psi}(t),\ X(t)) = -F_o(x(t)) + \psi_1 F_1(x_1(t)) + \psi_2 F_2(x_1(t))$$

$$+ \psi_3 u_m(x_1(t)) = 0 \tag{3.51}$$

We have now found a non-zero continuous vector $\bar{\psi}$ that fulfils the two conditions in the theorem from part 3.1.

3.12. Conclusion

The absorber strategy giving the maximum average burn-up for a minimum power-peaking factor is achieved in a two-region reactor by running the reactor at a constant power shape in the part of the cycle where there are control absorbers in both regions. In the remainder of the cycle, the reactor is kept critical with the control absorber in one of the regions. The problem will be further synthetized in the next chapter.

4. SYNTHETIZATION OF THE OPTIMIZATION PROBLEM

We know from chapter 3 that there is a control strategy giving maximum average discharge burn-up for minimum power-peaking factor for each material buckling x_1. Normally, the power peaking factor is not allowed to exceed a prescribed limit during operation of the reactor. The control strategies that fulfil the condition that the power-peaking factor does not exceed the prescribed limit are called permissible control strategies. In this chapter a search is made among the permissible control strategies for the strategy giving minimum energy-generating costs.

4.1. Method of Calculation

The calculations used in the synthetization process are performed in two dimensions with the program SELMA-2[1]. This program has an option for calculation of the spatial distribution of the control absorber concentration necessary to retain a prescribed power shape. The two-dimensional reactor core is divided into a number of control regions. A power density is ascribed to each control region and an average control absorber concentration is then calculated for each control region.

The method used in SELMA-2 to calculate the absorber concentration is briefly described here.

It is further assumed that the absorber is a thermal absorber, i.e. the epithermal absorption cross section is equal to zero. This is an acceptable approach for the possible burnable poison materials, as shown in chapter 7.

The two-group cross sections and diffusion constant are calculated in the following way. The basic data are 76-group cross sections created on the basis of the UKND library. The 76-group cross sections are condensed to 10-group cross sections with the program CRS[4], which condenses the cross sections with a homogeneized asymptotical pin cell spectrum. The 10-group cross sections are condensed to two-group macroscopic assembly-averaged cross sections with the assembly code CDB[5].

4.2. The Reactor Model

The PWR reactor Haddam Neck was chosen for study. The Haddam Neck core is usually divided into three zones with three

different enrichments, but for simplicity this study only uses one type of fuel with an average enrichment of 3%. The calculations are performed on a quarter of the core, which is divided into two control regions of almost equal size, an inner control region with 24 assemblies and an outer with 23 assemblies. Core geometry and data are given in fig. 1 and table 1. The meshes used in the diffusion calculation are equal in size to an assembly, and the maximum power-peaking factor is calculated as the ratio between the maximum power achieved in an assembly and the average power produced.

4.3. Results of the Calculations

In accordance with the optimal control strategy found in chapter 3, the power densities ascribed to the two control regions are kept constant until the control absorber concentration is zero in either of the regions. The reactor is then kept critical with the control absorber in the control region retaining control absorption, as the control absorber concentration in the other control region is restored to zero.

The results used in the synthetization are given in fig. 2, which shows the average burn-up of the outer region versus the average burn-up of the inner region. In other words, fig. 2 shows several permissible absorber management strategies, i.e. strategies for which the maximum power-peaking factor achieved during the cycle does not exceed the design limit f_{lim} for f. The curves marked A and E represent two strategies where f reaches the design limit at least once during the cycle. f_{lim} is here put equal to the maximum power-peaking factor for the homogeneously controlled reactor.

Any control strategy that gives burn-up curves between the A- and E-curves fulfils the condition that $f < f_{lim}$; on the other hand, any strategy giving burn-up curves outside the A- and E-curves gives $f > f_{lim}$. The optimal strategy should be found among the permissible control strategies; this strategy is that that gives maximum average burn-up for minimum power-peaking factor. It is obvious that the A-curve gives the maximum average discharge burn-up. This curve results from a strategy where the control absorber in the outer control region disappears first,and

criticality is retained with the control absorber in the inner control region. The variation of the control absorber versus time is shown in fig. 3; f versus time is shown in fig. 4.

Figure 5 shows the power-peaking factor versus maximum burn-up in the inner region. From this figure it is seen that the minimum power-peaking factor is achieved in case C, that is when the control absorber disappears simultaneously in the two regions. The power shape is constant during the cycle; in other words, the reactor has been run according to Haling's principle.

When choosing the optimal strategy, it should be kept in mind that the average burn-up is related to the 35% of the kWh price that can be ascribed to the fuel price, and that the power-peaking factor is related to the 65% of the kWh price that results from the capital investment.

The gain in average burn-up is calculated using table 2. Homogeneous poison control gives a burn-up of 15640 Mwd/TU with a power-peaking factor of 1.91. The maximum average burn-up for the same peaking factor is 16830, which means a gain in burn-up of

$$\frac{16830 - 15640}{15640} \cdot 100\% = 7.6\%.$$

The minimum peaking factor is 1.32, which means a reduction of

$$\frac{1.91 - 1.32}{1.91} \cdot 100\% = 31.7\%,$$

and there is no loss in the burn-up.

It seems that the optimal way of running a reactor is to keep the power-peaking factor as low as possible, which means that the reactor must be run at a constant power shape.

5. ABSORBER MATERIAL AND GEOMETRY

Having found the optimal way of running the reactor, the problem is now to find materials that can be used as burnable poisons and a suitable lumping that satisfies the optimal control strategy. This problem is discussed in this chapter.

5.1. Lumped Absorbers

The burn-up of lumped poison is studied under the following assumptions:

1) The poison is lumped in a sphere, cylinder or slab.
2) The lumped absorber is placed in an infinite medium and the neutron flux is not disturbed.
3) The absorption of neutrons takes places at the surface of the lump.

The burn-up is then described by the following differential equation:

$$\frac{dN}{dt} = -N\sigma\phi F \qquad (5.1)$$

where

$$dN = S \cdot C \cdot dX$$

where

- C is the absorber concentration
- N is the number of absorber atoms
- σ the absorption cross section
- ϕ the neutron flux
- S the surface of the lump
- F the self-shielding factor
- X the direction perpendicular to the surface.

The self-shielding for a black body is found from

$$\frac{dN}{dt} = -N\sigma\phi F = -\frac{\phi}{4} \cdot S.$$

With $N = C \cdot V$, we get:

$$F = \frac{S}{4VC\sigma} \qquad (5.2)$$

where V is the volume of the absorber lump.

Substitution of (5.2) into equation (5.1) gives

$$SC \cdot \frac{dX}{dt} = -VC\sigma\phi \cdot \frac{S}{4V\rho\sigma} \qquad (5.3)$$

which is transformed into

$$C \frac{dX}{dt} = - \frac{\phi}{4} , \tag{5.4}$$

which gives

$$x(t) = X(o) - \frac{\phi t}{4C} , \tag{5.5}$$

where t is the irradiation time.

Since the effective cross section is proportional to the absorber surface

$$\frac{\sigma_{eff}(\phi t)}{\sigma_{eff}(o)} = \left(\frac{X(t)}{X(o)}\right)^n = \left(1 - \frac{\phi t}{4CX(o)}\right)^n , \tag{5.6}$$

where $\sigma_{eff}(\phi t)$ is the effective cross section after an irradiation of ϕt and

n = 0 for a slab
n = 1 for a cylinder
n = 2 for a sphere.

It is seen from equation (5.6) that the rate of change depends upon the flux, the absorber density, the "thickness" of the absorber lump, and the geometry of the absorber lump.

The variation in effective absorption versus burn-up is illustrated in fig. 6. Absorber material in a cylinder geometry seems to offer the possibility of perfect control, bearing in mind the optimal variation of the control absorber found in chapter 4.

5.2. Choice of Absorber Material

Burnable poison materials must fulfil the following conditions:

1. At the end of the cycle less than 10% of the absorber must remain. This puts a limit to the absorption cross section.
2. The daughter isotopes of the burnable poison isotopes must have small absorption cross sections compared to the cross sections of their precursors.

At a flux time of 10^{21} n/cm^2, which is a typical flux time

for a light-water reactor, the first condition gives the following inequality

$$e^{-\sigma 10^{21}} < \frac{1}{10} = >$$

$$\sigma > \ln 10 \cdot 10^{-21} = 2.3 \cdot 10^{-24} \cdot 1000 = 2.300 \text{ barn}$$

where σ is the microscopic absorption cross section of the absorber.

In other words, the burnable poison isotopes should be sought among isotopes with cross sections larger than the cross section of ^{10}B, which has a thermal absorption cross section of $\sim$ 1600 barn (0 - 1.855 ev).

Possible burnable poison materials are given in table 3.

Of these possibilities, Eu is immediately rejected because of the large cross section of the daughter isotopes. Sm consists of two isotopes of considerable cross section. ^{149}Sm has a large thermal cross section and ^{152}Sm a large resonance integral. A small thermal self-shielding factor, usually of the order of one tenth, means that there is no burn-up of ^{152}Sm until ^{149}Sm has disappeared, and then ^{152}Sm gives a "tail" of poison, making Sm useless as a burnable poison.

Cd melts at 300°C which implies that Cd metal cannot be used as poison. CdO decomposes at 900°C, and CdO is thus a possible burnable poison.

Gadolinium and boron can both be used as burnable poisons. The melting point of B is 2300°C and the melting point of Gd is 1312°C. Boron is usually used in a mixture of B and SiC, while Gd is used in the ceramic form Gd_2O_3, which has a melting point of 2330°C. In this form Gd is usually mixed homogeneously with UO_2 in a few of the fuel pins in an assembly or distributed axially in selected fuel pellets in a few of the fuel pins.

6. CALCULATION OF ABSORBER DISTRIBUTION

The problem now is to find a way of distributing the absorber in the assembly, and then to control that the distribution and poison used are able to control the reactor in accordance with the prescribed way of running it. The important thing to

test is whether there are any of the suggested burnable poisons able to keep the power-peaking factor within the prescribed limits, thus preserving the optimistically suggested reduction in capital costs. This leaves two problems: the calculation of a suitable distribution and the control of burn-up calculation methods. The first problem is solved in this chapter.

6.1. Simple Calculations

The calculations used to determine the geometry of the lump can be used to calculate the poison concentration and the number of poison pins. The rate of change of the radius of a black cylinder is determined from equation (5.5). All poison has burned away for t = T. X(T) is therefore equal to zero and equation 5.5 is tranformed into

$$X(o) = r(o) = \frac{\phi T}{4C} . \qquad (6.1)$$

For a given unperturbed flux ϕ, cycle time T and cylinder radius at beginning of cycle r(o), the concentration of poison C is determined from

$$C = \frac{\phi T}{4r(o)} . \qquad (6.2)$$

In this report r(o) is put equal to the radius of the fuel pins.

The number of poison pins is determined from the assembly-averaged macroscopic thermal poison cross section at the beginning of the cycle $\Sigma_c(o)$ calculated with SELMA 2 by putting the absorption in the poison pins equal to the poison absorption calculated from $\Sigma_c(o)$

$$A \phi \Sigma_c(o) = 2\pi r(o) J \cdot n \qquad (6.3)$$

where

$$J = \frac{\phi}{4} ,$$

n is the number of poison pins in each assembly and A the assembly area.

Equation (6.3) is transformed into

$$n = \frac{2I_c(o)}{\pi r(o)} A \ . \tag{6.4}$$

This very rough method does not consider any perturbation in the flux caused by the poison pin.

6.2. Perturbation of the Flux

The perturbation could be accounted for by assuming that the poison pin is placed in an infinite, homogeneous medium and then calculating the flux by means of diffusion theory, using the extrapolation length in a black pin as a boundary condition.

The one-group diffusion equation describing the flux in the homogeneous medium is:

$$\nabla^2\phi(\bar{r}) - \kappa^2\phi(\bar{r}) = - \frac{S_o}{D} \tag{6.5}$$

$$\lim_{r \to \infty} \phi(\bar{r}) = \phi_o = \frac{S_o}{\Sigma_a}$$

where

S_o is a uniform source intensity

Σ_a is the macroscopic cross section for the homogeneous medium

D is the diffusion constant for the homogeneous medium

$$\kappa^2 = \frac{\Sigma_a}{D}$$

and

ϕ_o is the flux at the location of the poison pin prior to its introduction.

It is assumed that the source intensity is unaffected by the poison pin since this is a second-order effect.

The flux equation is, in cylindrical coordinates,

$$\frac{\partial^2\phi(\rho)}{\partial\rho^2} + \frac{1}{\rho}\frac{\partial\phi(\rho)}{\partial\rho} - \kappa^2\phi(\rho) = - \frac{S_o}{D} \ , \tag{6.6}$$

where ρ is the distance from the cylinder centerline. The symmetry of the geometry means that only the differentiation with respect to ρ remains.

The complete solution to this equation is

$$\phi(\rho) = A\, I_o(\kappa\rho) + B\, K_o(\kappa\rho) + \phi_o \,, \tag{6.7}$$

where I_o and K_o are modified Bessel's functions of first and second kind.

As $\phi(\rho)$ is limited for $\rho \to \infty$, A is equal to zero and $\phi(\rho) = B\, K_o(\kappa\rho) + \phi_o$.

The constant is determined from the boundary condition that ϕ is zero at the extrapolation distance d from the cylinder surface.

That is

$$\frac{d\phi}{d\rho} = \frac{\phi}{d} \,. \tag{6.8}$$

The sign of $\frac{\phi}{d}$ is positive because both $d\phi$ and $d\rho$ are negative.

The expression (6.7) is used for ϕ in (6.8), which is transformed into

$$\frac{d\phi}{d\rho} = - B\kappa\, K_1(\kappa\rho) = \frac{1}{d}(B\, K_o(\kappa\rho) + \phi_o) \tag{6.9}$$

which gives

$$B = - \frac{d\phi_o}{\kappa d\, K_1(\kappa\rho) + K_o(\kappa\rho)} \,. \tag{6.10}$$

The current of neutrons towards the cylinder surface is

$$D\,\frac{d\phi}{d\rho} = \frac{\phi_o D\kappa \cdot K_1(\kappa\rho)}{\kappa d\, K_1(\kappa\rho) + K_o(\kappa\rho)} = \frac{\phi_o}{4}\,\frac{4 \cdot D \cdot \kappa}{d\kappa + \dfrac{K_o(\kappa\rho)}{K_1(\kappa\rho)}} = \frac{\phi_o}{4}\, g. \tag{6.11}$$

d depends upon the size of the cylinder and it is two-thirds of a free mean path length for an infinitely large cylinder, and four-thirds of a free mean path length for an infinitely small cylinder[8].

The flux depression is accounted for by putting J equal to $\frac{\phi_o}{4} \cdot g$ and equations (6.2) and (6.4) are then transformed into

$$C = \frac{\phi T}{4r(o)}\, g \tag{6.12}$$

and

$$n = \frac{2\Sigma_c(o)}{\pi r(o)\, g}\, A. \tag{6.13}$$

The radius of fuel pins used in light-water reactors is of the order of 0.5 to 1 free mean path length. Several authors have studied the subject and given formulas for small and large cylinders. Sizes of interest in the present case require more complicated calculations.

An approximate way of calculating d, which in 9) is used on a sphere, is here used on a cylinder.

6.3. Calculation of Extrapolation Length

It is assumed that the poison lump is placed in an infinite medium in which a stationary flux of monochromatic neutrons is maintained.

The Peierl's neutron density equation, with all distances in units of the mean free path of the neutron, is

$$\phi(\bar{r}) = \frac{1}{4\pi} \int_{v'} \frac{\phi(\bar{r}')}{R^2}\, e^{-R}\, dv_{\bar{r}}, \tag{6.14}$$

where

$\phi(\bar{r})$ is the neutron track length per unit volume per unit time which is the flux at $\bar{r}$

R the distance between $\bar{r}$ and $\bar{r}'$

v' is the volume occupied by the non-capturing, isotropically scattering medium.

All distances are measured in units of mean free path.

For an infinite, homogeneous medium with a black cylinder of infinite height and radius r equation (6.11) is written in cylinder coordinates.

$$\phi(\rho) = \frac{1}{\pi} \int_r^\infty \phi(\rho')\, \rho'\, d\rho' \int_0^{\arccos \frac{r}{\rho} + \arccos \frac{r}{\rho'}} d\theta \tag{6.15}$$

$$\int_0^\infty \frac{e^{-\sqrt{\rho'^2+\rho^2+z^2-2\rho'\rho\cos\theta}}}{\rho'^2+\rho^2+z^2-2\rho\rho'\cos\theta}\, dz$$

The substitution $t = \sqrt{\rho^2+\rho'^2-2\rho\rho'\cos\theta}$ is used in equation (6.15), which becomes

$$\phi(\rho) = \frac{2}{\pi} \int_r^\infty \phi(\rho')\rho' d\rho' \int_{|\rho-\rho'|}^{\sqrt{\rho^2-r^2}+\sqrt{\rho'^2-r^2}} \frac{t\, dt \int_0^\infty \frac{e^{-\sqrt{z^2+t^2}}}{z^2+t^2}\, dz}{\sqrt{4\rho^2\rho'^2-(\rho^2+\rho'^2-t^2)^2}} \tag{6.16}$$

It is known from the theory of Bessel function that

$$\int_t^\infty K_o(x)\, dx = t \int_0^\infty \frac{e^{-\sqrt{z^2+t^2}}}{z^2+t^2}\, dz. \tag{6.17}$$

The integral on the left side is Bickley's function of the first kind $ki_1(t)$.

The solution of equation (6.16) at large distances from the cylinder boundary tends towards the solution of the corresponding diffusion equation

$$\nabla^2\phi = 0, \tag{6.18}$$

which has the solution

$$\phi(\rho) = A(1 + Q(\infty)\, \ln\rho), \tag{6.19}$$

where $Q(\infty)$ is a constant and A a non-essential constant.

Because

$$\phi(\rho) \underset{\rho \to \infty}{\to} (1+Q(\infty)\ \ln\ \rho) \tag{6.20}$$

$\phi(\rho)$ may be represented by

$$\phi(\rho) = 1+Q(\rho), \tag{6.21}$$

where

$$|Q(\rho) - Q(\infty)\ \ln\ (\rho)| \underset{\rho \to \infty}{\to} 0.$$

The expression (6.21) for $\phi(\rho)$ is used in the integral equation (6.16) giving

$$1+Q(\rho) = \frac{2}{\pi} \int_r^\infty (1+Q(\rho'))\ \rho'\ d\rho' \int_{|\rho-\rho'|}^{\sqrt{\rho^2-r^2}+\sqrt{\rho'^2-r^2}} \frac{dt\ ki_1(t)}{\sqrt{4\rho^2\rho'^2-(\rho^2+\rho'^2-t^2)^2}} \tag{6.22}$$

which is transformed into an equation for $Q(\rho)$

$$Q(\rho) = \int_r^\infty Q(\rho')\ k(\rho,\rho')\ \rho' d\rho' + f(\rho) \tag{6.23}$$

where

$$k(\rho,\rho') = \frac{2}{\pi} \int_{|\rho-\rho'|}^{\sqrt{\rho^2-r^2}+\sqrt{\rho'^2-r^2}} \frac{dt\ ki_1(t)}{\sqrt{4\rho^2\rho'^2-(\rho'^2+\rho'^2-t^2)^2}} \tag{6.24}$$

and

$$f(\rho) = \int_r^\infty \rho'\ k(\rho,\rho')\ d\rho' - 1 \tag{6.25}$$

This equation is used to find an expression for $Q(\infty)$ and thus for ϕ and $\frac{d\phi}{d\rho}$, which gives the extrapolation length d as

$$d = \frac{\phi}{\frac{d\phi}{d\rho}}. \tag{6.26}$$

The auxiliary functions $k'(\rho,\rho')$ and $f'(\rho)$ are introduced and $Q(\rho)$ is written

$$Q(\rho) = \int_r^\infty Q(\rho')\ k'(\rho,\rho')\ \rho'\ d\rho' + f'(\rho) \tag{6.27}$$

where

$$k'(\rho,\rho') = \begin{cases} k(\rho,\rho') & \text{for} \quad \rho > r \text{ and } \rho > r' \\ \frac{2}{\pi} \int_{\rho-\rho'}^{\rho+\rho'} \dfrac{dt\ k_i(t)}{\sqrt{4\rho^2\rho'^2-(\rho^2+\rho'^2-t^2)^2}} & \end{cases} \tag{6.28}$$

$f'(\rho)$ is defined from equation (6.25) by replacing $k(\rho,\rho')$ $k'(\rho,\rho')$. Equation (6.27) is then written as

$$\begin{aligned} Q(\rho) &= \int_o^\infty Q(\rho')\ G(\rho,\rho')\ \rho'\ d\rho' - \int_o^\infty Q(\rho')\ G(\rho,\rho')\ \rho'\ d\rho' \\ &\quad + \int_r^\infty Q(\rho')\ (k'(\rho,\rho') - G(\rho,\rho'))\ \rho'\ d\rho' + f'(\rho) \\ &= \int_o^\infty Q(\rho')\ G(\rho,\rho')\ \rho'\ d\rho' + F(\rho)\ . \end{aligned} \tag{6.29}$$

Using Taylor's expansion as described in 8), equation (6.29) is transformed into

$$-\frac{1}{3}\ \nabla^2\ Q(\rho) = F(\rho). \tag{6.30}$$

Integration of equation (6.39) gives

$$\begin{aligned} -\frac{1}{3} \int \nabla^2\ Q(\rho')\ dv &= -\frac{1}{3} \int_o^\rho \nabla^2\ Q(\rho')\ \rho'\ 2\pi\ d\rho' \\ &= -\frac{1}{3}\ 2\pi\ Q'(\rho')\ \rho' - \int_o^\rho F(\rho')\ \rho'\ 2\pi\ d\rho' = > \\ Q'(\rho)\ \rho &= -\int_o^\rho F(\rho')\ \rho'\ d\rho' \end{aligned} \tag{6.31}$$

where $Q'(\rho)$ is derived from $Q(\rho)$ by differentiation with respect to ρ.

For $\rho \to \infty$, $Q(\rho) \to Q(\infty)\ \ln\rho$ and equation (6.31) then becomes

$$Q(\infty) = -3 \int_0^\infty F(\rho)\, \rho\, d\rho. \tag{6.32}$$

The right side of equation (6.32) is transformed using the expression for $F(\rho)$ from equation (6.29)

$$\begin{aligned} &- 3\Big(- \int_0^\infty \int_0^r Q(\rho)\ G(\rho,\rho')\ \rho'\ d\rho'\ \rho\ d\rho \\ &+ \int_0^\infty \int_0^\infty Q(\rho')\ k'(\rho,\rho')\ \rho'\ d\rho'\ \rho\ d\rho - \\ &\int_0^\infty \int_r^\infty Q(\rho')\ G(\rho,\rho')\ \rho'\ d\rho'\ \rho\ d\rho + \int_0^\infty f'(\rho)\ \rho\ d\rho. \end{aligned} \tag{6.33}$$

The second and fourth terms give

$$\begin{aligned} &\int_r^\infty \int_r^\infty Q(\rho')\ k(\rho,\rho')\ \rho'\ d\rho'\ \rho\ d\rho + \int_0^r \int_r^\infty Q(\rho')\ G(\rho,\rho')\ \rho'\ d\rho' \\ &+ \int_r^\infty f(\rho')\ \rho\ d\rho + \int_0^r f'(\rho)\ \rho\ d\rho = \\ &\int_r^\infty Q(\rho')(1 + f(\rho'))\ \rho'\ d\rho + \int_r^\infty f(\rho)\ \rho\ d\rho + \int_0^r Q(\rho)\ \rho\ d\rho. \end{aligned} \tag{6.34}$$

Using Peierl's neutron density equation, the first and third terms give

$$- \int_0^\infty \int_0^\infty Q(\rho')\ G(\rho,\rho')\ \rho'\ d\rho'\ \rho\ d\rho = - \int_0^\infty Q(\rho)\ \rho\ d\rho. \tag{6.35}$$

Equations (6.33), (6.34) and (6.35), used together with equation (6.32), give

$$Q(\infty) = -3 \int_r^\infty Q(\rho)\ f(\rho)\ \rho\ d\rho - 3 \int_r^\infty f(\rho)\ \rho\ d\rho. \tag{6.36}$$

It is obvious that $Q(\rho)$ far from the cylinder boundary can be replaced by $Q(\infty)\ \ln\rho$. The idea now is to do this for all ρ and then check that the error in the extrapolation length is within acceptable limits. The asymptotic expression for $Q(\rho)$

is used in equation (6.36), which is then solved for $Q(\infty)$

$$Q(\infty) = - \frac{3 \int_r^\infty f(\rho)\ \rho\ d\rho}{\frac{1}{3} + \int_r^\infty \ln \rho\ f(\rho)\ \rho\ d\rho} \tag{6.37}$$

The extrapolation length is calculated from (6.36). This gives

$$d = \frac{1 + Q(\infty)\ \ln r}{\frac{Q(\infty)}{r}} = \frac{r}{Q(\infty)} + r \ln r\ . \tag{6.38}$$

Equation (6.37) does not give $Q(\infty)$ in a form suitable for a computer. The integrals must be transformed and this is done in the appendix.

It is found in the appendix that

$$d \xrightarrow[r \to 0]{} \frac{4}{3} \tag{6.39}$$

and

$$d \xrightarrow[r \to \infty]{} \frac{2}{3}\ . \tag{6.40}$$

The correct value for d with r = o is $\frac{4}{3}$. The correct value for d in the limit $r \to \infty$ is 0.71 and the error is 6%.

The extrapolation length calculated with this method has been compared with exact, but more laborious methods. The results of the comparison are shown in fig. 7.

The errors for r = 0.5 and r = 1.0 are

$$\frac{0.99 - 0.9487}{0.99} \cdot 100\% = 4.17\%$$

and

$$\frac{0.889 - 0.86609}{0.889} \cdot 100\% = 2.5\%.$$

These errors are acceptable in this work.

6.4. Distribution in Grey Cylinders

It was assumed in the preceding chapters that the absorbing cylinder was a black cylinder, which means that the excape probability α is equal to zero. This is not necessarily true for all poison materials.

α is the ratio between the number of neutrons that pass through a lump without being absorbed and the number of neutrons incident upon the surface of the lump. Using this definition, a relation between α, J_{black} and J_{grey} is found

$$\alpha = \frac{J_{black} - J_{grey}}{J_{black}} \tag{6.41}$$

where J_{grey} and J_{black} are the net neutron currents toward equalized grey and black cylinders, respectively.

Equation (6.41) is transformed into an expression for J_{grey}

$$J_{grey} = (1-\alpha)\ J_{black}. \tag{6.42}$$

By replacing J in expression (6.2) and (6.4) with J_{grey}, expressions for the poison concentration in grey cylinders and the number of grey poison pins are found.

Using the above mentioned definition, α is found from

$$\alpha = \frac{\int_{-\frac{\pi}{2}}^{\frac{\pi}{2}} \int_{-\frac{\pi}{2}}^{\frac{\pi}{2}} j(\theta,\theta')\ e^{-\Sigma_c \ell(\theta,\theta')} \cos\theta'\ d\theta'\ d\theta}{\int_{-\frac{\pi}{2}}^{\frac{\pi}{2}} \int_{-\frac{\pi}{2}}^{\frac{\pi}{2}} j(\theta,\theta')\ \cos\theta'\ d\theta\ d\theta'} \tag{6.43}$$

where

$j(\theta,\theta')$ is the current into the absorber

θ and θ' angles defined in fig. 8.

Σ_c the macroscopic absorption cross section of the absorber.

ℓ the maximal distance travelled by a neutron $\ell = \frac{2r(o)\cos\theta}{\cos\theta'}$.

In the diffusion approximation assuming an isotropic flux, the neutron current is

$$j(\phi,\phi') = \frac{\phi_\cdot}{2}\,\mu \qquad (6.44)$$

where

$\phi_\cdot$ is the neutron flux and

μ is the cosine of the angle between the surface normal and the entering line and then $\mu = \cos\theta\,\cos\theta'$.

Equation (6.44) in equation (6.43) gives

$$\alpha = \frac{\int_{-\frac{\pi}{2}}^{\frac{\pi}{2}}\int_{-\frac{\pi}{2}}^{\frac{\pi}{2}} \mu e^{-\Sigma_c \ell}\cos\theta'\,d\theta\,d\theta'}{\int_{-\frac{\pi}{2}}^{\frac{\pi}{2}}\int_{-\frac{\pi}{2}}^{\frac{\pi}{2}} \mu\cos\theta'\,d\theta\,d\theta'} = \frac{\int_{-\frac{\pi}{2}}^{\frac{\pi}{2}}\int_{-\frac{\pi}{2}}^{\frac{\pi}{2}} e^{-\Sigma_c \frac{2r(o)\cos\theta}{\cos\theta'}}\cos\theta\,\cos^2\theta'\,d\theta d\theta'}{\int_{-\frac{\pi}{2}}^{\frac{\pi}{2}}\int_{-\frac{\pi}{2}}^{\frac{\pi}{2}} \cos\theta\,\cos^2\theta'\,d\theta\,d\theta'} \qquad (6.45)$$

This expression is used to calculate α on a computer.

The neutron current is, of course, not isotropic near the border of heavily absorbing material unless the heavy absorber lump is small, i.e. for cylinders $2r \ll 1$. The formulas in which α is used calculate only estimates of poison concentration and the number of poison pins, thus it is therefore a reasonable assumption.

The general equations which take both flux depression and greyness into account are found from equations (6.2) and (6.4) by putting J equal to $(1 - \alpha)\, g\frac{\phi}{4}$ and this gives

$$C = (1 - \alpha)\cdot g\,\frac{\phi}{4}\,\frac{T}{r(o)}$$

$$n = \frac{\Sigma_c(o)}{\pi r(o)}\;\frac{2}{g(1-\alpha)}\,A\,. \qquad (6.46)$$

7. TEST OF BURN-UP CALCULATION METHODS

The burn-up calculations are performed with the CDB program described in 6). The calculation of burn-up is performed in two steps. A one-dimensional collision probability calculation gives the flux distribution in the cylincrical pin cells and diffusion theory is used in the overall assembly calculation. The pin cells are for fuel without poison divided into three regions - a fuel region, a cladding region and a moderator region - and this geometry gives satisfactory results as shown in 6). If the fuel region contains heavily absorbing material, the flux is anisotropic and it could be expected that this relatively simple way of calculation would give unsatisfactory results. Therefore the method of calculation has been tested against measurement.

7.1. Comparison of Measurements and Calculations for Boron and Cadmium

Reference 11 gives results for burn-up experiments with boron and cadmium. The geometry of the experiment facility is shown in fig. 9 and material data in table 4. The flux time is measured with Co(0.48%)-Al-monitors placed in the moderator. The calculations were performed with the CDB program using 10 energy groups in the collision probability calculation and 5 energy groups in the diffusion calculation. The 10-group cross sections are calculated with the program CRS[5], which condensates cross sections in 76 groups taken from a master tape. The 10-group cross sections are not changed during burn-up, but the 5-group cross sections are condensated from the 10-group cross sections for each time step. The flux time is calculated from the average flux in the moderator. The fuel rod is divided into 10 subregions and the poison concentration in each subregion is considered to be the concentration at the middle of the subregion. The power is assumed to be constant during the radiation periods between examination of the poison disk, because only the flux time at the time of examination is given. The results from the calculations and measurements of the concentration profiles are shown in figs. 10 and 11. The calculated and experimental integral burn-up values versus flux time are shown in fig. 12.

In [11] the errors in measurements are given as 10% for the radial concentration profile measurements, 5% for the integral burn-up measurements and 5% for the flux time measurements. The flux time is used to normalize the power used in the calculations and this thus introduces an error of 5% in the calculations.

The boron is distributed as grains of B_4C, which probably causes the variation in the experimental results shown in fig.10.

The integral burn-up calculations give faster burn-up of boron than the experimentally determined boron burn-up. This might be explained by the fact that the boron is distributed in grains with diameters of 90-100 μm, and this geometrical shielding is not considered in the calculations. The integral burn-up calculations for cadmium show a slower burn-up than the experimentally determined cadmium burn-up. No explanation is found for this discrepancy.

The integral results are within the errors in the measurements and calculations, and it is therefore concluded that the method of calculation can be used for integral burn-up calculations for boron and cadmium.

Figure 12 also shows the integral burn-up calculations performed with the epithermal cross sections, that is cross sections above 1.855 eV equal to zero. The results support the assumption that the absorber materials are purely thermal absorbers.

7.2. Comparison of Calculations for Gadolinium

Experimental results for burn-up of the burnable poison gadolinium have not been found, but the method of calculation has been compared with burn-up calculations performed in Norway[15] and Sweden[16]. These calculations are also used to investigate the dependence upon the number of regions used in the fuel and in the moderator region.

The geometry used in the gadolinium burn-up calculations is shown in fig. 13. It is a one-dimensional model of an infinite number of fuel pins with one poison pin containing a homogeneous mixture of fuel and gadolinium. The data used in the calculations are shown in table 5.

Calculations have been made with 1, 2, 4 and 8 subregions in the fuel and with 8 subregions in the fuel and 4 subregions in the moderator. The subregions in the fuel have equal volumes and subregions in the moderator have equal volumes. The results are shown in fig. 14, from which it is seen that 4 regions in the fuel and 1 in the moderator give acceptable accuracy. Calculations with 4 regions in the fuel are used in the comparison with Norwegian and Swedish calculations shown in fig. 15. The agreement is satisfactory.

The same type of calculation is used to test the influence of the epithermal cross sections on gadolinium burn-up by putting all cross sections above 1.8555 eV equal to zero. This does not influence the burn-up.

8. BORON, CADMIUM AND GADOLINIUM AS BURNABLE POISONS

This chapter describes calculations with boron, cadmium and gadolinium as burnable poisons distributed according the the formulas given in chapter 6. The results are discussed.

8.1. Distribution According to the Simple Formula

Equation (6.2) tells us that the absorber concentration is known when the absorber pin radius, the undisturbed flux and the cycle time are known.

The absorber pin radius is for practical reasons chosen equal to the fuel pin radius. The time it takes for the poison to burn away is known from SELMA 2, and is in this case 713 days. The flux which is taken as the thermal flux, because the absorber is considered to be a pure thermal absorber, is calculated with CDB using the power densities calculated with SELMA 2. It is assumed in equation (6.2) that the flux is constant. This is not entirely correct. There is a slight variation in the thermal flux, and therefore the flux used to calculate the absorber concentration is an average value of thermal flux over the cycle time.

The number of absorber pins is known when the thermal macroscopic control absorber cross section at the beginning of the cycle is known and the area of the assembly is known. The control absorber cross section is known from the SELMA 2 calcu-

lation and taken as the control absorber cross section when xenon equilibrium is established. The results are shown in table 6.

The fuel pins are placed in positions as indicated in fig. 15. It is assumed that the poison is mixed homogeneously with the fuel in the fuel pins.

The concentrations calculated with formula (6.2) are ascribed to boron, cadmium and gadolinium in the following way. Natural boron contains two isotopes, ^{10}B and ^{11}B. The ^{11}B absorption cross section is very small and the absorption in ^{11}B is therefore neglected, and all absorption in boron is due to ^{10}B. The concentration calculated with formula (6.2) is therefore equal to the concentration of ^{10}B.

Natural cadmium contains one isotope with large cross section, namely ^{113}Cd, and the concentration calculated with (6.2) is equal to the ^{113}Cd concentration.

Natural gadolinium contains two isotopes with large absorption cross sections, ^{155}Gd and ^{157}Gd. The thermal cross section of ^{157}Gd is four times as large as the thermal cross section of ^{155}Gd, thus they do not absorb equally well. In spite of this fact, the concentration is divided among the two isotopes according to their natural abundance, that is as if they absorbed equally well. The microscopic 10-group sections are calculated in the usual way with CRS. The burn-up-dependent, two-group assembly-averaged macroscopic cross sections for the two control regions are calculated with CDB. The two-dimensional calculations are performed with diffusion theory using the program DBU[6] and the same geometry as in the SELMA 2 calculations (fig.1).

The results of the burn-up calculations with CDB and the overall calculations with DBU giving the power-peaking factor and k_{eff} versus burn-up are shown in figs. 17-19 for boron, cadmium and gadolinium, respectively, as burnable poisons.

It is seen that none of the poisons has disappeared at the end of the cycle, that is after 713 days. The burn-up of the poison is too slow as the concentration of poison in the pins is too high, because the flux perturbation due to the poison pin was not considered in the concentration calculation. For boron, the small absorption causes an even slower burn-up, which is seen in fig. 17a. The decrease in the macroscopic absorption cross section is not perfectly linear at the end of the cycle.

The slow burn-up is also seen in the k_{eff}, which becomes less than 1 after 400-600 days.

The power-peaking factor is rather constant when boron and gadolinium are used as burnable poisons, and it is equal to or below the ideal value, 1.32, calculated with SELMA 2.

When cadmium is used as burnable poison, the power-peaking factor increases very rapidly at the end of the cycle. This increase in power-peaking factor is also seen in the k_{eff}, which increases too. This increase is partly due to the fact that the macroscopic thermal absorption cross sections in the two control regions decrease equally fast at the end of cycle and do not disappear simultaneously. No explanation has been found for this behaviour.

8.2. Absorber Distribution Using Formula (6.46)

The geometrical correction factor g for a black cylinder depends only upon the radius of the poison pin and the properties of the surrounding material and is, in this case, 0.78 calculated with the formulas from chapter 6 using the thermal values of the diffusion constant and diffusion length. The greyness of an absorber pin is calculated from the knowledge of the thermal capture cross sections of the poison and the concentration calculated with 6.2. The microscopic thermal cross section for boron is 1594.1 barn, which gives the following macroscopic cross section in the fuel pins in the inner and outer fuel region, respectively, of 1.75 cm^{-1}, which again gives α values of 0.25 and 0.32.

The microscopic thermal absorption cross section for ^{113}Cd is 22479, which gives macroscopic cross sections of 24.738 cm^{-1} and 16.257 cm^{-1} for the inner and outer control regions, respectively; these give α values less than 10^{-4} and the cadmium poison pin is in fact black.

The microscopic thermal cross sections of ^{155}Gd and ^{157}Gd are 12968 and 59282 barn, which give macroscopic cross sections of 40.552 cm^{-1} and 26.648 cm^{-1} for the inner and outer control regions, respectively, which again give α values less than 10^{-4} and the gadolinium poison pin is in fact black.

Burn-up calculations with the concentrations from table 7 given in figs. 20-22 for boron, cadmium and gadolinium, respect-

ively, show that there is no absorption left when cadmium and gadolinium are used as burnable poison, but that there still is absorption left when boron is used as burnable poison, because of the relatively small ^{10}B absorption cross section. Therefore isotopes with a thermal absorption cross section smaller than that of ^{10}B should not be used as burnable poison. The slow burn-up of boron is also seen in the k_{eff}, which reaches 1 after 600 days.

Both gadolinium and cadmium are suitable as burnable poison although formulas 6.46 do not give the correct concentrations. The power-peaking factor increases at the end of the cycle when the 6.46 formula concentrations are used. The concentration in the outer region is increased by 5% for gadolinium and by 5%, 10% and 15% for cadmium and this decreases the maximum value of the power-peaking factor. It is possible to operate the reactor at an almost constant power shape with the power-peaking factor below the ideal value and k_{eff} close to the prescribed value, in this case 1.0.

8.3. Local Power-Peaking Factors

It is assumed that the control absorber is mixed homogeneously with the fuel. The fuel in the pin with the control absorber does not produce power as long as there is any absorber left. The moment that the absorber is burned up, power production starts; but the concentration of fissile material is now larger in the former absorber pin than in the remaining fuel pins, and this gives a power peaking in the former absorber pin that counteracts the gain in the overall power-peaking factor calculated with DBU.

Calculations without fuel in the absorber pin show that the local power peaking is smaller at the end of the cycle, but that there is still a power peaking from the fuel pins around the absorber pin. The flux in these pins is depressed as long as there is any control absorber left. The burn-up of the fuel is thus less in these pins than in the other fuel pins.

In this case, the overall power-peaking factor is not seriously disturbed and the conclusion in chapter 4 is still valid, but the problem should be investigated in each particular case.

8.4. Remarks on Gadolinium Burn-up

Figure 24a shows the absorption versus time in gadolinium and the two gadolinium isotopes ^{155}Gd and ^{157}Gd. The absorption in gadolinium and ^{157}Gd decreases. But the absorption in ^{155}Gd increases during the first 120 days and then decreases. The concentrations of both ^{155}Gd and ^{157}Gd decrease during the cycle and the increase in the absorption of ^{155}Gd is due to the different radial burn-up of the two isotopes. Because ^{157}Gd has a cross section which is four times that of ^{155}Gd, the burn-up of ^{157}Gd is faster than that of ^{155}Gd, as is seen in fig. 24b.

The faster burn-up of ^{157}Gd causes an increase in the flux in the outer region of the absorber pin and this gives the ^{155}Gd absorption an increasing weight at the beginning of the cycle.

9. THREE-DIMENSIONAL CALCULATIONS

In the previous chapters the optimal control strategy was determined for a two-dimensional reactor. In this chapter the optimal poison strategy for a three-dimensional reactor is determined.

9.1. Control Strategy for a Three-dimensional Reactor

The diffusion equations describing the three-dimensional reactor are

$$\nabla^2 \phi_i (\bar{r}) + x_i \phi(\bar{r}) = 0 \qquad i = 1, 2, \ldots\ldots n$$

where n is the number of control regions.

Conditions 1-8 from 3.2 and conditions 1-3 from 3.8 are also valid for a three-dimensional reactor.

It was found in chapter 3 that the maximum average burn-up is achieved when no poison is left in the reactor, and that the optimal control stretegy was to run the reactor at constant power-shape until poison is left in one control region only and then maintain criticality with the poison in this region.

In the three-dimensional case, the optimal poison strategy shows the same characteristics as the two-dimensional case. The criticality condition for the end of cycle gives

$$F_c\ (e_1^T,\ \ldots\ldots\ldots,\ e_n^T) \;=\; 0, \tag{9.1}$$

where n is the number of control regions.

Increase of the burn-up in any region leads to subcriticality, that is

$$\frac{dF_c}{de_i} < 0 \qquad i = 1,\ 2,\ \ldots\ldots\ n \tag{9.2}$$

and the maximum value of the average burn-up is thus obtained when no poison is left in the reactor core.

The state equations are

$$\frac{de_i}{dt} = F_i\ (x_1, \ldots\ldots\ x_{n-1}) \quad i = 1,\ldots\ldots n \tag{9.3}$$

$$\frac{dx_i}{dt} = u_i \qquad\qquad i = 1,\ldots.n-1$$

These equations describe the system together with the criticality equation

$$F_c\ (x_1,\ldots\ldots\ldots x_n) = 0 \tag{9.4}$$

The Hamilton function is

$$H = F_o + \sum_{i=1}^{n} \Psi_i F_i + \sum_{i-1}^{n-1} \Psi_{i+n} u_i \tag{9.5}$$

and the adjoint equations are

$$\frac{d\Psi_i}{dt} = 0 \qquad\qquad i = 1,\ 2\ldots n$$

$$\frac{d\Psi_{i+n}}{dt} = -\frac{dF_o}{dx_i} - \sum_{i=1}^{n} \frac{dF_i}{dx_i} \qquad i = 1,\ldots.n-1 \tag{9.6}$$

During the period when the control bounds are state-independent, the following conditions are satisfied.

$$\Psi_{i+n} = 0 \qquad i = 1,\ldots\ldots n-1$$

$$\frac{d\Psi_{i+n}}{dt} = 0 \qquad i = 1,\ldots\ldots n-1 \qquad (9.7)$$

Equation 9.6 means that Ψ_i is constant for all i, and the x_i's, which satisfy equation(9.7),are constant. This is equivalent to constant power shape.

The many elements complicate the variable power shape control strategy. From the two-region problem it is known that one element in the control region takes its maximum value when all the others take their minimum value.

The optimal strategy could therefore be a period of constant power shape followed by a period of variable power shape, when criticality is maintained with the poison in one region.

The three-dimensional control strategy has thus the same characteristics as the two-dimensional control strategy.

9.2. Three-dimensional Calculations for PWRs

Three-dimensional calculations for a PWR are performed with SELMA 2 in RZ-geometry with the same fuel data as used in the two-dimensional calculations. The four control regions used in these calculations are shown in fig. 25. The three-dimensional case is not synthesized as for the two-dimensional case. Considering the conclusions in 9.1, the conclusion from the two-dimensional case - that the reactor should be run at constant power shape - is also used here. The absorption calculated with SELMA 2 for this case is shown in fig. 26, and the power-peaking factor for the homogeneously controlled reactor and the reactor controlled with lumped absorbers according to Haling's principle is shown in fig. 27. There is no significant loss in average burn-up and a considerable decrease in the power-peaking factor from the homogeneously controlled reactor to the reactor controlled with lumped absorbers.

In the three-dimensional case, the reduction is

$$\frac{2.74 - 1.46}{2.74} \cdot 100\% = 46.7\%.$$

The gain in capital costs is thus considerable, and this seems to support the use of burnable poison in PWRs to shape the power in the radial and axial directions.

9.3. Three-dimensional Calculations for BWRs

The use of burnable poison in boiling-water reactors must be investigated in three dimensions. The three-dimensional nodal program NOTAM[14], used at Risø for three-dimensional burn-up calculations on boiling water reactors, is used in the investigation of this problem.

The program is rewritten to calculate a macroscopic absorption cross section that retains a prescribed power shape. The reactor core is divided into a number of control regions. A power density is prescribed to each region and the absorption cross sections are calculated in the following way.

The two-group neutron equations describing the neutron balance of a node j are

$$L_j^1 - \lambda(\Sigma_a^1+\Sigma_s^{2,1})_j \phi_j^1 + \nu(\Sigma_f^1\phi^1 + \Sigma_f^2\phi^2)_j = 0 \qquad (9.8)$$

$$\Sigma_{s,j}^{2,1}\phi_j^1 = \Sigma_{a,j}^2\phi_j^2 \qquad (9.9)$$

where

$\Sigma_{a,j}^i$, $\Sigma_{s,j}^i$ $\Sigma_{f,j}^i$	are the macroscopic cross sections for absorption, scattering and fission in node j and group i
$\Sigma_{s,j}^{2,1}$	is the macroscopic cross section for scattering from group 1 to group 2.
λ	is the eigenvalue of the problem
ϕ_j^i	is the flux in group i, node j
ν	is the number of neutrons released per fission
L_j^i	is the leakage in group i, node j.

The equations are normally solved with λ as the eigenvalue.

In this case the power shape and λ are prescribed and the thermal poison concentration is used as eigenvalue.

It is assumed that the macroscopic poison cross sections are equal for nodes within a control region. This means that

$$(\Sigma_a^2 + \Sigma_c^2)_j \phi_j^2 = \Sigma_{s,j}^{2,1} \phi_j^1$$

and

$$\Sigma_{cl}^2 = \Sigma_{cj}^2$$

j number on node in a control region, j = 1 is an arbitrary node in the same control region

where

Σ_{cj}^2 is the thermal macroscopic control absorber cross section.

The equations are transformed into

$$\Sigma_{cl} = \Sigma_{s,j}^{2,1} \frac{\phi_j^1}{\phi_j^2} - \Sigma_{a,j}^2 = \Sigma_{s,1} \frac{\phi_1^1}{\phi_1^2} - \Sigma_{a1}^2. \qquad (9.10)$$

ϕ_j^2 is then expressed in the following way:

$$\phi_j^2 = \left(\frac{\Sigma_{1,1}}{\Sigma_{s,j}} \frac{\phi_1^1}{\phi_j^1} + (\Sigma_{a,j}^2 - \Sigma_{a,1}^2)/\Sigma_{s,j}^{2,1} \frac{\phi_1^2}{\phi_j^1}\right)^{-1} \cdot \phi_1^2 = B_j \cdot \phi_1^2 \qquad (9.11)$$

The equation for the fast flux is transformed giving

$$\phi_j^1 = \nu\Sigma_{f,j}^2 / \left(\lambda(\Sigma_a^1 - \Sigma_s^{2,1})_j - \nu\Sigma_{f,j}^1 - L_j^1/\phi_j^1\right) B_j \phi_1^2. \qquad (9.12)$$

This equation is used to calculate ϕ_1^2 iteratively from the prescribed power density p^*. The power density p is expressed in ϕ_1^2

$$p = \int_j \Sigma^2_{fj}(1+\nu\Sigma^2_{fj}/(\lambda(\Sigma^1_a-\Sigma^{2,1}_s)_j - \nu\Sigma^1_{fj} - L^1_j/\phi^1_j)\ B_j\ \phi^2_1 = z\phi^2_1 \tag{9.13}$$

where

$\int$ means summation over the nodes in a control region j.

The iteration is carried out in the following way:

$$\phi^{2,m+1}_1 = \phi^{2,m}_1 + (p^*-p^m)/z$$

$$\phi^{2,m+1}_j = B_j\phi^{2,m+1}_1 \tag{9.14}$$

$$\phi^{1,m+1}_j = \phi^{1,m}_j + \nu\Sigma^2_{fj}/(\lambda(\Sigma^1_a+\Sigma^{2,1}_s)_j - \nu\Sigma^1_{fj} - L^1_j/\phi^{1,m}_j)\cdot(\phi^{2,m+1}_j-\phi^{2,m}_j)$$

where m is an iteration index.

When the iteration has converged, the macroscopic absorption cross section is calculated from

$$\Sigma_c = \Sigma^{2,1}_{s,1}\frac{\phi^1_1}{\phi^2_1} - \Sigma^2_{a,1}. \tag{9.15}$$

Calculations performed with this program gave no definite solution to the optimal way of running a BWR reactor. It was not possible to use the trial and error method in three dimensions because of the long computer times.

Calculations with this program were performed on the DRESDEN 1 core. Data for the Dresden reactor are given in tables 8-10 and the geometry is shown in fig. 28. The Dresden 1 assembly is shown in fig. 29. The problem of finding optimal control for a BWR is more difficult than for a PWR because of the change in the power shape during the cycle as seen in fig. 30, which shows the acial power shape at the beginning and end of the cycle, and table 11, which shows an example of the constant power shape retaining macroscopic absorption cross sections in the six control regions into which the DRESDEN 1 core was divided. The variation in the macroscopic cross sections is considerable and no solutions were found to the problem.

One way to facilitate the synthesization would be to find the power shape corresponding to Haling's principle. This is easily done since the power shape is constant, and thus the burn-up shape is constant during the cycle. This is expressed in the following equations:

$$p_j = \bar{p} a_j \tag{9.16}$$

and

$$e_j = \bar{e} a_j \tag{9.17}$$

where

p_j and e_j are the power and burn-up in node j
$\bar{p}$ and $\bar{e}$ are the space-averaged power and burn-up values.

Equations (9.8) and (9.9) are then written

$$L'_j - (\Sigma'_a + \Sigma^{2,1}_s)_j \phi_j + \nu \frac{\bar{p} \cdot e_j}{\bar{e}} = 0 \tag{9.18}$$

$$\Sigma^{2,1}_{s,j} \phi'_j = \Sigma^2_{a,j} \phi^2_j$$

where

$p_j = \bar{p} \frac{e_j}{\bar{e}}$ and $\lambda = 1$ have been used.

The eigenvalue is now $\bar{e}$ and the equations can be solved by iterations.

10. CONCLUSIONS

From the investigations described in this report, it is consluded that the optimal absorber management strategy for a PWR-reactor with the same fuel all over the core is to run the reactor at a constant power shape. It is furthermore concluded that cadmium and gadolinium are excellent burnable poisons because both can be used to keep the power shape constant and k_{eff} equal to 1 during a cycle. The optimal control problem for a BWR was investigated but no solution was found to this problem.

11. ACKNOWLEDGEMENTS

The author wishes to thank S. Weber for fruitful discussions and G.K. Kristiansen for much help in solving the mathematical problems.

REFERENCES

1) S. Weber, The IBU2-SELMA2 Fuel-Management System. Risø Report No. 310 (1974) 75 pp.

2) K. Ladekarl Thomsen, Self-Management, An Approach to Optimum Core Management of Thermal Reactors by Means of Ideal Burn-up Distributions. Risø Report No. 232 (1971) 129 pp.

3) L.S. Pontryagin et al., The Mathematical Theory of Optimal Processes. (Interscience, New York, 1965) 360 pp.

4) S. Fadilah, Optimum Power Shape Strategies for Given Reactor End of Cycle Conditions, J. of Inst. Nucl. Eng., 16 (1975) 102-104.

5) A.M. Hvidtfeldt Larsen, CRS: A Code to Produce Multigroup Neutron Cross Sections for Reactor Physics Calculations. Risø-M-1568 (1973) 32 pp.

6) K.E. Lindstrøm Jensen, Development and Verification of Nuclear Calculation Methods for Light-Water Reactors. Risø Report 235 (1970) 161 pp.

7) R.V. Meghreblian and D.K. Holmes, Reactor Analysis. (McGraw--Hill, New York, 1960) 808 pp.

8) B. Davison and I.B. Sykes, Neutron Transport Theory (Clarendon Press, London, 1957) 450 pp.

9) D.F. Zaretsky, Effective Boundary Conditions for Grey Bodies. In: Proceedings of the International Conference on the Peaceful Uses of Atomic Energy. Held in Geneva 8 Aug - 20 Aug, 1955. Vol. 5 (United Nations, New York, 1956). 525-530.

10) S.A. Kushneriuk and C. McKay, Neutron Density in an Infinite, Non-Capturing Medium Surrounding a Long Cylindrical Body Which Scatters and Captures Neutrons. AECL-137, CRT-566 (1954) 68 pp.

11) J. Ahlf et al., Experimentelle und Theoretische Abbranduntersuchungen an Modellanordnungen mit Festen Abbrenbaren Giften. Atomkerneenergi 25 (1975) 91-97.

12) A.M. Hvidtfeldt Larsen, Sigma Master Tape, a Multi-Group Cross Section Library. Risø Report No. 262 (1972) 50 pp.

13) R. Peirls, Critical Conditions in Neutron Multiplication. Proc. of the Camoridge Phil. Soc. 35 (1939) 610-615.

14) T. Petersen, Private communication.

15) S. Børresen, Private communication.

16) M. Edenius, Private communication.

12. APPENDIX

In this appendix the integrals in equation (6.37) are transformed into a form suitable for a computer.

The first step is to transform the integral expression for $f(\rho)$

$$f(\rho) = \frac{2}{\pi} \int_r^\infty \rho' \, d\rho' \int_{|\rho-\rho'|}^{\sqrt{\rho^2-r^2} + \sqrt{\rho'^2-r^2}} \frac{dt \; ki_1(t)}{\sqrt{4\rho'^2\rho^2-(\rho^2+\rho'^2-t^2)^2}} - 1 \, . \tag{A.1}$$

The sequence of integration is interchanged

$$f(\rho) = \frac{2}{\pi} \int_0^{\rho-r} dt \; ki_1(t) \int_{\rho-t}^{\rho+t} \frac{\rho'}{\sqrt{4\rho^2\rho'^2-(\rho^2+\rho'^2-t^2)^2}} d\rho' +$$

$$\frac{2}{\pi} \int_{\rho-r}^{\sqrt{\rho^2-r^2}} dt \; ki_1(t) \int_r^{\rho+t} \frac{\rho'}{\sqrt{4\rho^2\rho'^2-(\rho^2+\rho'^2-t^2)^2}} d\rho' +$$

$$\frac{2}{\pi} \int_{\sqrt{\rho^2-r^2}}^\infty dt \; ki_1(t) \int_{\sqrt{t^2+\rho^2-2t\sqrt{\rho^2-r^2}}}^{\rho+t} \frac{\rho'}{\sqrt{4\rho^2\rho'^2-(\rho^2+\rho'^2-t^2)^2}} d\rho'$$

$$- \int_0^\infty ki(t) \, dt \tag{A.2}$$

where the well known relation

$$\int_0^\infty ki_1(t)\,dt = 1 \qquad \text{(A.3)}$$

is used for figure 1. Integration of the inner integrals give

$$f(\rho) = \frac{1}{\pi} \int_{\rho-r}^{\sqrt{\rho^2-r^2}} dt \arcsin \frac{\rho^2+t^2-r^2}{2\rho t}\, ki_1(t)$$

$$+ \frac{1}{\pi} \arcsin \frac{\sqrt{\rho^2-r^2}}{\rho} \int_{\sqrt{\rho^2-r^2}}^{\infty} ki_1(t)\,dt - \tfrac{1}{2} \int_{\rho-r}^{\infty} dt\, ki_1(t). \qquad \text{(A.4)}$$

$f(\rho)$ is a part of two types of integral

$$\int_r^\infty \rho\, f(\rho)\, d\rho \quad \text{and} \quad \int_r^\infty \rho \ln \rho\, f(\rho)\, d\rho,$$

which must now be solved.

This is done by interchanging the sequence of integration with respect to t and ρ, first for the integral

$$\int_r^\infty \rho\, f(\rho) d\rho \ .$$

$$\int_r^\infty \rho\, f(\rho)\, d\rho = \frac{1}{\pi} \int_r^\infty \rho\, d\rho \int_{\rho-r}^{\sqrt{\rho^2-r^2}} \arcsin \frac{\rho^2+t^2-r^2}{2\rho t}\, ki_1(t)\, dt$$

$$+ \frac{1}{\pi} \int_r^\infty \rho \arcsin \frac{\sqrt{\rho^2-r^2}}{\rho} d\rho \int_{\sqrt{\rho^2-r^2}}^\infty ki_1(t)\, dt$$

$$- \frac{1}{2} \int_r^\infty \rho\, d\rho \int_{\rho-r}^\infty ki_1(t)\, dt$$

$$= \frac{1}{\pi} \int_o^\infty ki_1(t)\, dt \int_{\sqrt{t^2+r^2}}^{t+r} r \arcsin \frac{\rho^2+t^2-r^2}{2\rho t} d\rho$$

$$+ \frac{1}{\pi} \int_o^\infty ki_1(t)\, dt \int_r^{\sqrt{t^2+r^2}} \rho \arcsin \frac{\sqrt{\rho^2-r^2}}{\rho} d\rho$$

$$- \frac{1}{2} \int_o^\infty ki_1(t)\, dt \int_r^{t+r} \rho\, d\rho$$

$$= \int_o^\infty \left(\frac{1}{\pi} \left(- \frac{r^2+t^2}{2} \operatorname{arc\,tg} \frac{t}{r} + \frac{\pi}{4} t(t+2r) - \frac{rt}{2}\right)\right.$$

$$+ \frac{1}{\pi} r^2 (\operatorname{arc\,tg} \frac{t}{r}) (\frac{t}{r})^2 \cdot \frac{1}{2}$$

$$\left. - \frac{1}{2} (\frac{r}{r} - \operatorname{arc\,tg} \frac{t}{r})) - \frac{1}{2} \cdot \frac{1}{2} t(t+2r)) ki_1(t)\, dt \right.$$

$$= -\frac{r}{\pi} \int_0^\infty t\, ki_1(t)\, dt \,. \qquad (A.5)$$

A series is used for the Bickley function and the integral is calculated on a computer.

The $\int_r^\infty \rho \ln\rho\, f(\rho)d\rho$ integral is transformed in the same way

$$\int_r^\infty \rho \ln \rho\, f(\rho)\, d\rho$$

$$= \frac{1}{\pi} \int_r^\infty \rho \ln \rho\, d\rho \int_{\rho-r}^{\sqrt{\rho^2-r^2}} \arcsin \frac{\rho^2+t^2-r^2}{2\rho t}\, ki_1(t)\, dt$$

$$+ \frac{1}{\pi} \int_r^\infty \rho \ln \rho \arcsin \frac{\sqrt{\rho^2-r^2}}{\rho}\, d\rho \int_{\sqrt{\rho^2-r^2}}^\infty ki_1(t)\, dt$$

$$- \frac{1}{2} \int_r^\infty \rho \ln \rho\, d\rho \int_{\rho-r}^\infty ki_1(t)\, dt$$

$$= \frac{1}{\pi} \int_c^\infty ki_1(t)\, dt \int_{\sqrt{t^2+r^2}}^{t+r} \rho \ln \rho \arcsin \frac{\rho^2+r^2-r^2}{2rt}\, d\rho$$

$$+ \frac{1}{\pi} \int_0^\infty ki_1(t)\, dt \int_r^{\sqrt{t^2+r^2}} \rho \ln \rho \arcsin \frac{\sqrt{\rho^2-r^2}}{\rho}\, d\rho$$

$$- \frac{1}{2} \int_0^{\infty} ki_1(t)\, dt \int_r^{t+r} \rho \ln \rho \, d\rho$$

$$= \frac{1}{\pi} \int_0^{\infty} (\ln \sqrt{t^2+r^2} \left(\frac{1}{2} (t^2+r^2) \text{ arc tg } \frac{t}{r} + \frac{\pi r^2}{4}\right)$$

$$- \ln(t+r) \left(\frac{\pi}{4} (t+r)^2 + \frac{rt}{2}\right)$$

$$- \frac{1}{2} \left(\frac{t^2+r^2}{2} \text{ arc tg } \frac{t}{r} - \frac{\pi}{4} t(t+2r) - \frac{rt}{2}\right)$$

$$+ \frac{1}{4} \int_0^1 r^2 \frac{\text{arc sin } \sigma}{2rt\sigma r^2+t^2} 2rt \, d\sigma$$

$$- \frac{1}{4} \int_0^1 rt \frac{2rt\sqrt{1-\sigma^2}}{2rt\sigma+r^2+t^2} d\sigma) \, ki_1(t)\, dt$$

$$= \frac{1}{\pi} \int_0^{\infty} (\ln \sqrt{t^2+r^2} \left(r^2 \left(\frac{1}{2} \text{ arc tg } \frac{t}{r} \left(\frac{t}{r}\right)^2 - \frac{1}{2} \left(\frac{t}{r} - \text{arc tg } \frac{t}{r}\right)\right)\right.$$

$$\left. - \frac{1}{4} r^2 \text{ arc tg } \frac{t}{r} \frac{t^2}{r^2} + \frac{3}{4} r^2 \left(\frac{t}{r^2} - \text{arc tg } \frac{t}{a}\right)\right) ki_1(t)\, dt$$

$$- \frac{1}{2} \int_0^\infty \left(\frac{1}{2} (t+r)^2 \ln(t+r) - \frac{1}{4} t(t+2r) - \frac{1}{2} r^2 \ln r\right) ki_1(t)\, dt$$

$$= \int_0^\infty \left(\frac{1}{\pi} \left\{-\ln \sqrt{t^2+r^2}\, rt - \text{arc tg} \frac{t}{r} \frac{r^2}{2} + rt \right.\right.$$

$$+ \frac{1}{4} \int_0^1 r^2 \frac{\text{arc sin } \sigma}{2rt\sigma+r^2+r^2} 2rt\, d\sigma - \frac{1}{4} \int_0^1 rt \frac{2rt\sqrt{1-\sigma^2}}{2rt\sigma+r^2+t^2} d\sigma)$$

$$\left.\left. - \frac{1}{4} \ln(t+r) \frac{r^2}{4} + \frac{1}{4} r^2 \ln r\right) ki_1(t)\, dt = I \,. \qquad \text{(A.5)}\right.$$

This integral is calculated on a computer using the same series for the Bickley function as mentioned above. The integrals of the form $\int_0^1 h(\rho)d\rho$ are calculated using Gauss integration.

The extrapolation length values for $r \to 0$ and $r \to \infty$ are calculated from the following asymptotic expressions:

$$d = r \ln r + \frac{\pi}{3 \int_0^\infty t\, ki_1(t)\, dt} + \frac{I\, \pi}{\int_0^\infty t\, ki_1(t)\, dt} \qquad \text{(A.6)}$$

$I \underset{r \to 0}{\to} 0$ and $r \ln r \underset{r \to 0}{\to} 0$, which gives

$$d \underset{r \to 0}{\to} \frac{\pi}{3 \int_0^\infty t\, ki_1(t)\, dt} = \frac{4}{3}. \qquad (A.7)$$

This is the correct d value for $r \to 0$. The value of I for $r \to \infty$ must be found to calculate the extrapolation length in this limit. The integral terms of I give

$$\frac{1}{4} \int_0^1 r^2 \frac{2rt \arcsin \sigma}{2rt\sigma r^2 + t} d\sigma \underset{r \to \infty}{\to} \frac{rt}{2} \frac{\pi}{2} - \frac{rt}{2} \qquad (A.8)$$

and

$$-\frac{1}{4} \int_0^1 2r^2 r^2 \frac{\sqrt{1-\sigma^2}}{2rt\sigma + r^2 + t^2} d\sigma \underset{r \to \infty}{\to} -\frac{t^2}{2} \frac{\pi}{4}. \qquad (A.9)$$

The remaining integrand is

$$\frac{1}{\pi} \left(-\ln \sqrt{t^2+r^2}\, rt - \operatorname{arc\,tg} \frac{t}{r} \frac{r^2}{2} + rt\right) - \ln(t+r) \frac{r^2}{4} + \frac{1}{4} r^2 \ln r \underset{r \to \infty}{\to}$$

$$\frac{1}{\pi} \left(-rt \ln r + \frac{rt}{2}\right) + \frac{rt}{4} \qquad (A.10)$$

and the limit for I is then

$$I \underset{r \to \infty}{\to} \int_0^\infty \left(\frac{1}{\pi}\left\{-rt \ln r + \frac{rt}{2} + \frac{rt\pi}{4} - \frac{rt}{2} - \frac{\pi t^2}{8}\right) - \frac{rt}{4}\right) k_i(t)\, dt$$

$$= \int_0^\infty \frac{1}{\pi}\left(-rt \ln r - \frac{\pi t^2}{8}\right) ki_1(t)\, dt$$

$$= -r \ln r \frac{1}{\pi} \int_0^\infty t\, ki_1(t)\, dt - \frac{1}{8} \int t^2\, ki_1(t)\, dt\,, \qquad \text{(A.11)}$$

which gives for d

$$d \underset{r \to \infty}{\to} r \ln r + \frac{\pi}{3 \int_0^\infty t\, ki_1(t)\, dt} + \frac{\pi \frac{1}{\pi}(-r \ln r) \int_0^\infty t\, k_i(t)\, dt}{\int_0^\infty t\, ki_1(t)\, dt}$$

$$- \frac{\frac{\pi}{8} \int_0^\infty t^2\, ki_1(t)\, dt}{\int_0^\infty t\, k_i(t)\, dt}$$

$$= \frac{\pi}{3 \int_0^\infty t\, ki_i(t)\, dt} - \frac{\frac{\pi}{8} \int_0^\infty t^2\, ki_1(t)\, dt}{\int_0^\infty t\, ki_1(t)\, dt} = \frac{2}{3}. \qquad \text{(A.12)}$$

Table 1

Main plant data for the reference reactor Haddam Neck

Reactor thermal power initial cycle	MWt	1465
Average power density initial cycle	MWt/tU	22.2
core diameter	cm	303.5
Active core height	cm	309.4
Number of fuel elements		157
Number of fuel rods		32028
Fuel rod pitch	cm	1.43
Fuel rod outside diameter	cm	1.07
Cladding thickness	cm	0.0419
Pellet diameter	cm	0.9741
Fuel enrichment Initial cycle	w/o U^{235}	3.00

Table 2

Maximum average burn-up values and maximum power peaking factors

Control form*	Max. burn-up MWd/TU	Power-peaking factor
A	16830	1.92
B	16100	1.58
C	15656	1.32
D	15780	1.57
E	16050	1.92
Homogeneous poison	15640	1.92

*The letters refer to the curves in fig. 2.

Table 3

Possible burnable poison materials

Element	Isotopes (abundance)	σ_{2200} barn	RI barn	$\sigma_{daughter}$ barn
Cd		2450		
	113 (12.26%)	19910		0.336
Sm		5800	1400	
	149 (13.83%)	41000		102
	152 (76.72%)	206	3300	
Eu		4600	2430	
	151 (47.82%)	9200	3300	2300
	153 (52.18%)	390	1635	1500
Gd		49000		
	155 (14.73%)	61000	1550	1.5
	157 (15.68%	254000	730	2.5
B		759	341	
	10 (19.6%)	3837	1722	

Table 4

Material data for the burn-up experiment

Fuel pin

Fuel	UO_2
Density g/cm^3	10.26
Enrichment (W%)	3.234
Average fuel temp. (^oC)	110-740

Poison pin	1	2
Material	binal	Cd-Mg-alloy
Density (g/cm^3)	2.68	2.55
Composition (W%)	Al: 94.05%	Cd: 38.0
	B: 4.60	Mg: 62.0
	C: 1.00	
	Fe: 0.22	
	Si: 0.13	
Poison (atom %)	B^{10}: 19.8^o	Cd^{113}: 12.26
Poison distribution	grains 90-100 um in diameter	
Average water temperature (^oC)	40	

Table 5

Material data for gadolinium burn-up calculations

Fuel pins	
Material	UO_2
Enrichment W/%	3.00 ^{o}k
Density g/cm^3	10.4
Temperature ^{o}C	600
Poison pin	
Material	$UO_2 + Gd_2O_3$
Enrichment W/%	3.00
Gadolinium conc. mg Gd_2O_3/cm^3	200
Density	10.4
Temperature ^{o}C	600
Cladding	
Material	Zircaloy
Density g/cm^3	6.4
Temperature ^{o}C	380
Moderator	
Material	H_2O
Density g/cm^3	0.457
Temperature ^{o}C	286
Power density in unpoisoned pins W/g UO_2	15

Table 6

Poison number densities calculated with equations 6.2

Outer control region

Average thermal flux $2.3 \cdot 10^{13}$ n/cm^2/s

Poison isotope	^{10}B	^{113}Cd	^{155}Gd	^{157}Gd
Number densities (cm^{-3} 10^{-24})	$7.2318 \cdot 10^{-4}$	$7.2318 \cdot 10^{-4}$	$3.5029 \cdot 10^{-4}$	$3.7289 \cdot 10^{-4}$

Macroscopic thermal poison cross section at beginning of cycle when xenon equilibrium is established $1.3572 \cdot 10^{-2}$ cm^{-1}.

Number of poison pins pr. assembly = 8.

Inner control region

Average thermal flux $3.5 \cdot 10^{13}$ n/cm^2/sec

Poison isotope	^{10}B	^{113}Cd	^{155}Gd	^{157}Gd
Number densities (cm^{-3} 10^{-24})	$1.1005 \cdot 10^{-3}$	$1.1005 \cdot 10^{-3}$	$5.3306 \cdot 10^{-4}$	$5.6744 \cdot 10^{-4}$

Macroscopic thermal poison cross section at beginning of cycle when xenon equilibrium is established $1.731 \cdot 10^{-2}$ cm^{-1}.

Number of poison pins pr. assembly = 10.

Table 7

Poison number densities calculated with equation 6.46

Thermal diffusion constant for the surrounding media 0.442019
Thermal diffusion length for the surrounding media 2.2483

Isotopes	Macroscopic cross section		Transmission coefficient α		Number densities $cm^{-3} \cdot 10^{-24}$	
	inner region (cm^{-1})	outer region (cm^{-1})	inner region	outer region	inner region	outer region
^{10}B	1.175	1.153	0.22	0.35	$6.6954 \cdot 10^{-4}$	$3.6427 \cdot 10^{-4}$
^{113}Cd	24.738	16.257	∿0	∿0	$8.5839 \cdot 10^{-4}$	$5.60418 \cdot 10^{-4}$
^{155}Gd	40.552	26.648	∿0	∿0	$4.1579 \cdot 10^{-4}$	$2.7323 \cdot 10^{-4}$
^{157}Gd					$4.4260 \cdot 10^{-4}$	$2.9085 \cdot 10^{-4}$

Number of pins

	inner region	outer region
Gadolinium and Cd	12	10
^{10}B	16	16

Table 8

DRESDEN 1 core 1 description

Core data	
Heat output (MW)	620
Net electrical output (MW)	180
Active core height (cm)	275.4
Equivalent diameter (cm)	326
Fuel enrichment (W/o U^{235})	1.5
Number of fuel boxes max.	488
Number of rods in each box	36
Number of cruciform control rods	80
Fuel element pitch (cm)	12.65
Fuel rod pitch (cm)	1.8034
Fuel rod outside diameter (cm)	1.448
Fuel rod zircaloy-2 cladding thickness (cm)	0.0762
Fuel pellet diameter (cm)	1.255
Average power density in core (W/cm^3)	31.2
Average power density (W/cm rod)	143.0
Connector length (cm)	4.45
Mass density UO_2 (g/cm^3)	10.44
Mass density zircaloy-2 (g/cm^3)	6.51
Mass density H_2O 284°C (g/cm^3)	0.7442
UO_2 linear expansion coefficient ($10^{-5}/°C$)	0.794
Zircaloy-2 linear expansion coefficient ($10^{-5}/°C$)	0.65

Table 9

DRESDEN 1 Core hydraulics data

System pressure (bar)	69
Total mass flow rate (kg/s)	$4.764 \cdot 10^3$
Inlet subcooling (°C)	21.8
Pressure drop across the core (bar)	0.53
Coolant channel flow area (cm^2)	61.50
Coolant channel hydraulic diam. (m)	0.1444
Moderator channel flow area (m^2)	1.691
Moderator channel hydraulic diam. (m)	0.02199
Shroud perimeter (m)	0.4420
Fuel pin perimeter per channel (m)	1.6174
Channel height (m)	2.7535

Table 10

DRESDEN 1 unit cell description

Region type		Hot full power
		Outer region radius (cm)
Fuel (UO_2)		0.6300
Clad (zircaloy-2)		0.7252
Moderator (H_2O)		1.0193
		Temperature (^oC)
Fuel		541
Clad		294
Moderator		284
		Number density (10^{24} atoms/cm^3)
Fuel	^{235}U	0.000350
	^{238}U	0.02268
	O	0.04604
Clad	Zr	0.0347
	Fe	0.000074
Moderator	H, O — 0 per cent void	H: 0.04980; O: 0.02490
	H, O — 25 per cent void	H: 0.03736; O: 0.01868
	H, O — 50 per cent void	H: 0.02490; O: 0.01245

Table 11

Macroscopic thermal cross section and power peaking factor vs. burn-up

	Days	Control regions*						Power-peaking factor
		1	2	3	4	5	6	
0	0	50.92	25.46	49.15	29.13	-0.26	15.55	1.681944
165.2	10	40.24	13.97	28.04	8.45	14.56	-10.40	1.693697
660.7	40	41.66	15.19	28.26	7.89	14.26	- 8.86	1.69807
1156.2	70	40.74	14.70	26.09	6.25	13.01	-12.47	1.6799
1651.7	100	38.00	12.87	22.35	3.67	10.60	-13.70	1.672813
2147.2	130	34.91	10.52	18.32	0.89	7.598	-13.81	1.65992
2642.7	160	30.80	7.75	14.47	-1.47	4.686	-14.70	1.65406
3138.2	190	27.55	5.80	11.32	-3.07	2.418	-14.91	1.65081

*Macroscopic thermal absorption cross section in $cm^{-1} \cdot 10^{-4}$

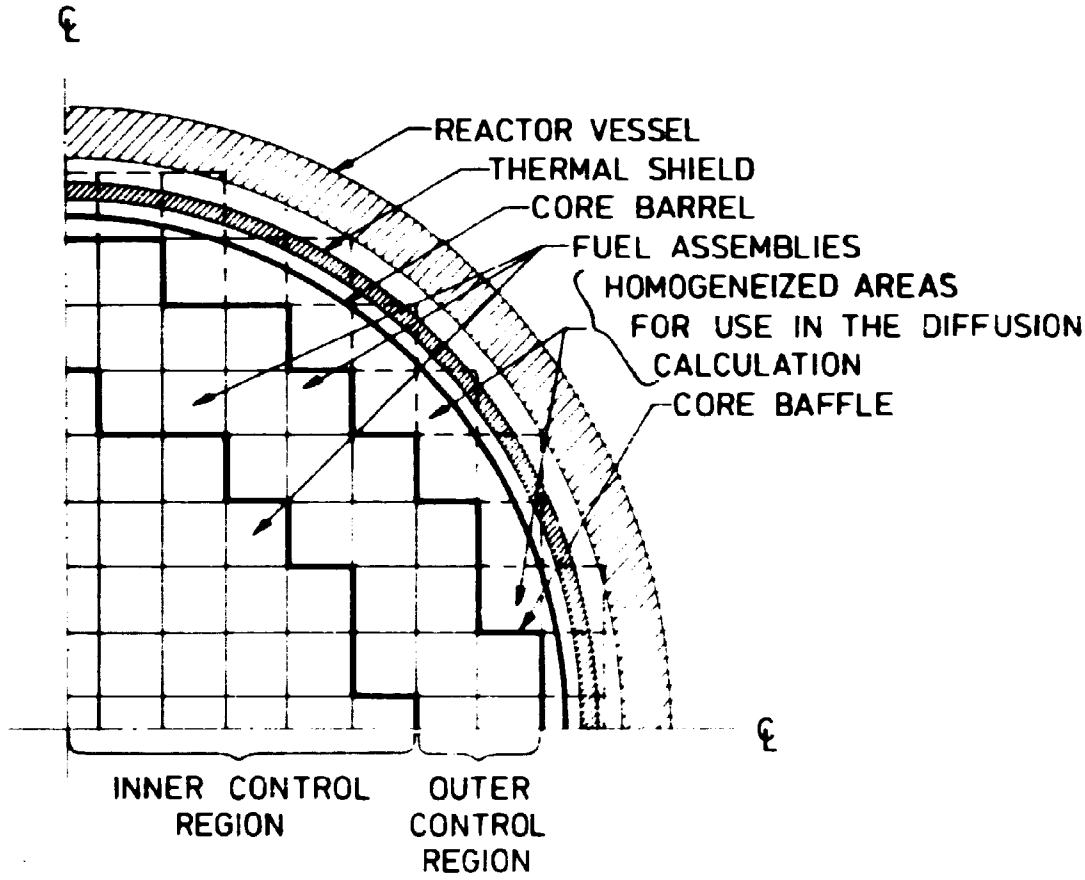

Fig. 1. Horizontal cross section of Haddam Neck showing the control regions used in the calculations with SELMA2 and DBU.

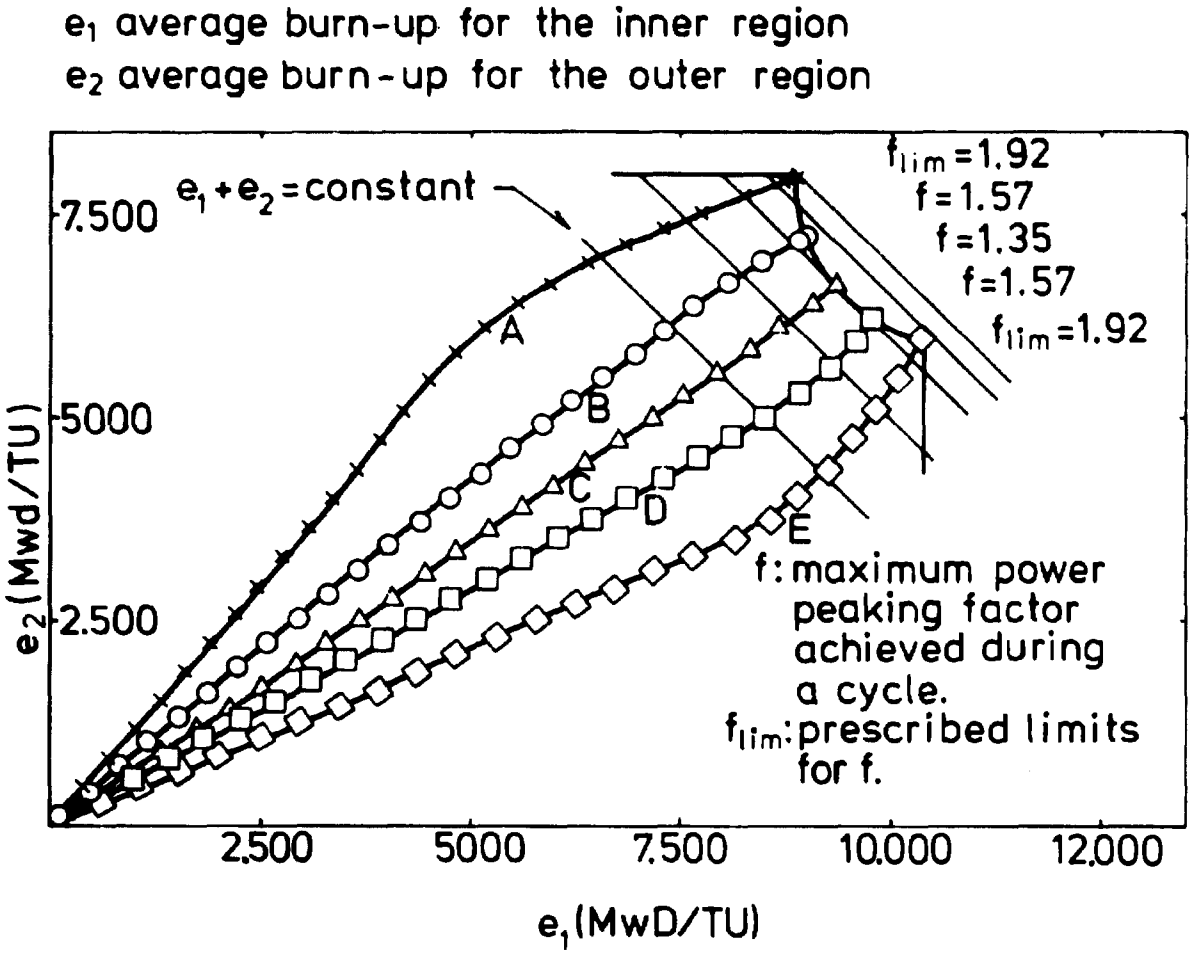

Fig. 2. Terminal state for discharge burn-up maximization.
Same fuel enrichment 3.00% in the two control regions.

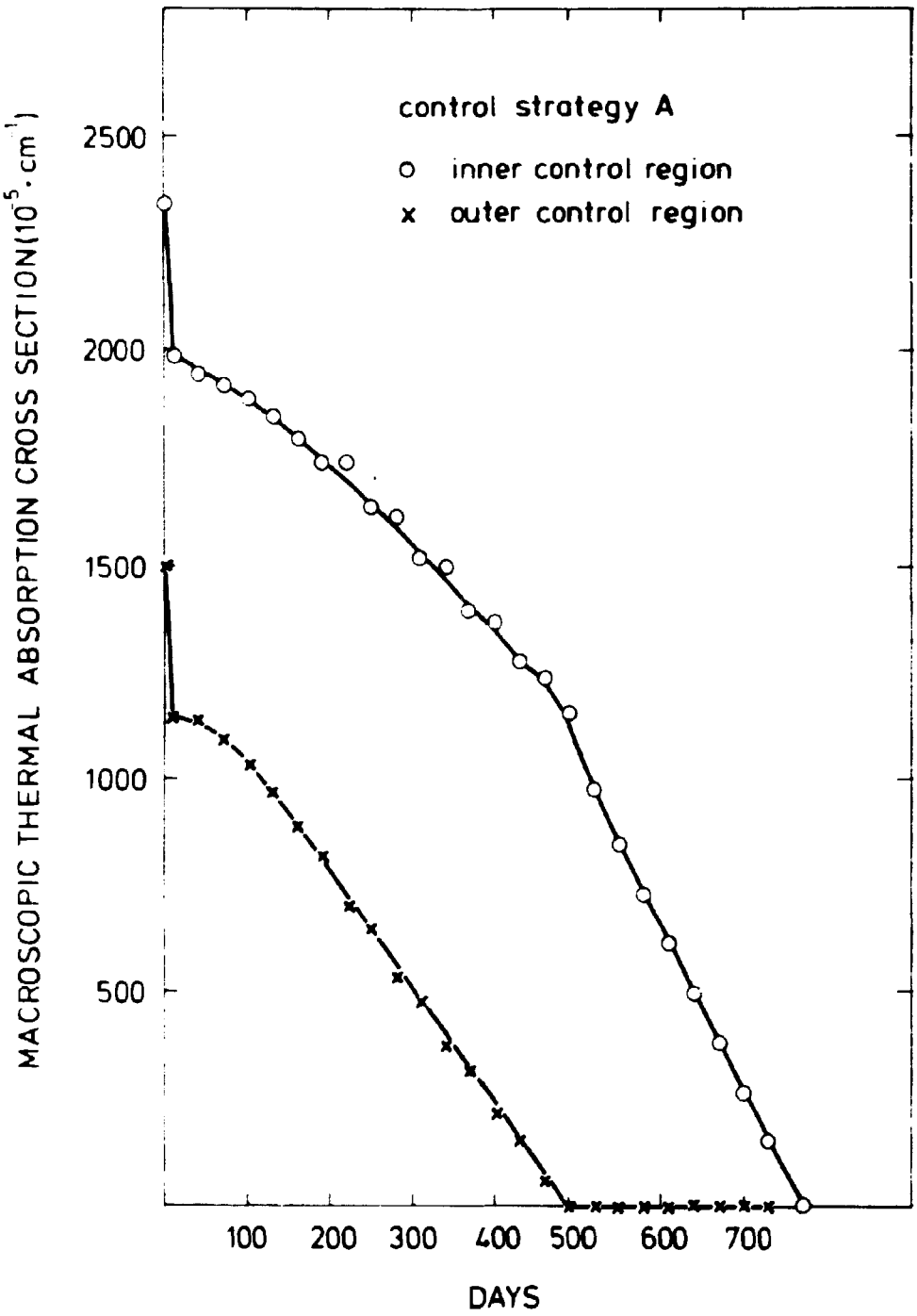

Fig. 3a. Macroscopic thermal absorber cross section vs. burn-up calculated with SELMA2.

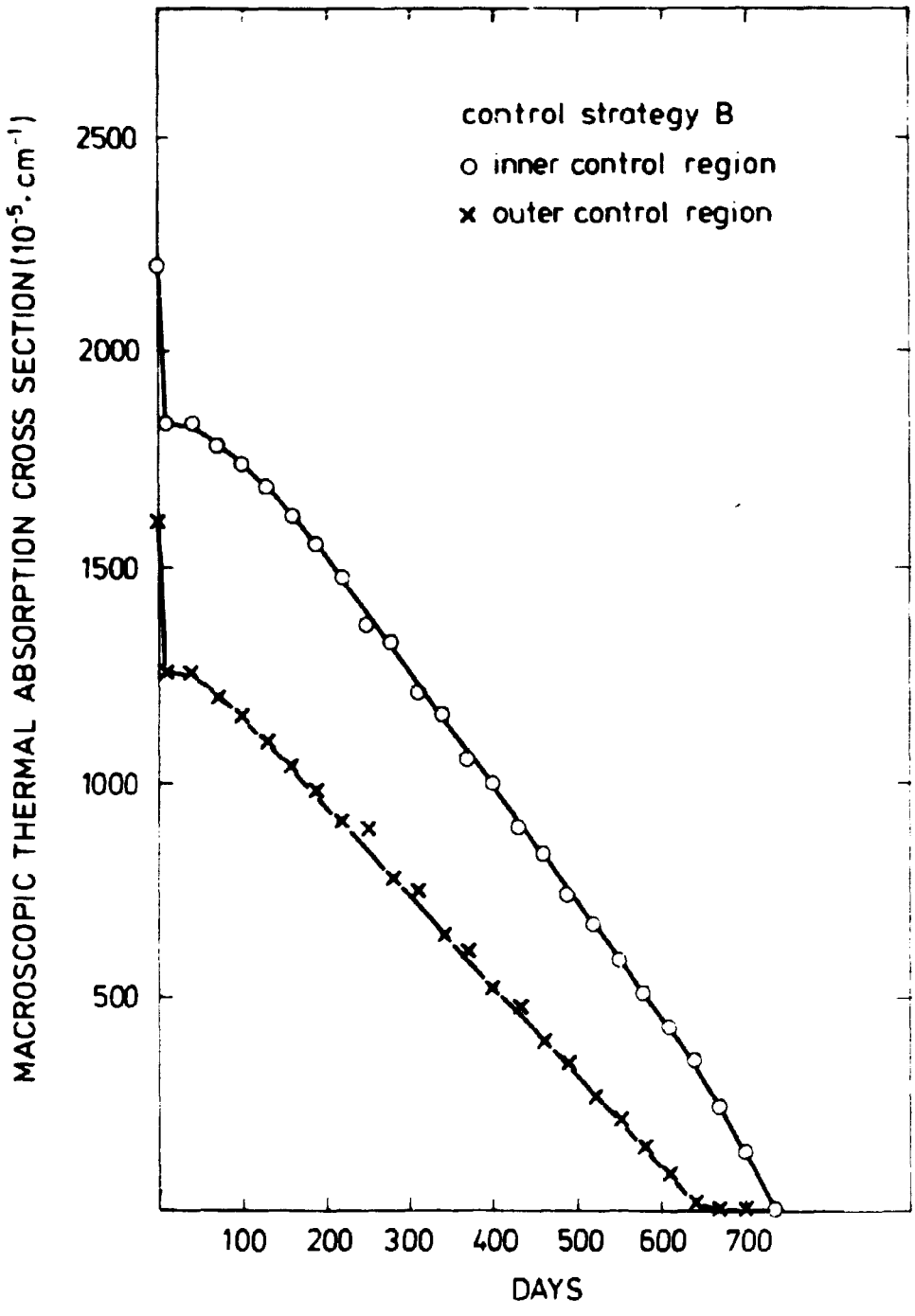

Fig. 3b. Macroscopic thermal absorption cross section vs. burn-up calculated with SELMA2.

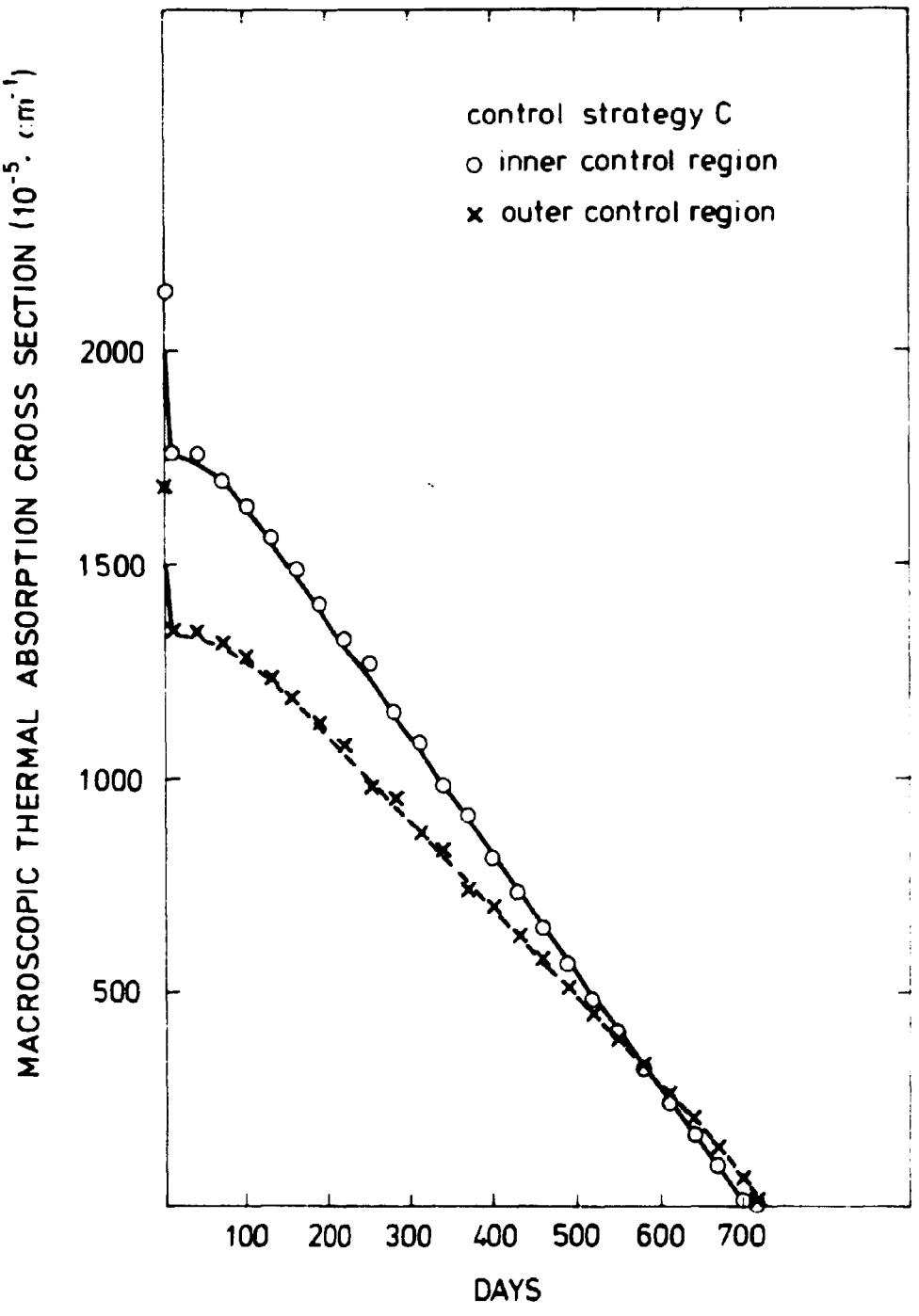

Fig. 3c. Macroscopic thermal absorption cross section vs. burn-up calculated with SELMA2.

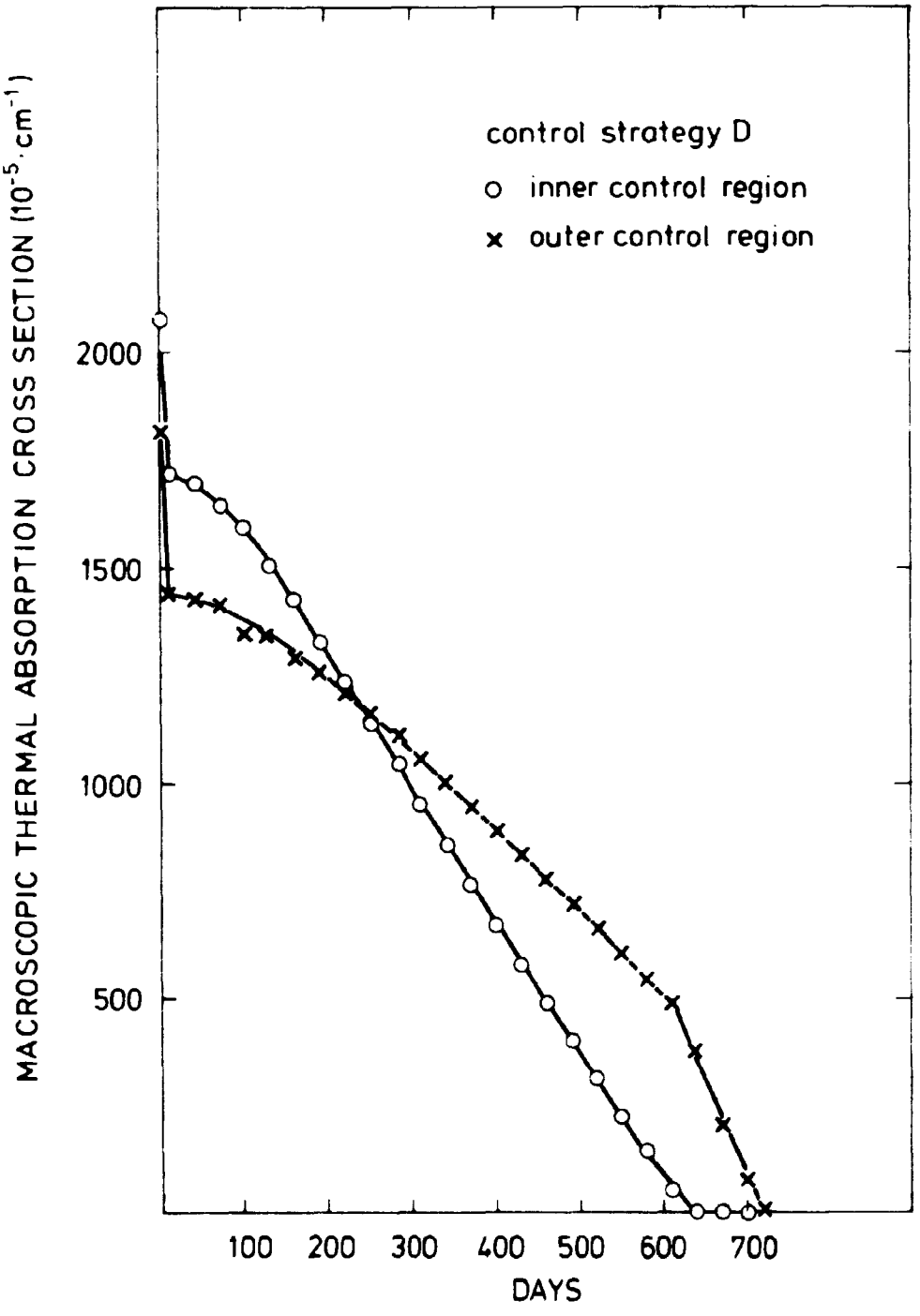

Fig. 3d. Macroscopic thermal absorption cross section vs. burn-up calculated with SELMA2.

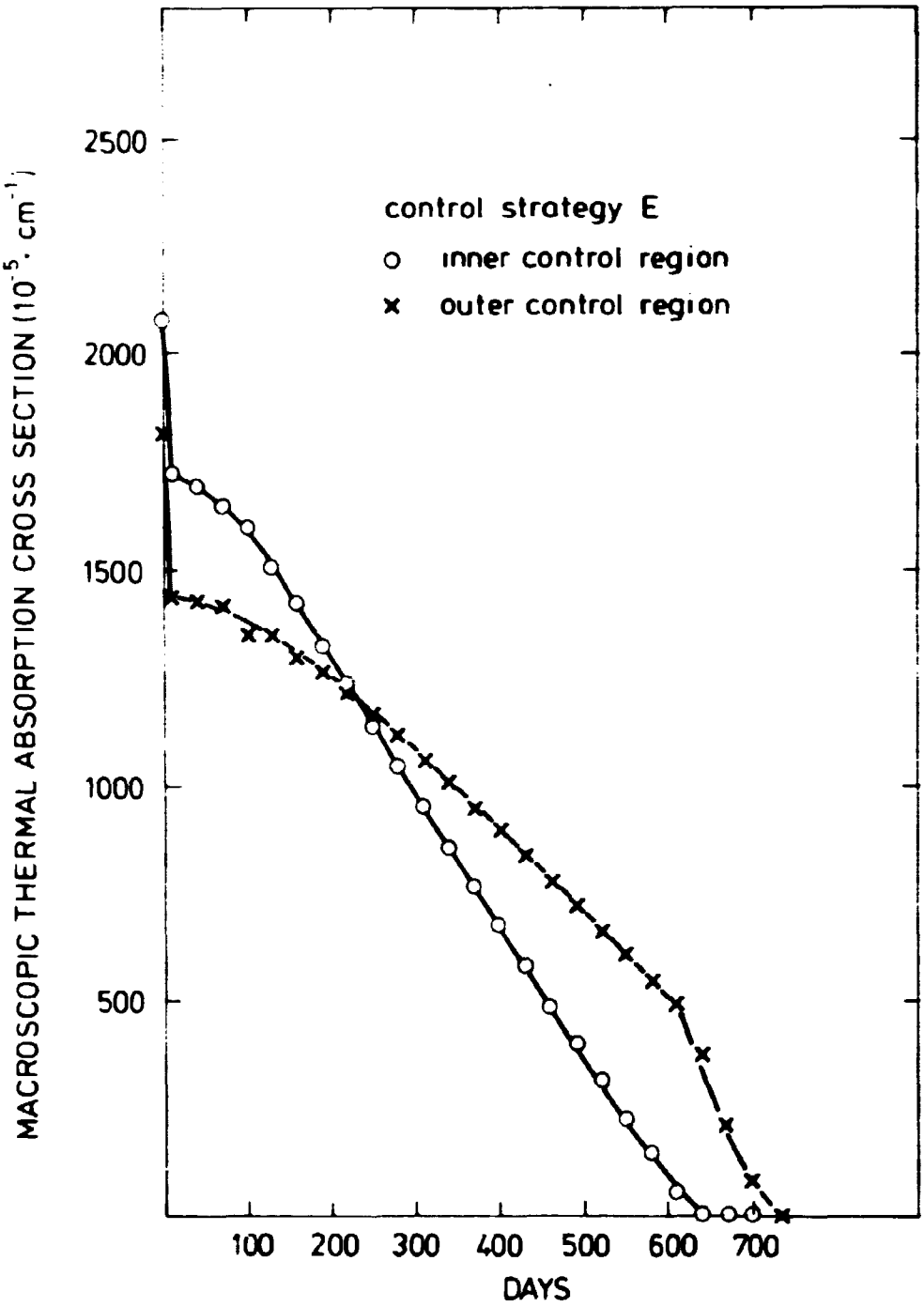

Fig. 3e. Macroscopic thermal absorption cross section vs. burn-up calculated with SELMA2.

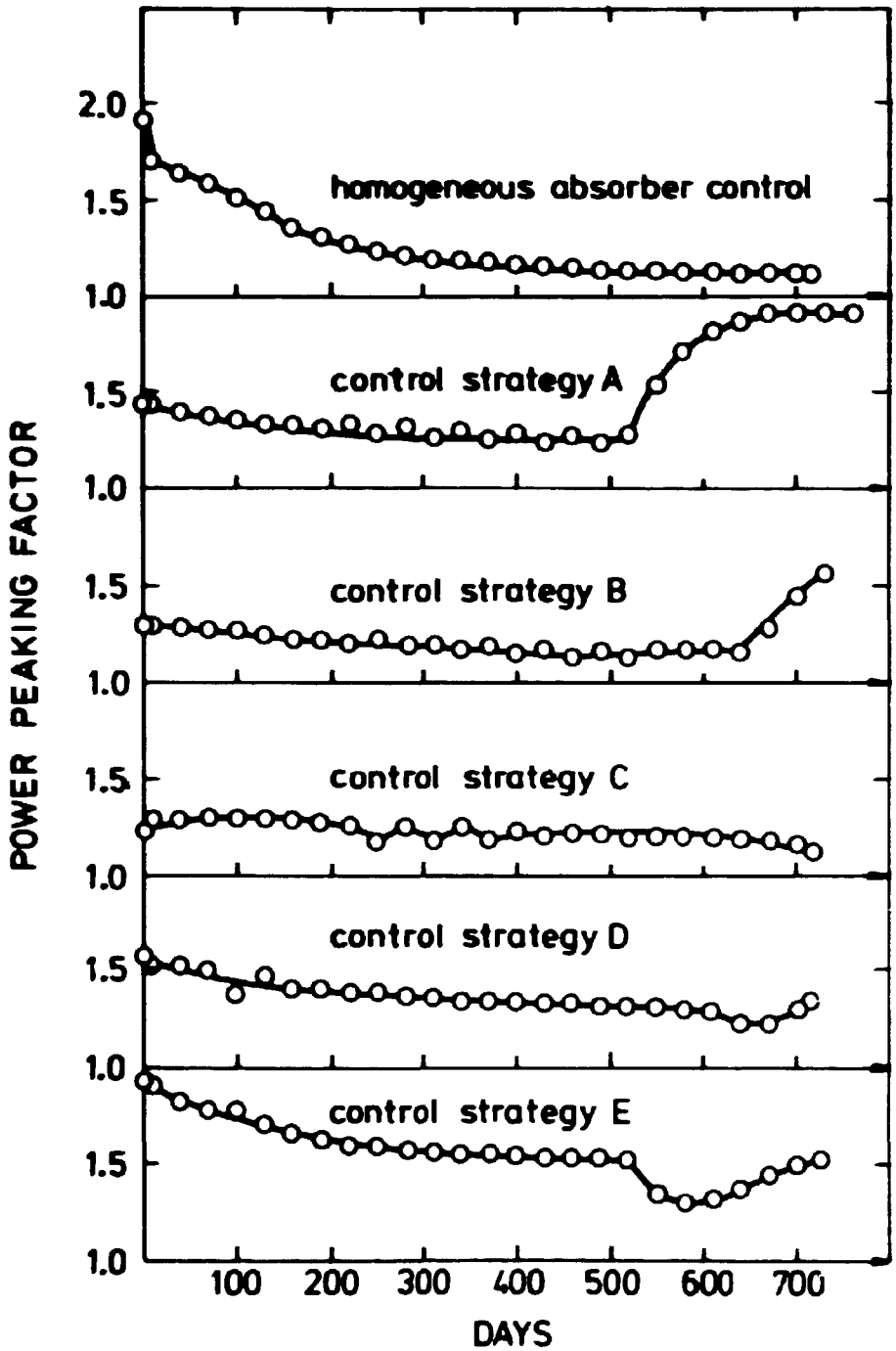

Fig. 4. Power peaking factor vs. burn-up for different control strategies calculated with SELMA2.

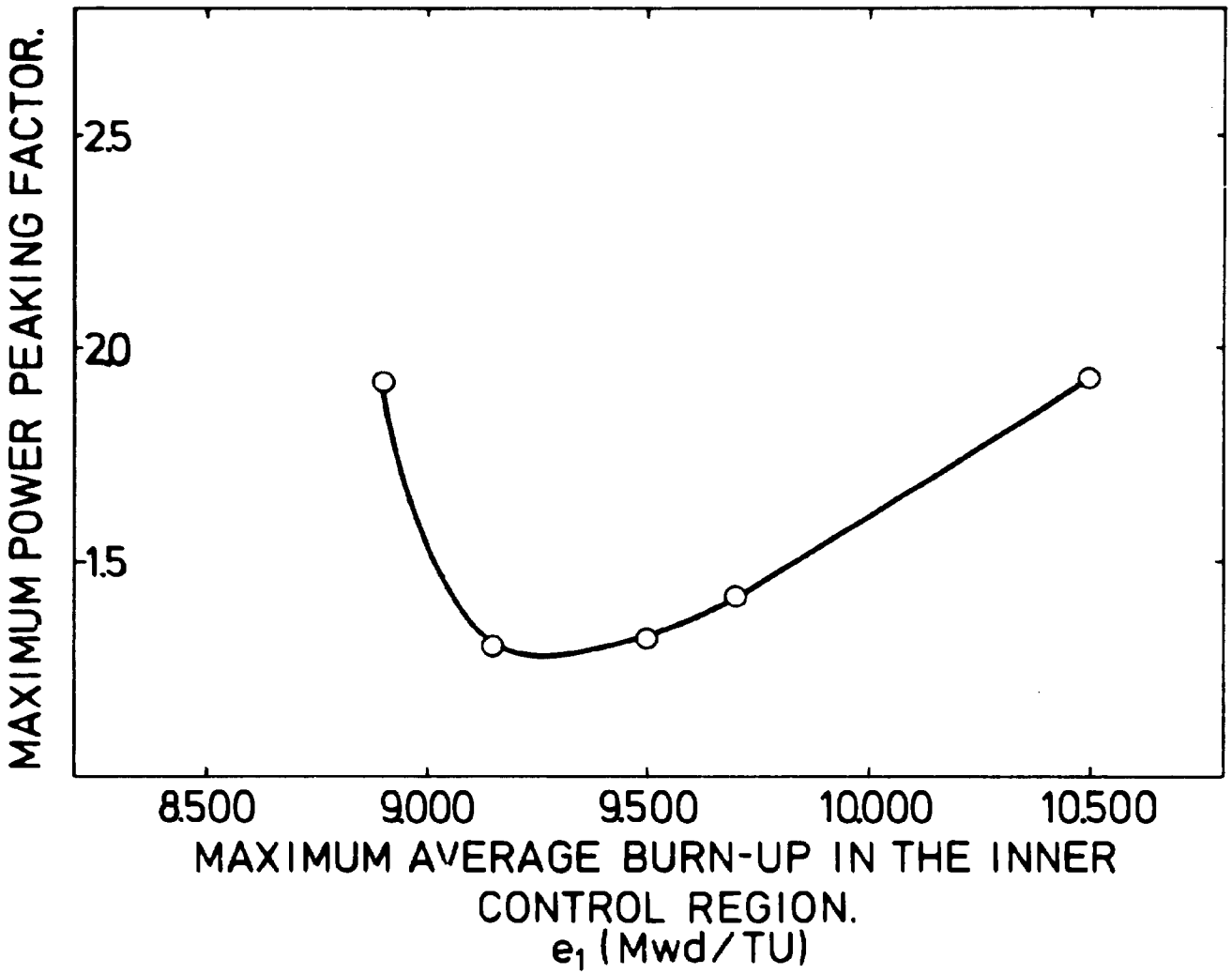

Fig. 5. Maximum power peaking factor vs. maximum average burn-up in the inner control region.

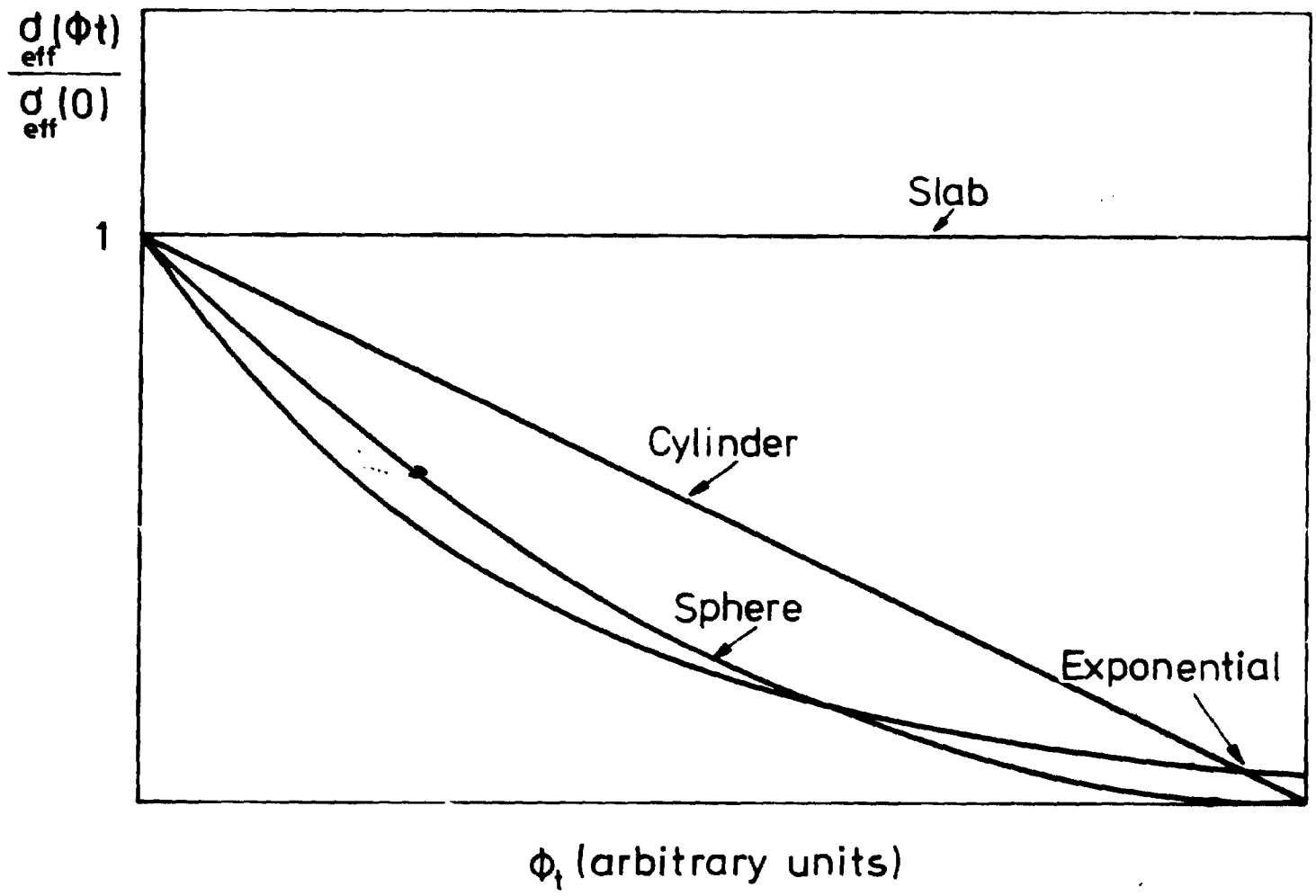

Fig. 6. Effective absorption cross section vs. burn-up.

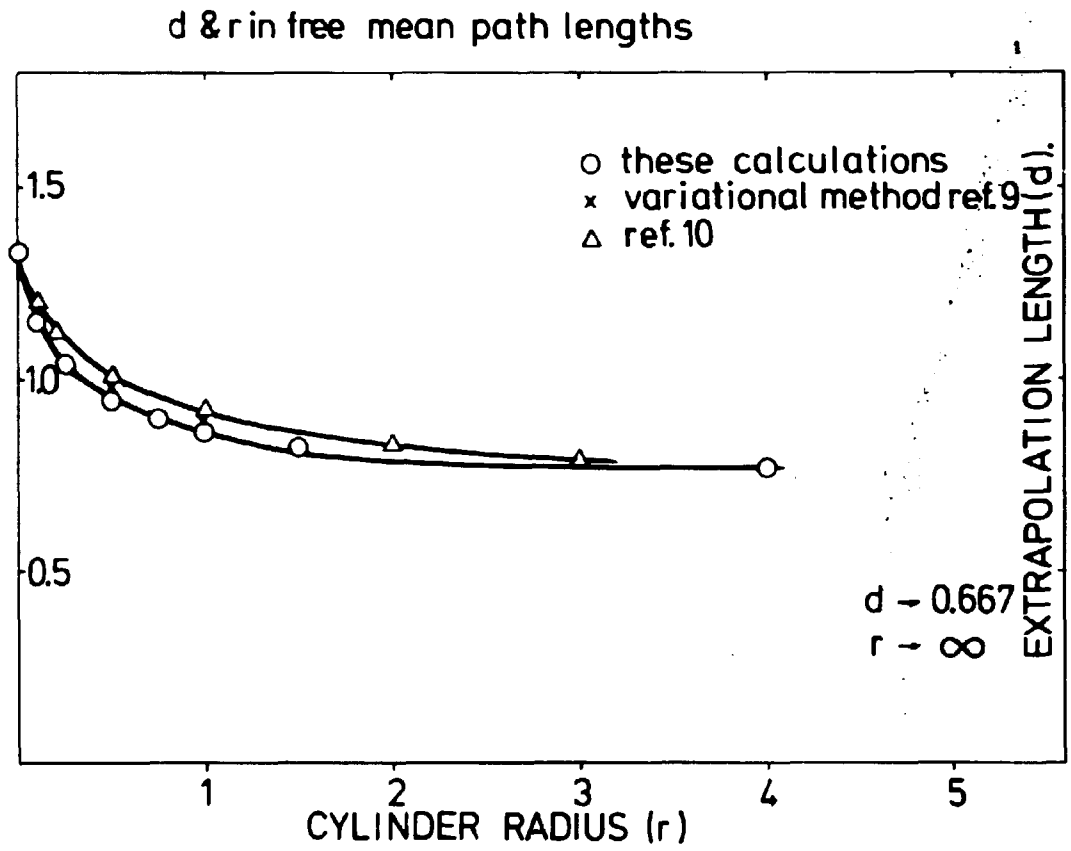

Fig. 7. Extrapolation length for a purely absorbing black cylinder.

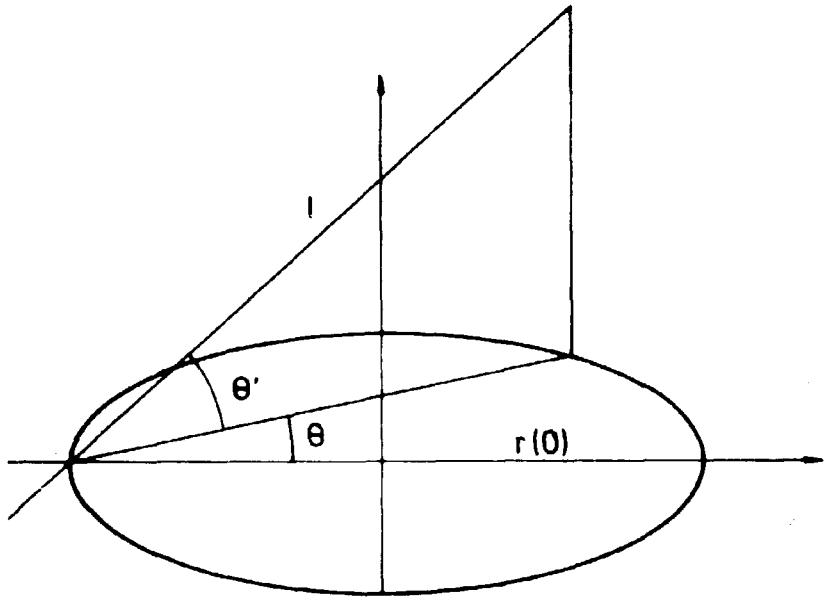

Fig. 8. The neutron path length l in a purely absorbing cylinder of radius r(0).

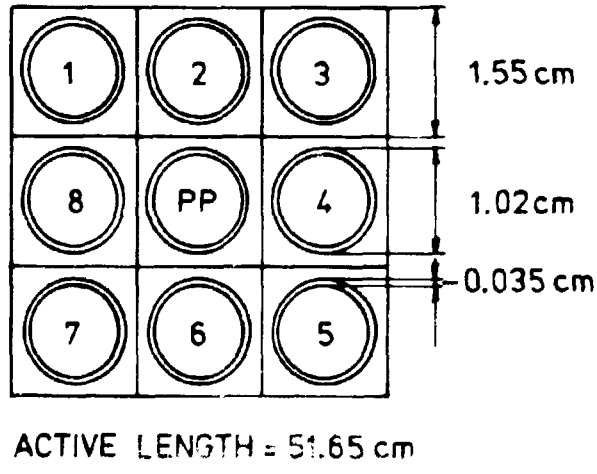

Fig. 9. Experimental facility for burn-up experiments. 1-8 are full pins and PP is a poison pin.

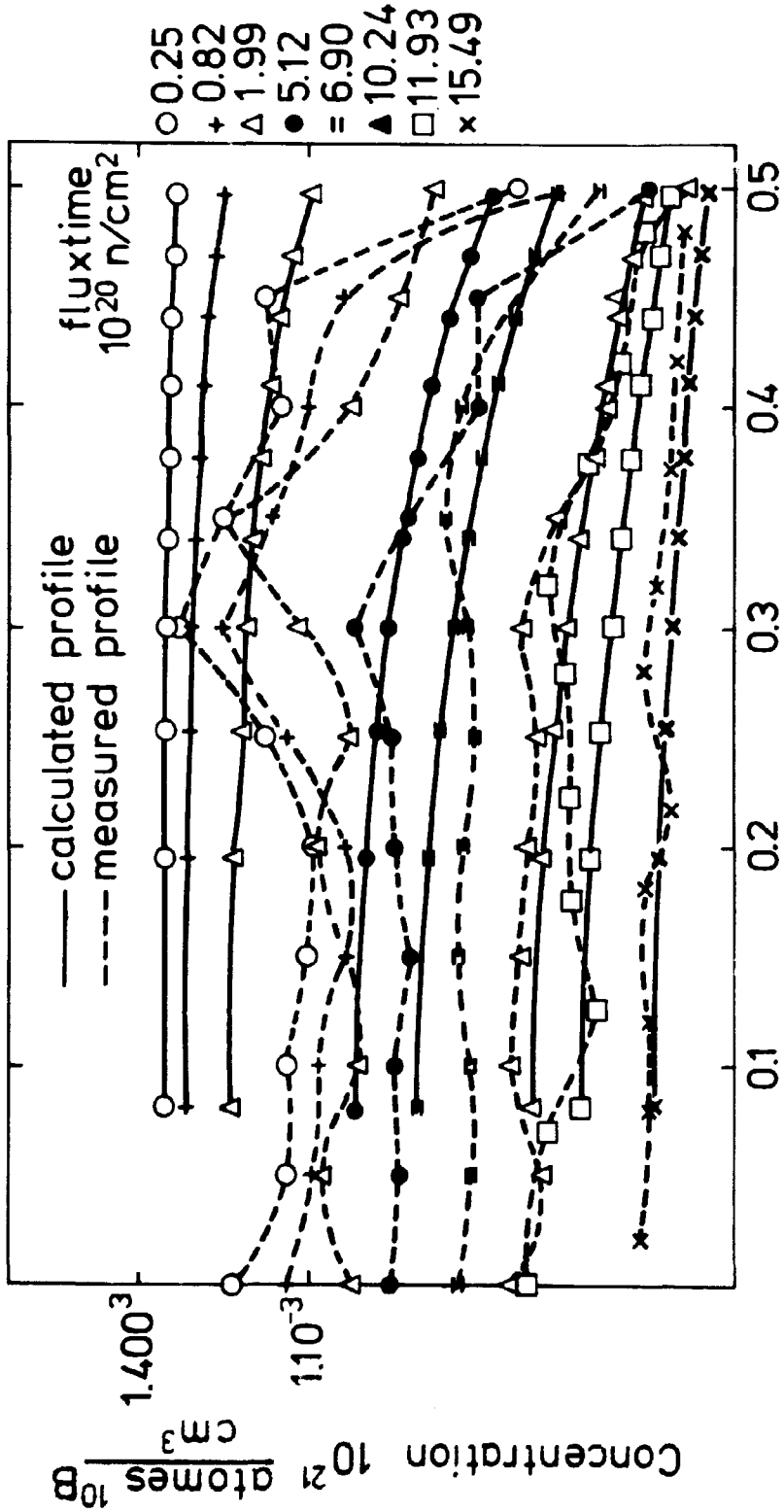

Fig. 10. Radial concentration profiles for boron.

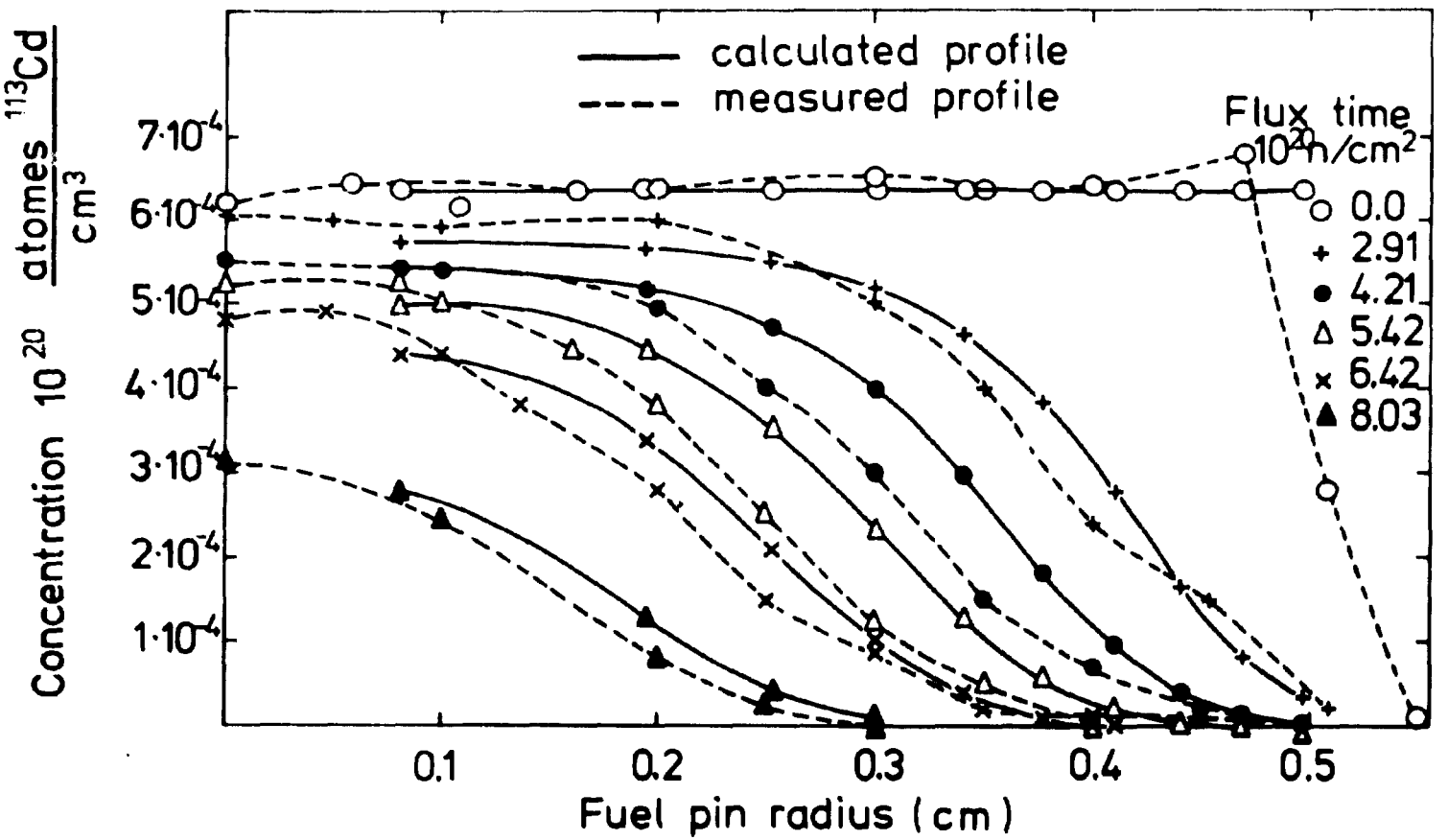

Fig. 11. Radial concentration profiles for cadmium.

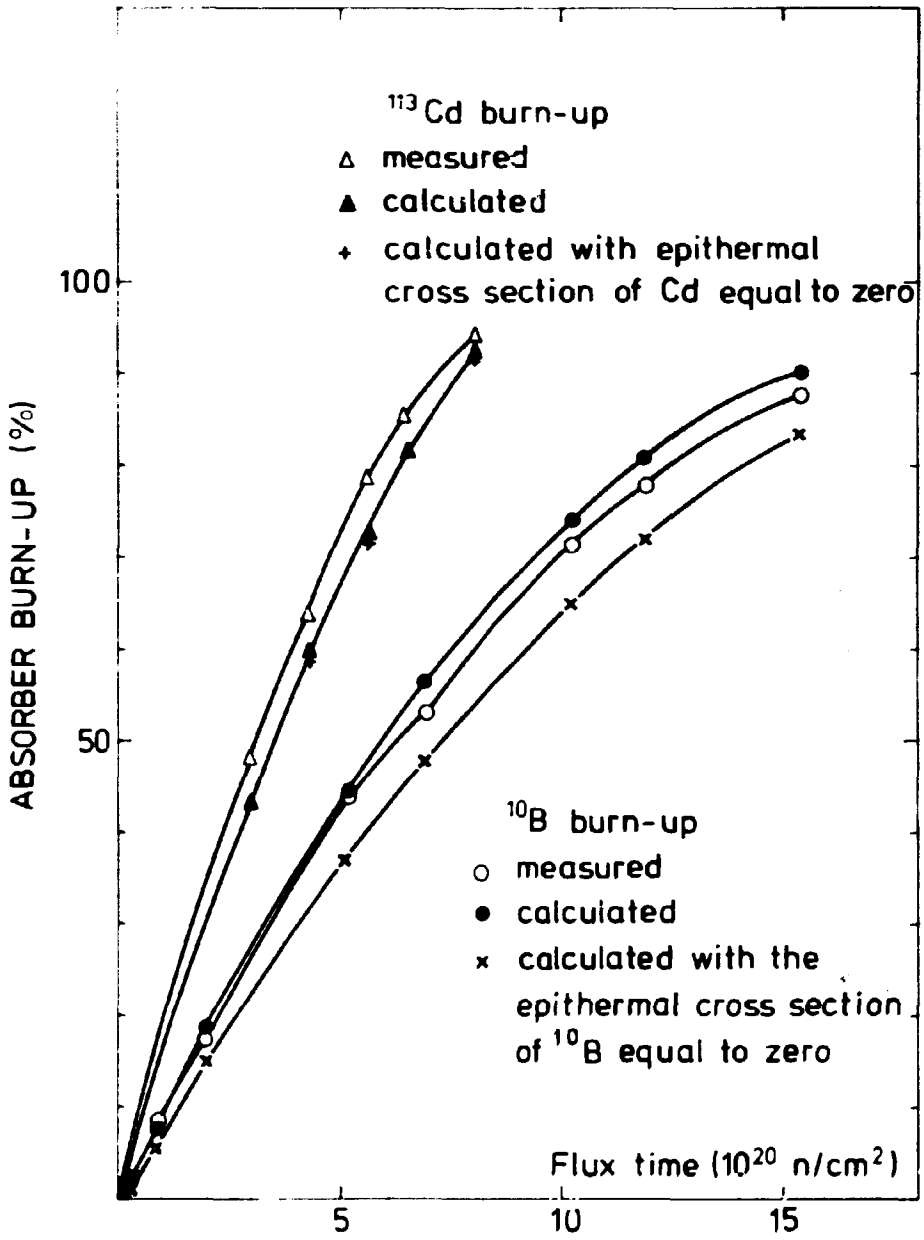

Fig. 12. Absorber burn-up vas. fluxtime.

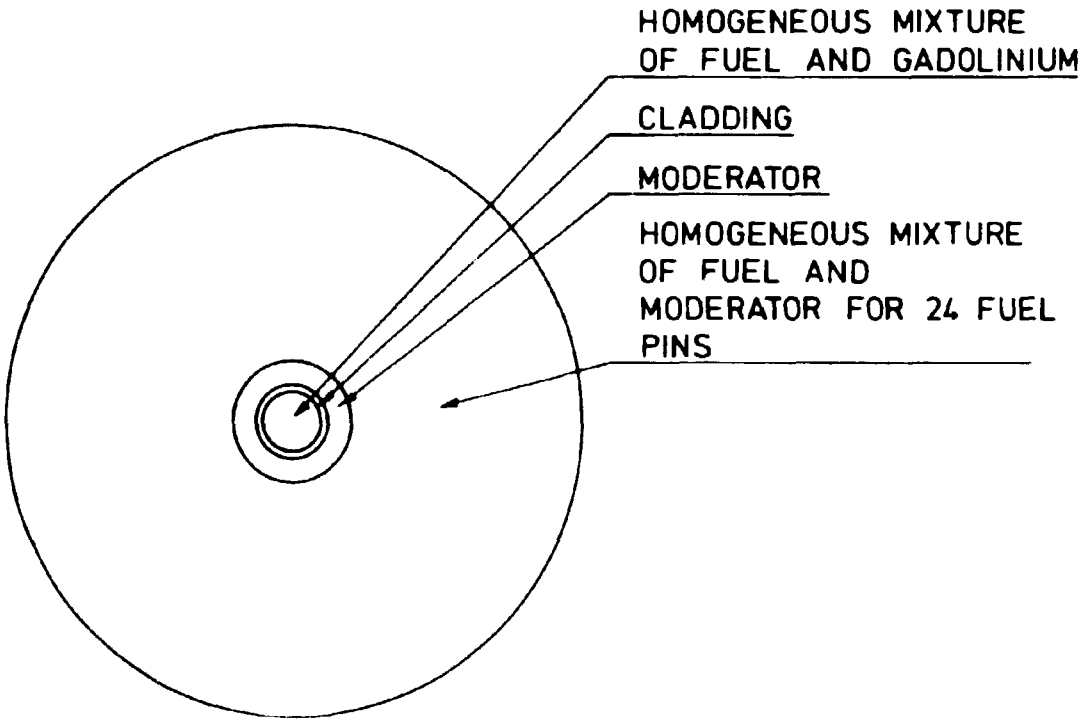

Fig. 13. One-dimensional model of the fuel assembly used in the gadolinium burn-up calculations.

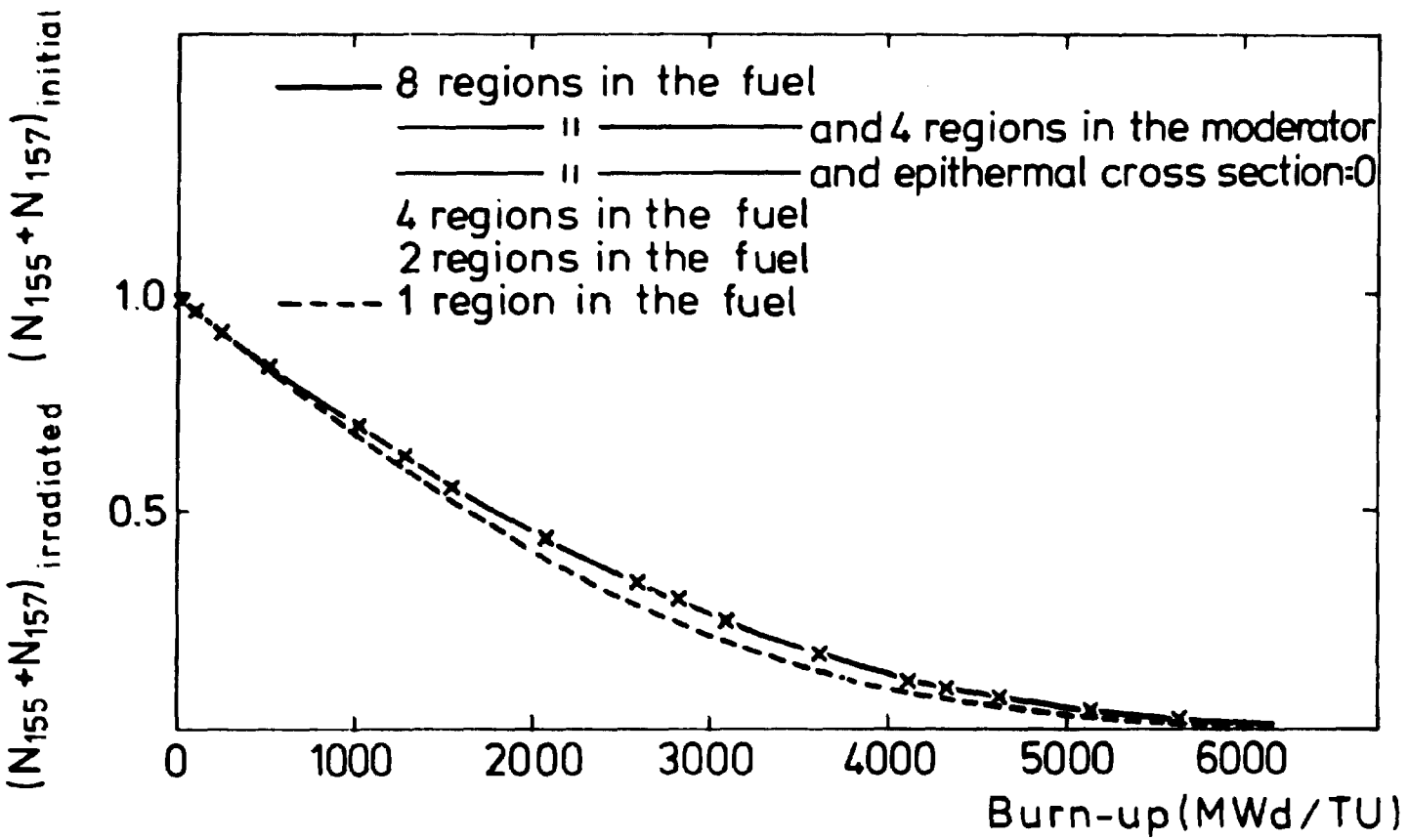

Fig. 14a. Gadolinium burn-up.

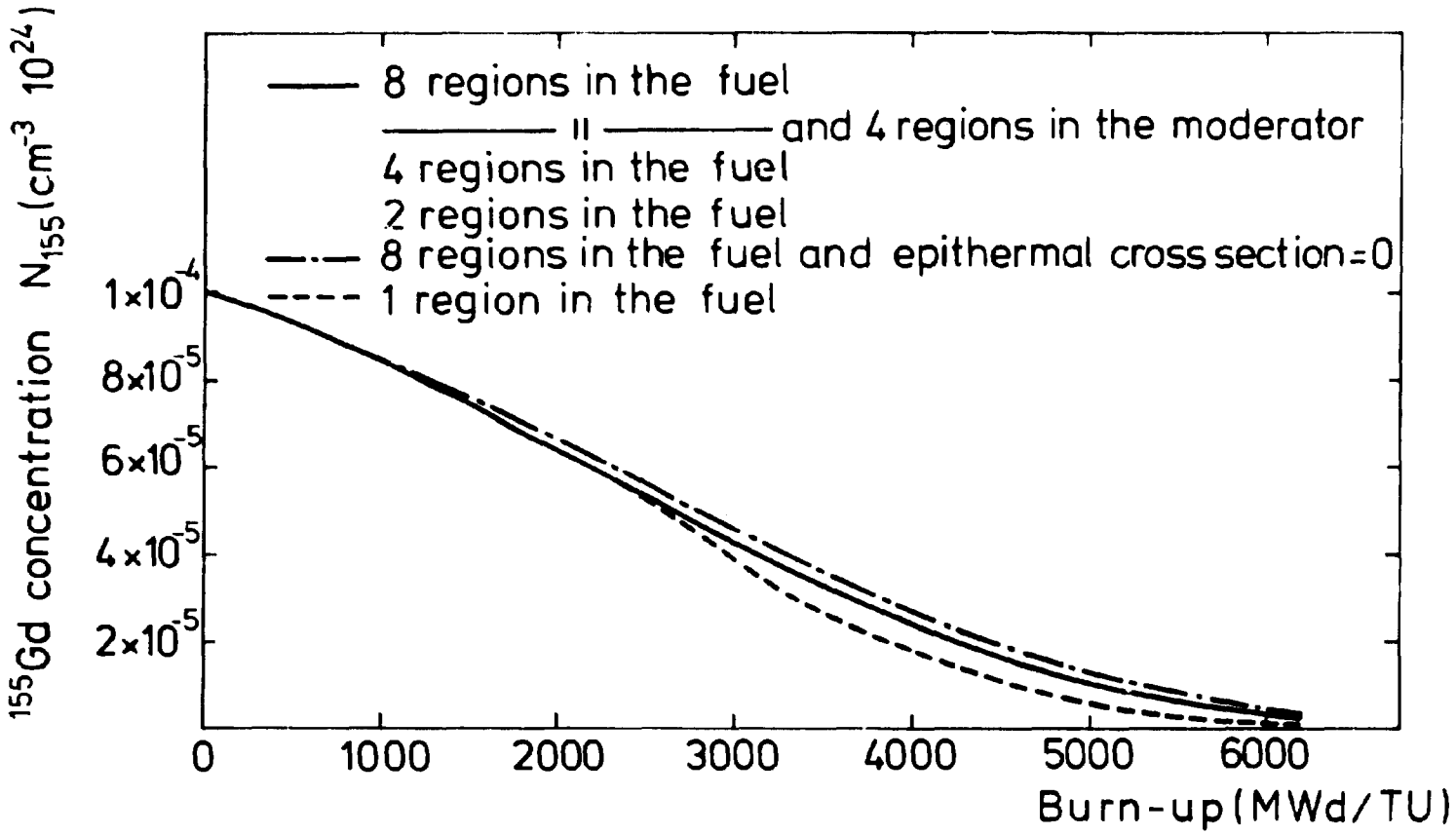

Fig. 14b. ^{155}Gd concentration vs. burn-up.

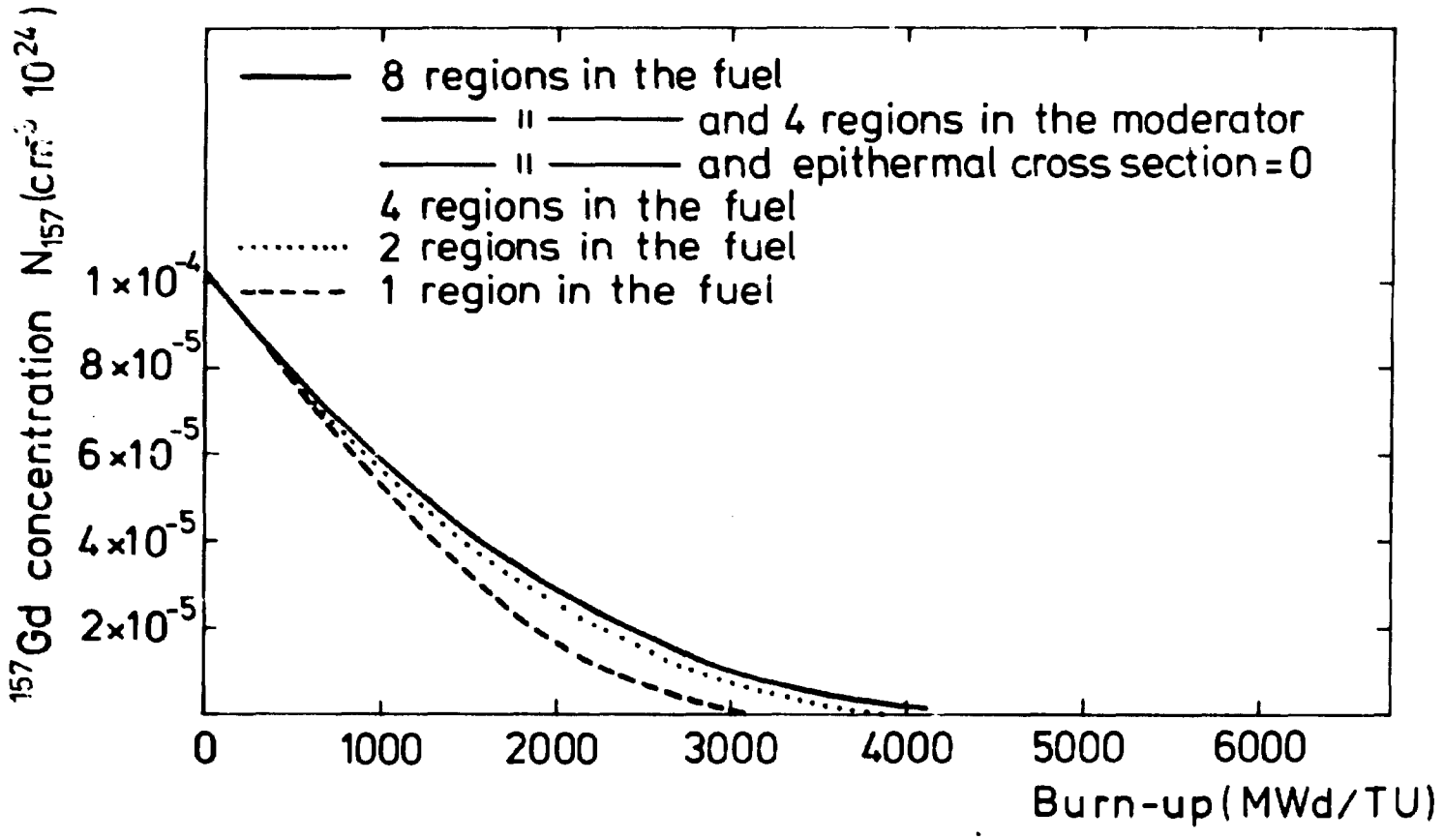

Fig. 14c. ^{157}Gd concentration vs. burn-up.

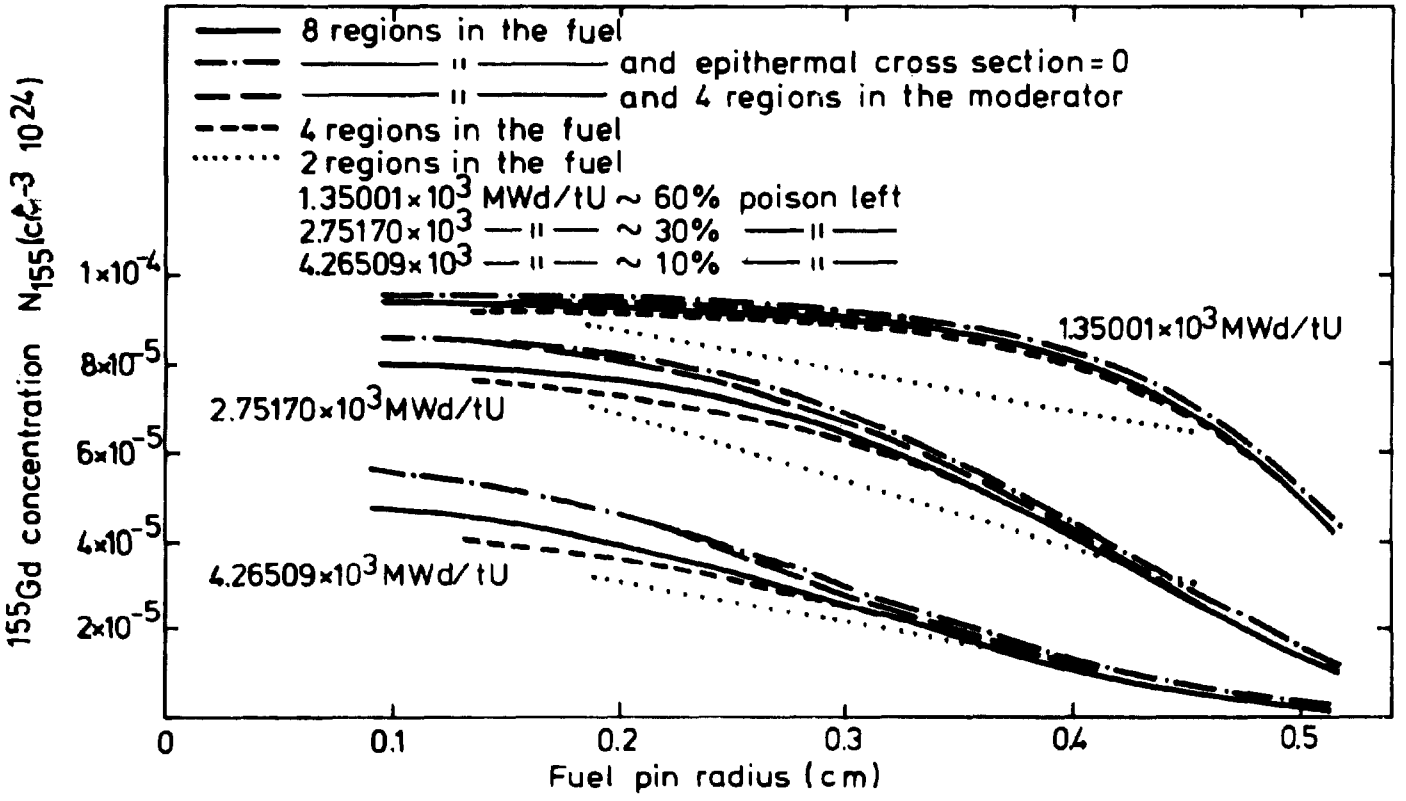

Fig. 14d. Radial concentration profiles for ^{155}Gd.

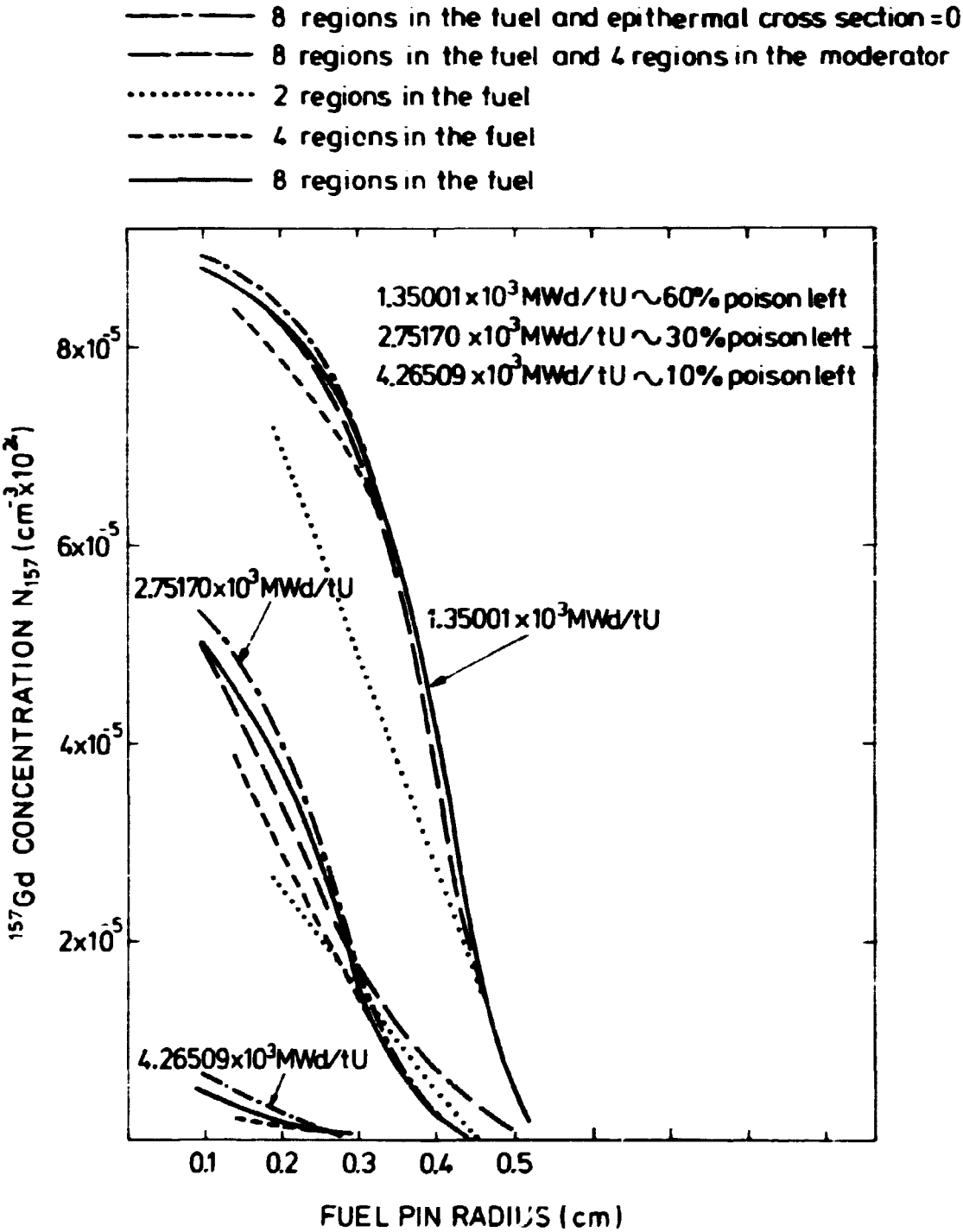

Fig. 14e. Radial concentration for ^{157}Gd.

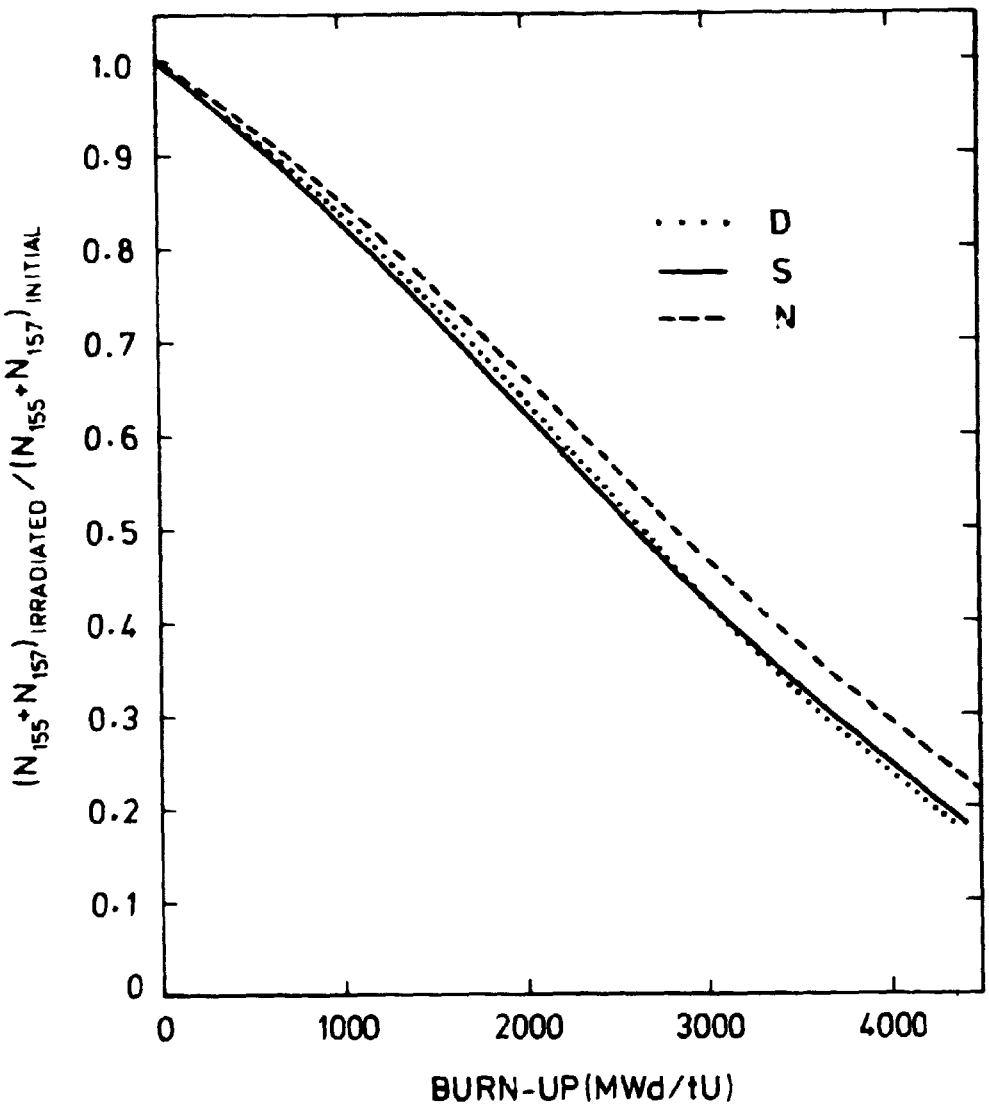

Fig. 15a. Gadolinium burn-up, D Danish calculations, N Norwegian calculations, S Swedish calculations.

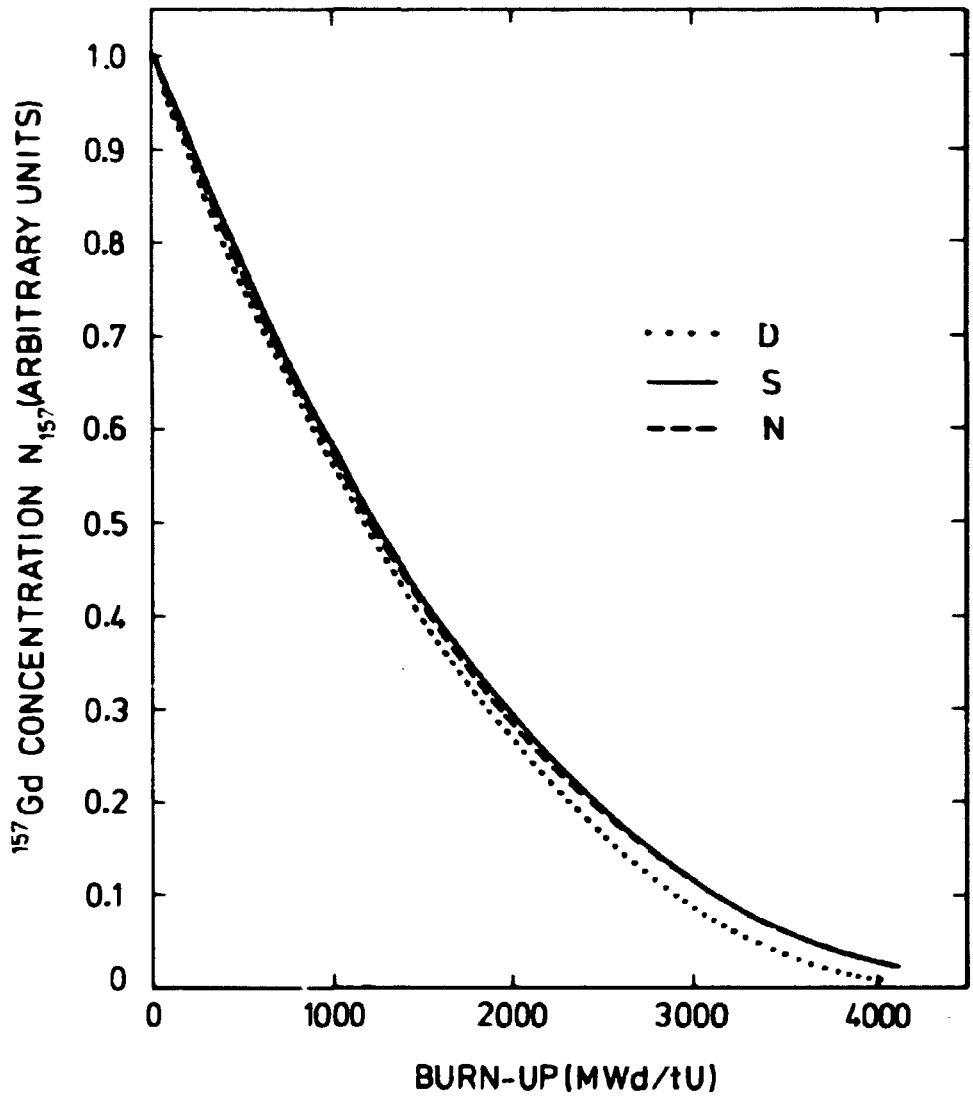

Fig. 15b. ^{157}Gd concentration vs. burn-up, D Danish calculations, N Norwegian calculations, S Swedish calculations.

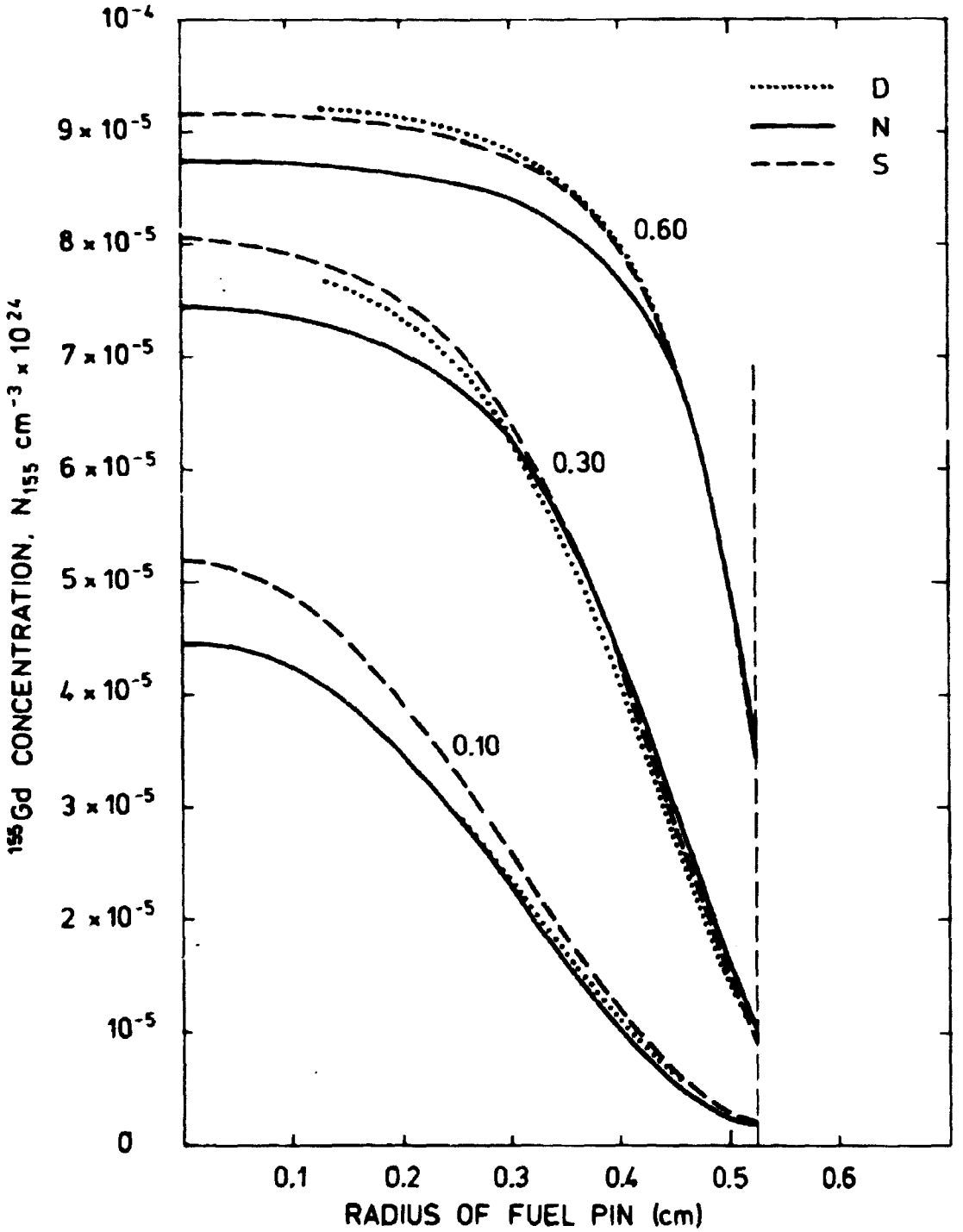

Fig. 15c. Radial concentration profiles for ^{155}Gd, D Danish calculations, N Norwegian calculations, S Swedish calculations.

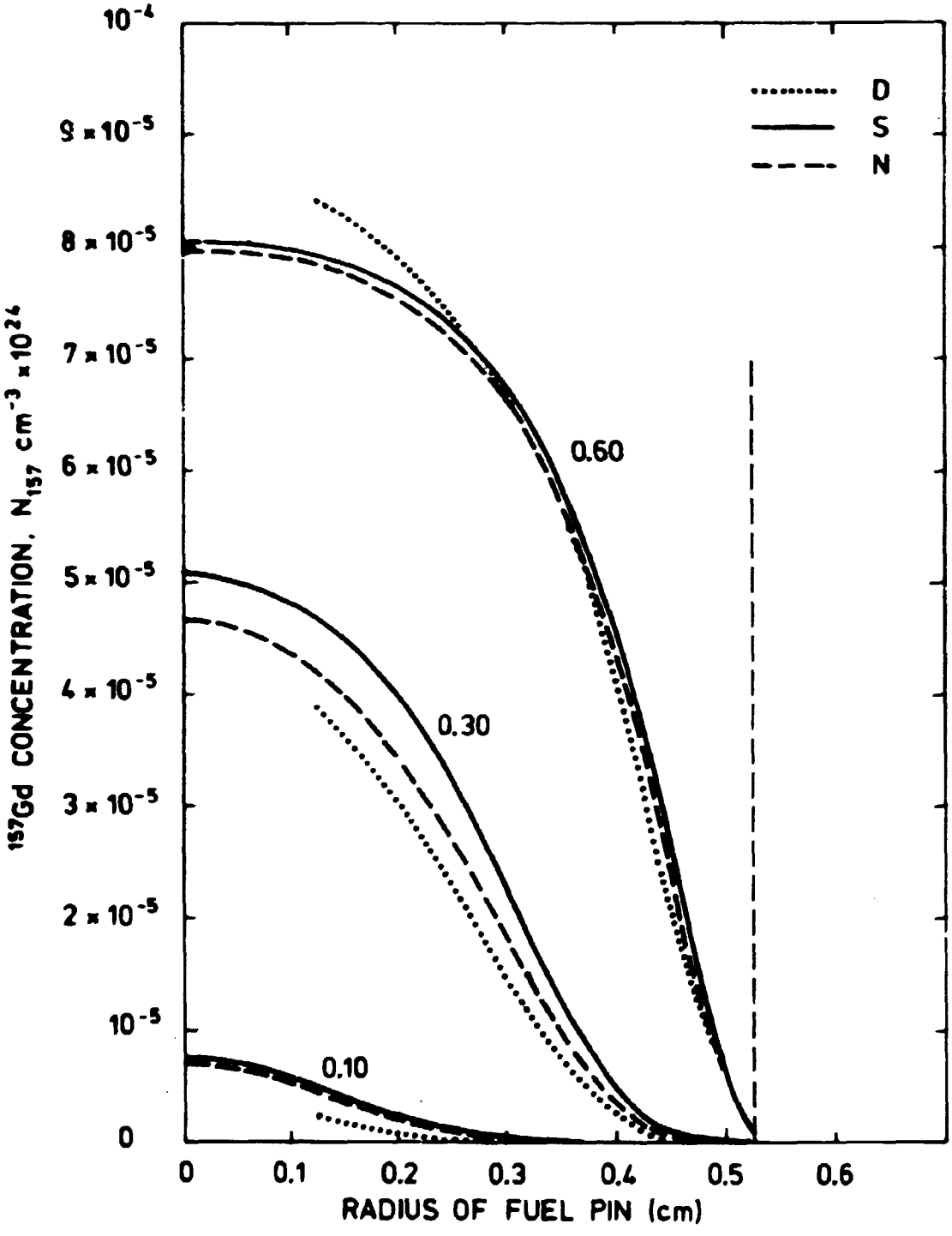

Fig. 15d. Radial concentration profiles for ^{157}Gd,
D Danish calculations, N Norwegian calculations,
S Swedish calculations.

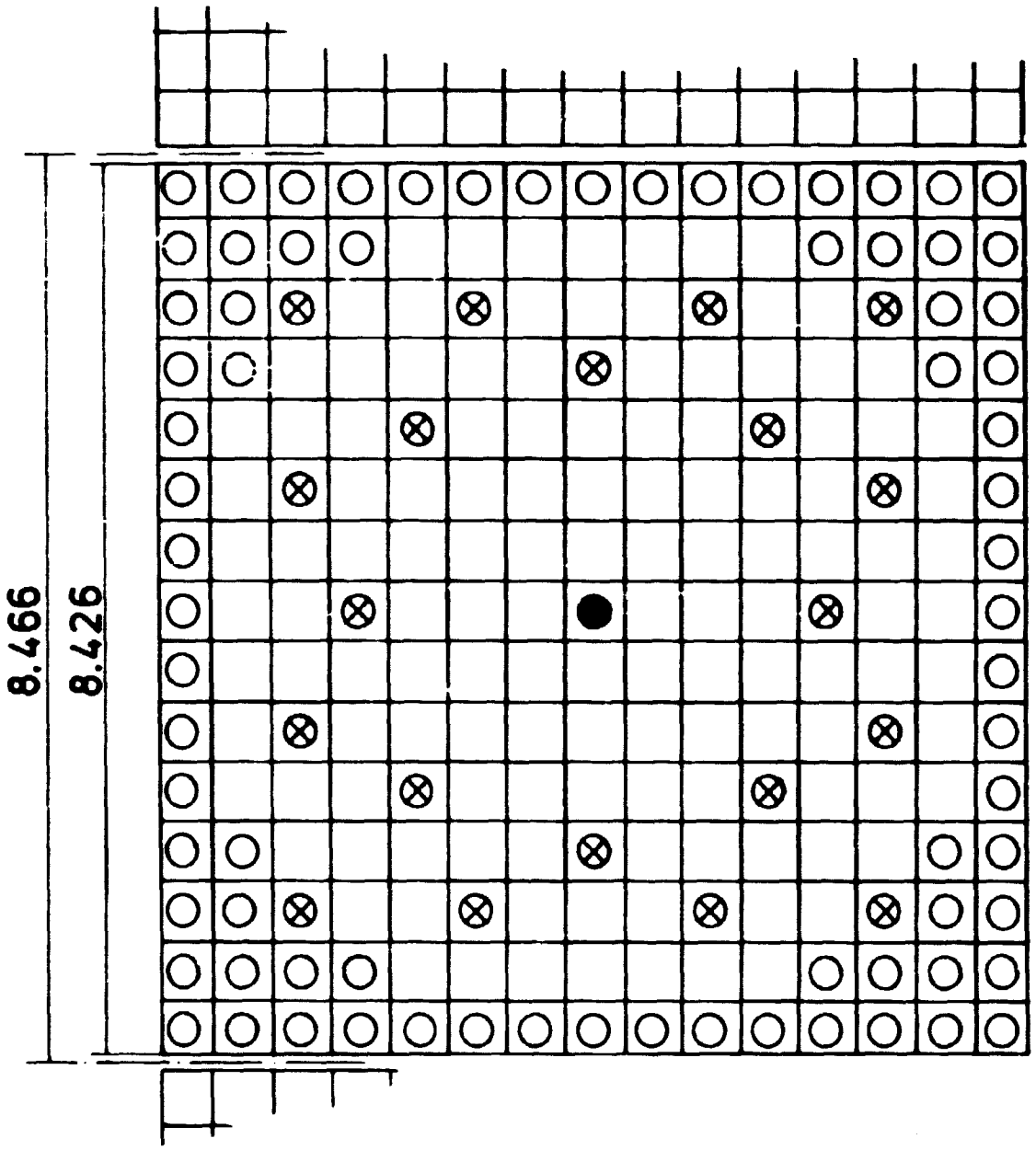

Fig. 16. Haddam Neck assembly showing possible poison pin positions.

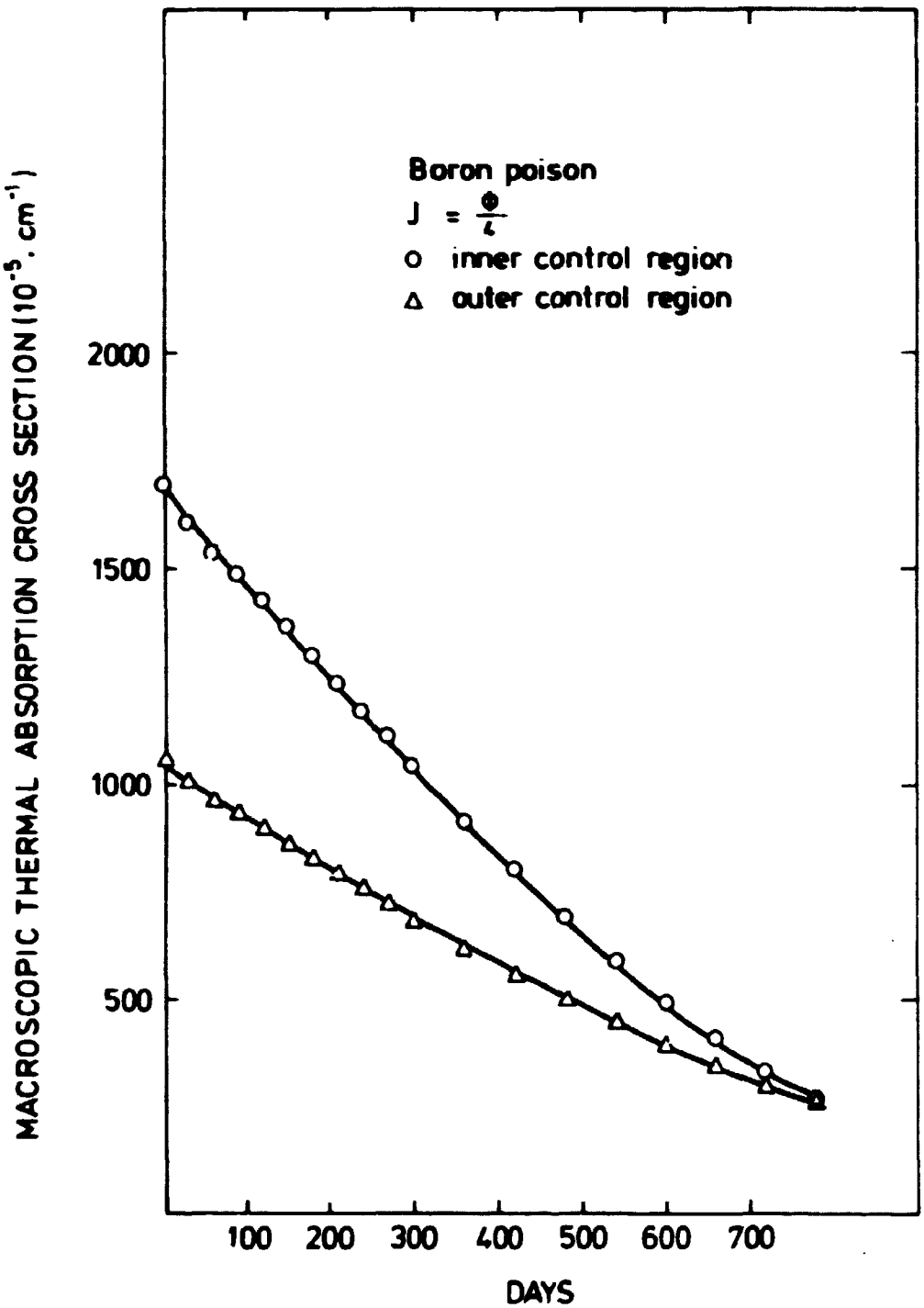

Fig. 17a. Boron burn-up calculated with CDB.

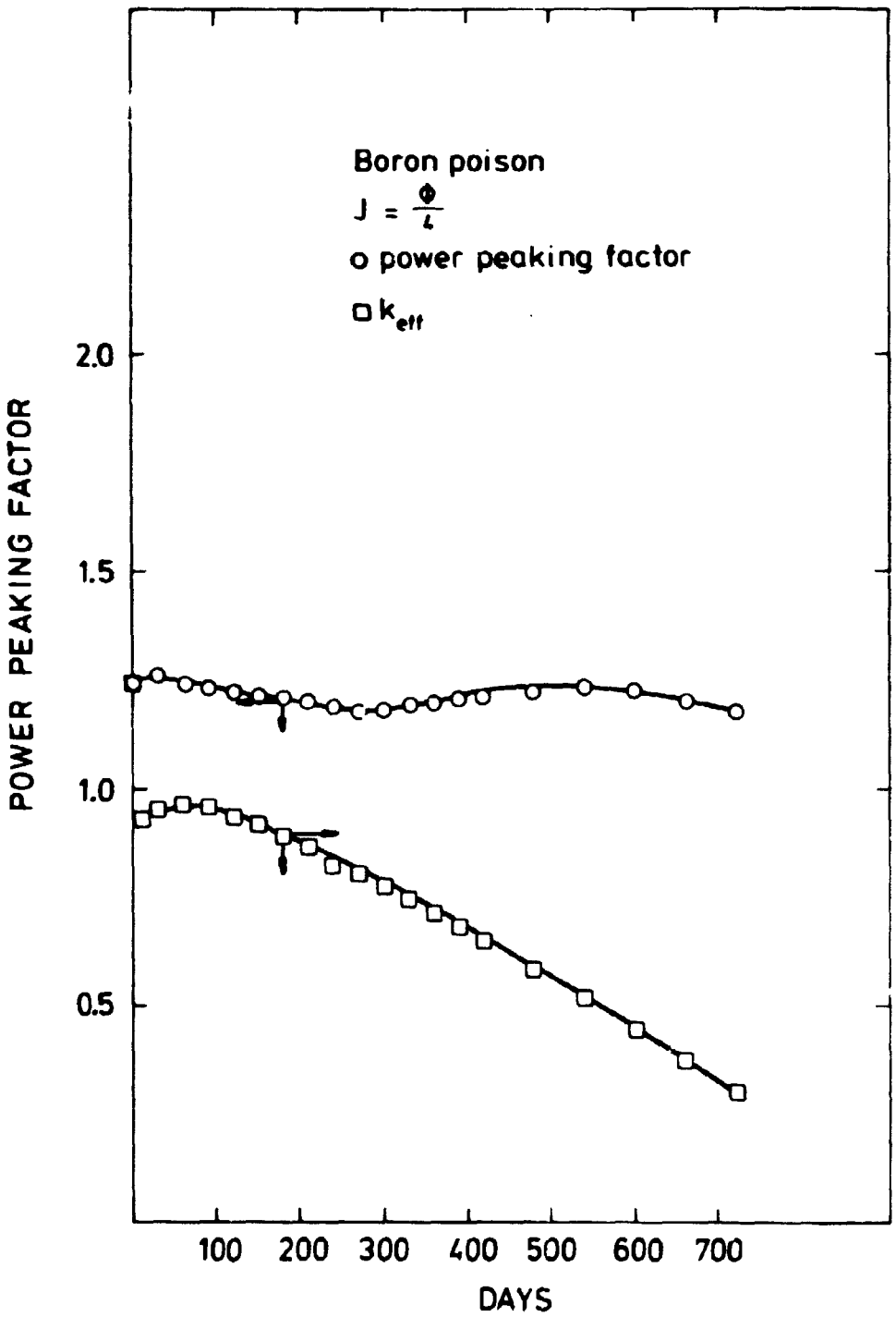

Fig. 17b. Power peaking factor and k_{eff} vs. burn-up using boron as burnable poison calculated with DBU.

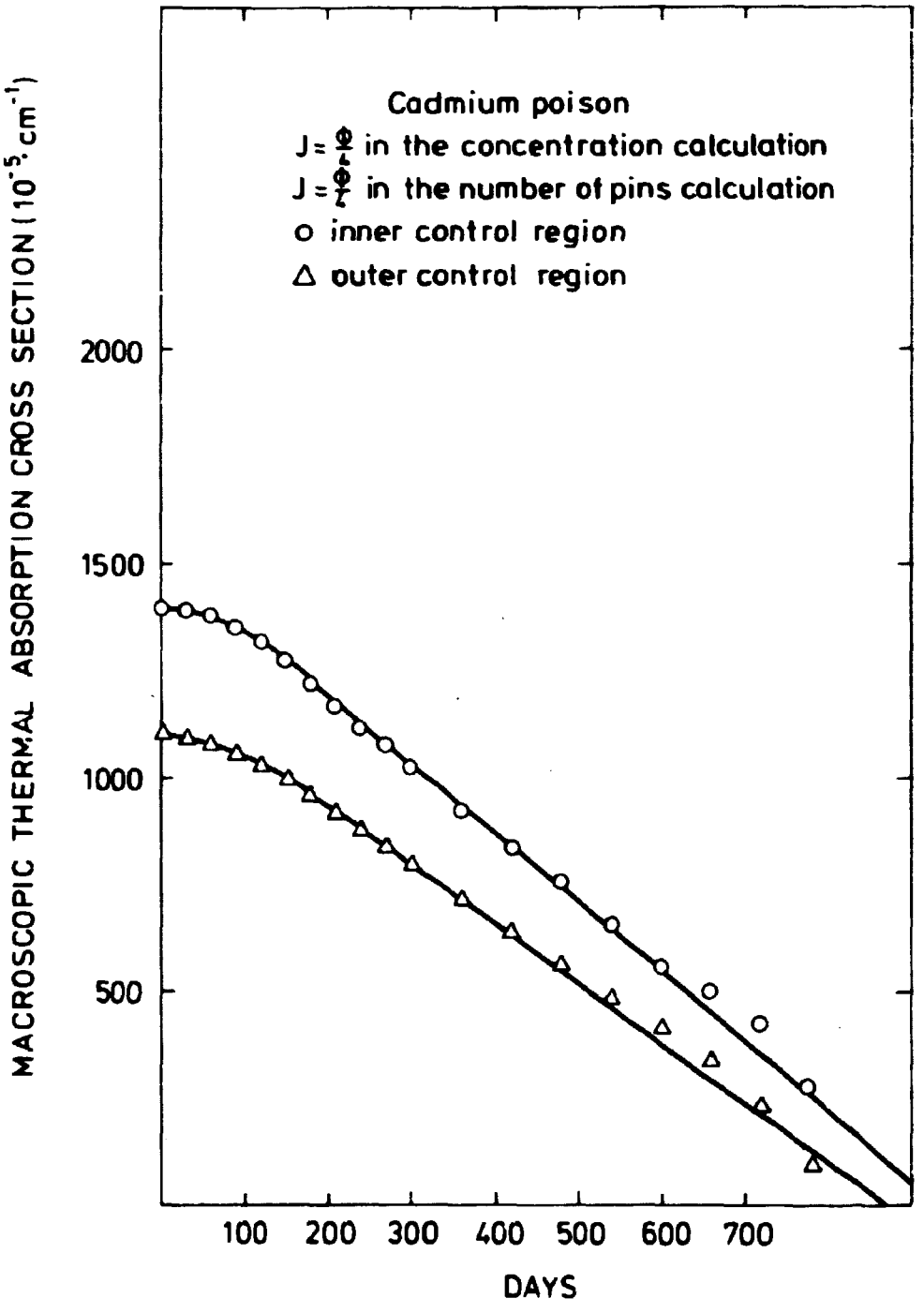

Fig. 18a. Cadmium burn-up calculated with CDB.

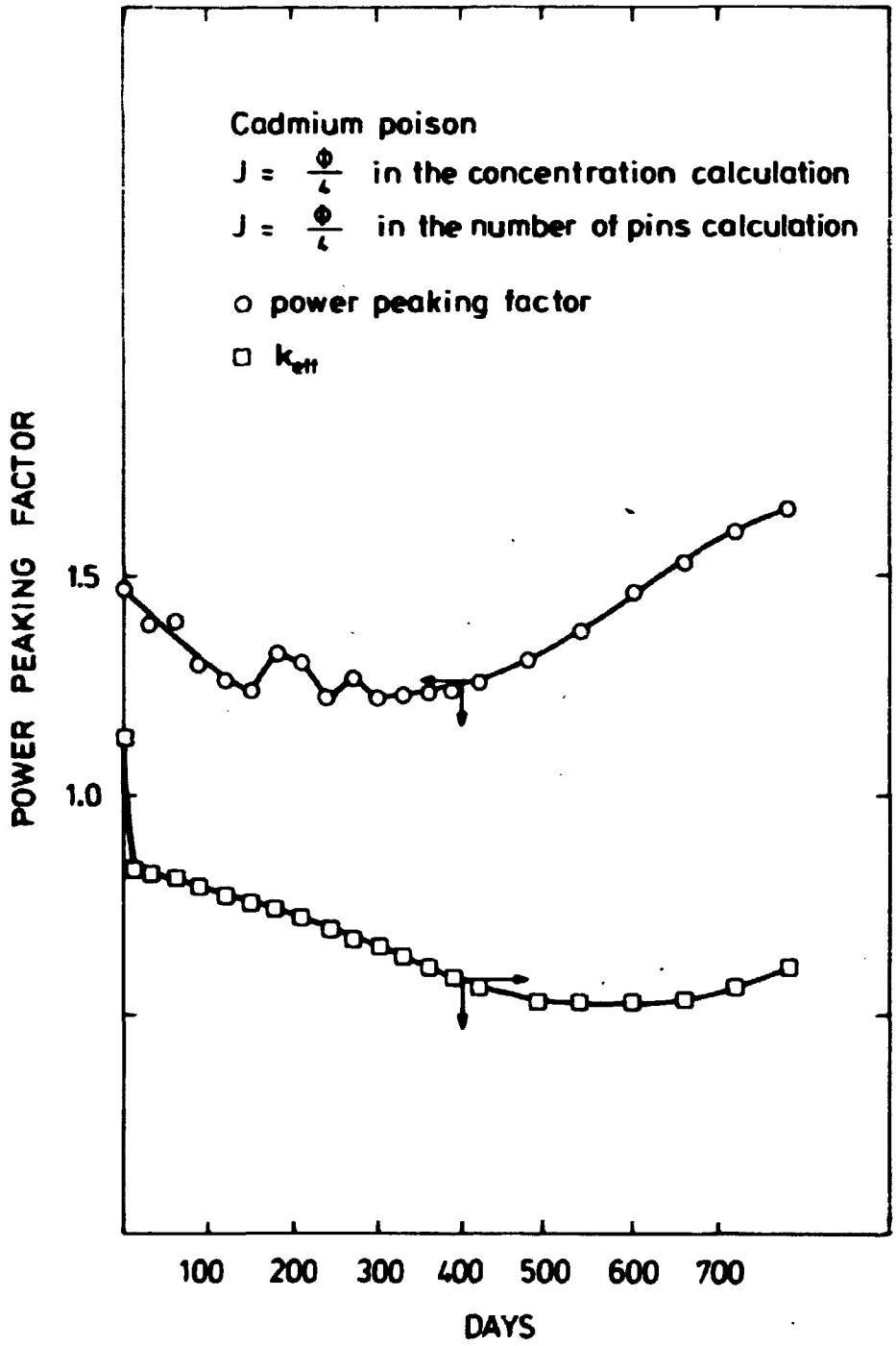

Fig. 18b. Power peaking factor and k_{eff} using cadmium as burnable poison calculated with DBU.

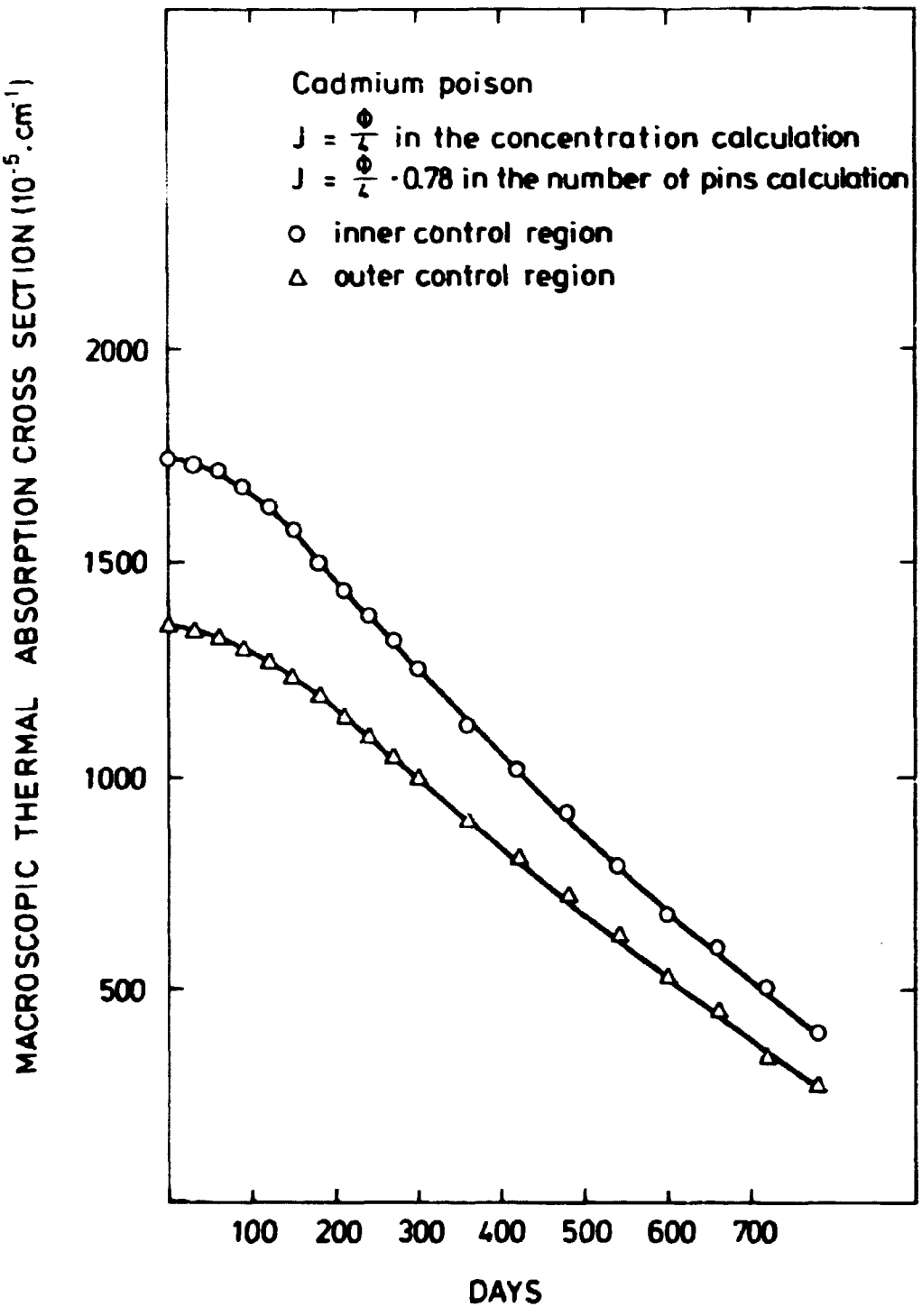

Fig. 18c. Cadmium burn-up calculated with CDB.

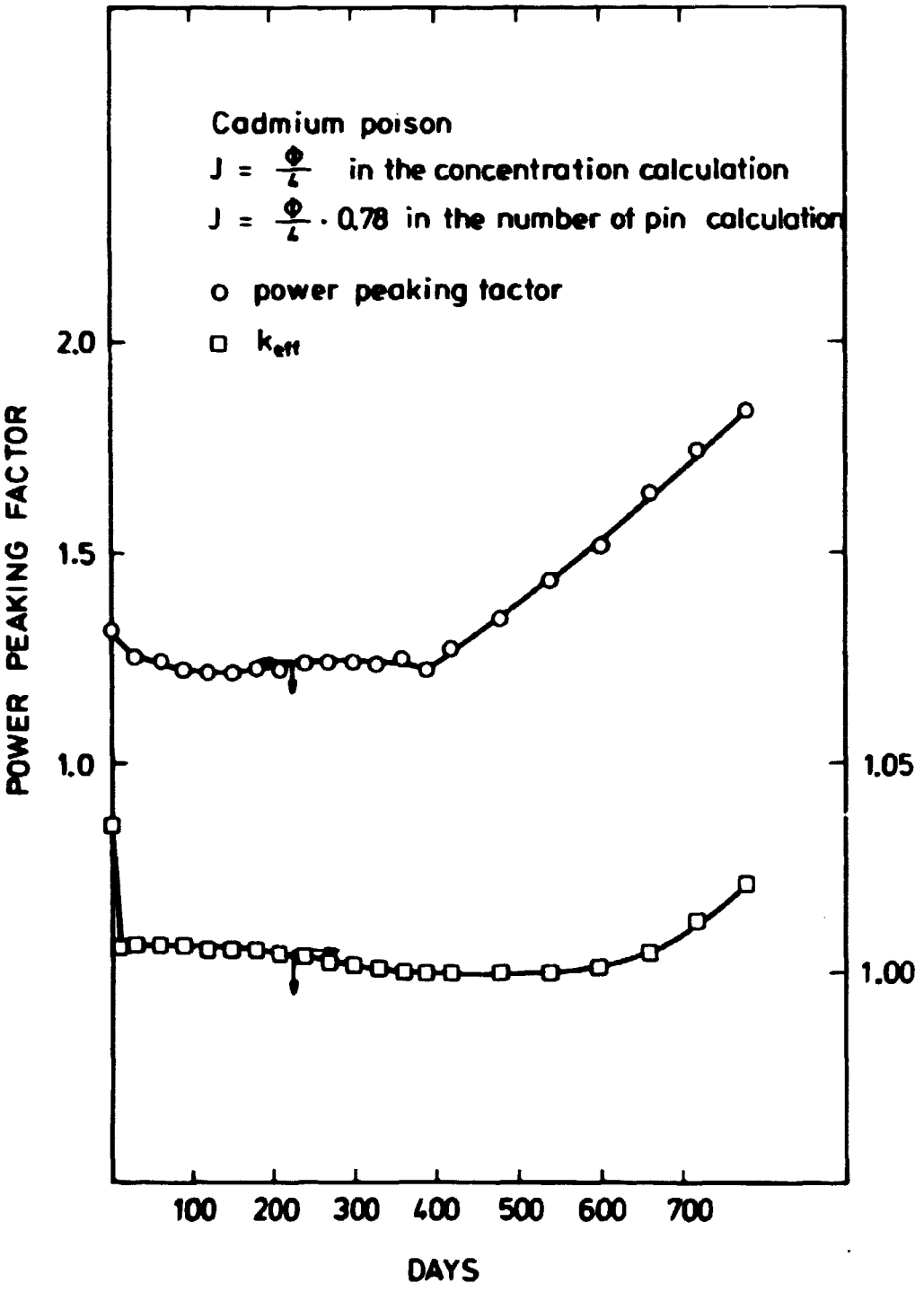

Fig. 10d. Power peaking factor and k_{eff} vs. burn-up using cadmium as burnable poison calculated with DBU.

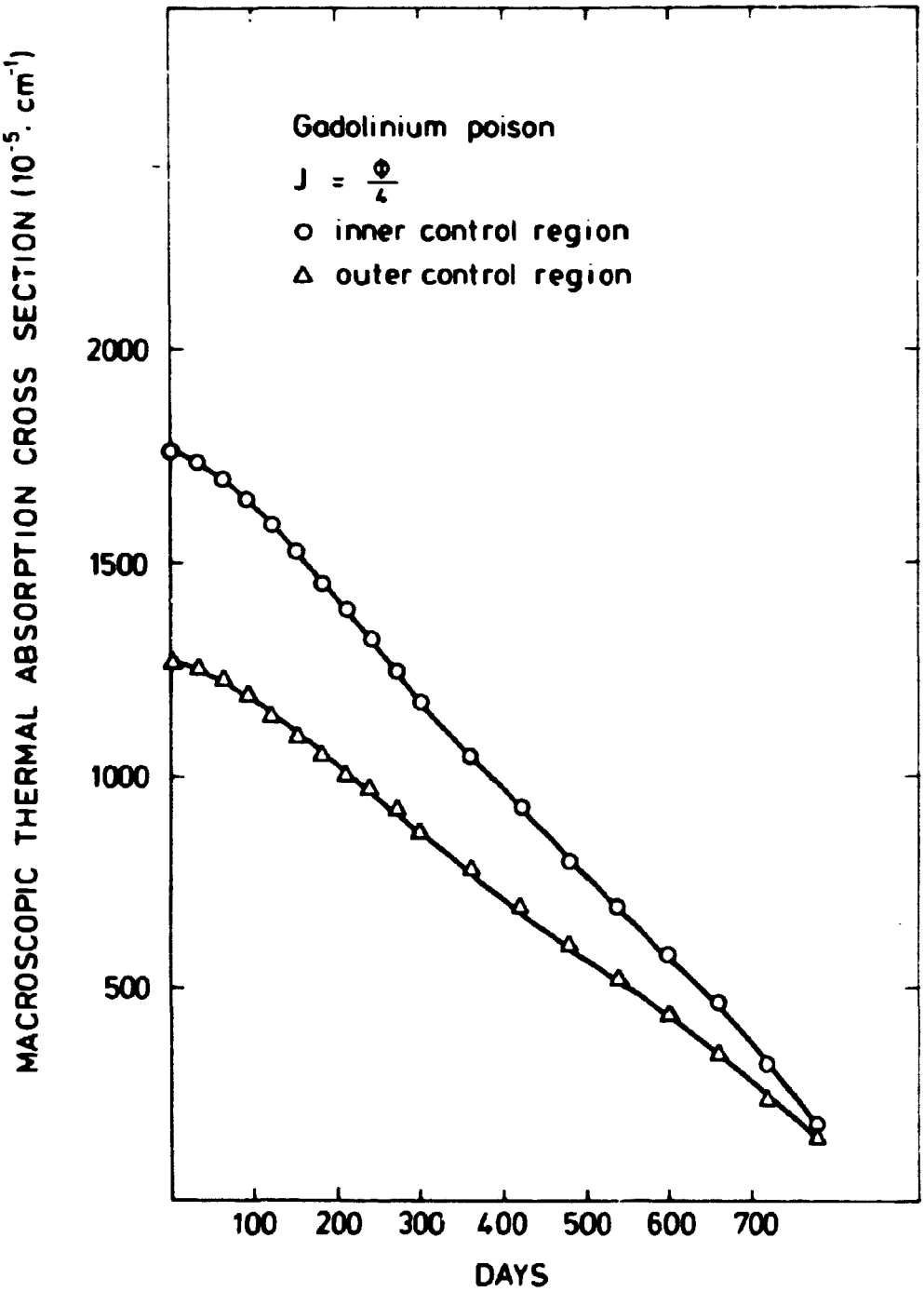

Fig. 19a. Gadolinium burn-up calculated with CDB.

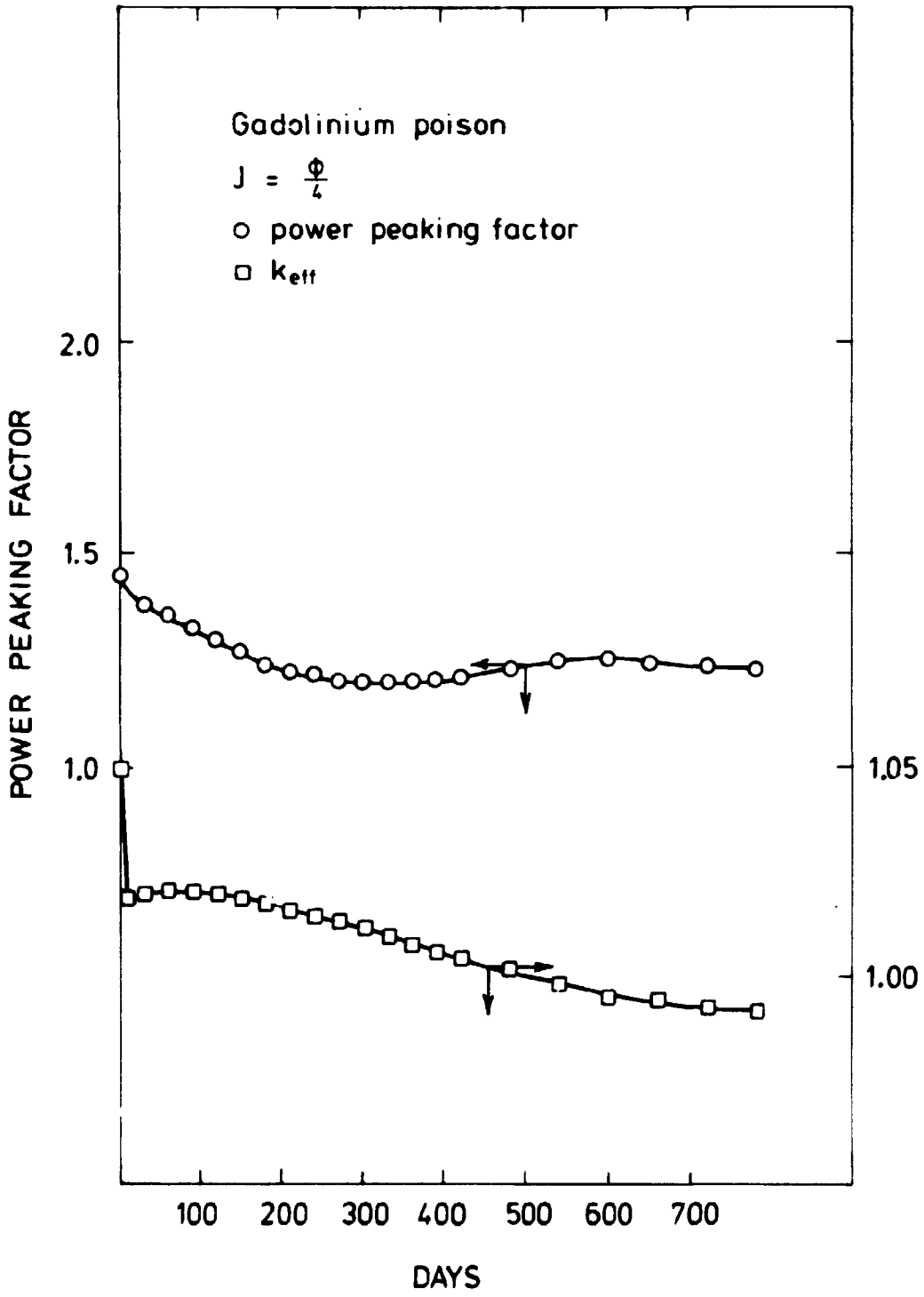

Fig. 19b. Power peaking and k_{eff} vs. burn-up using gadolinium as burnable poison calculated with DBU.

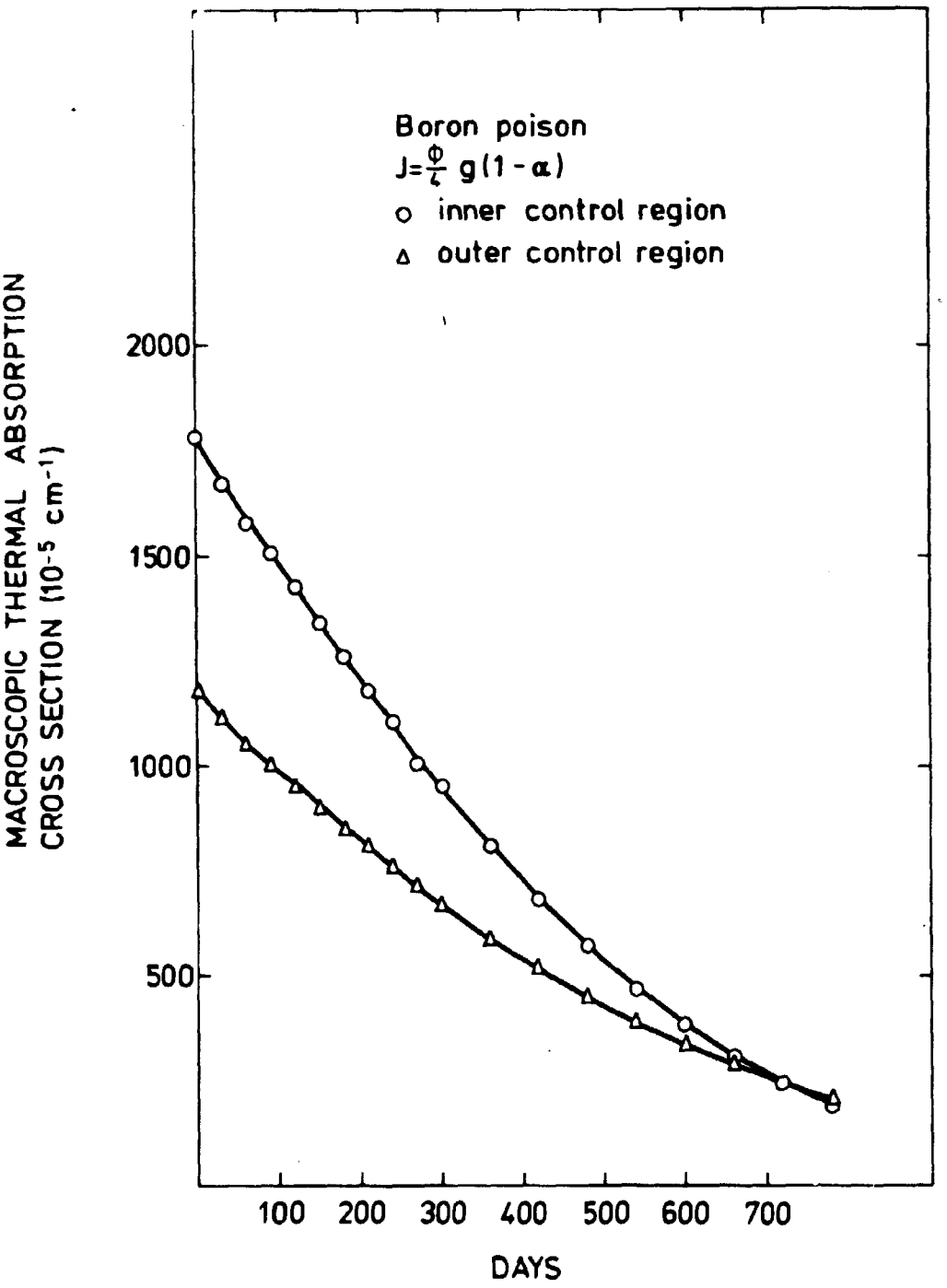

Fig. 20a. Boron burn-up calculated with CDB.

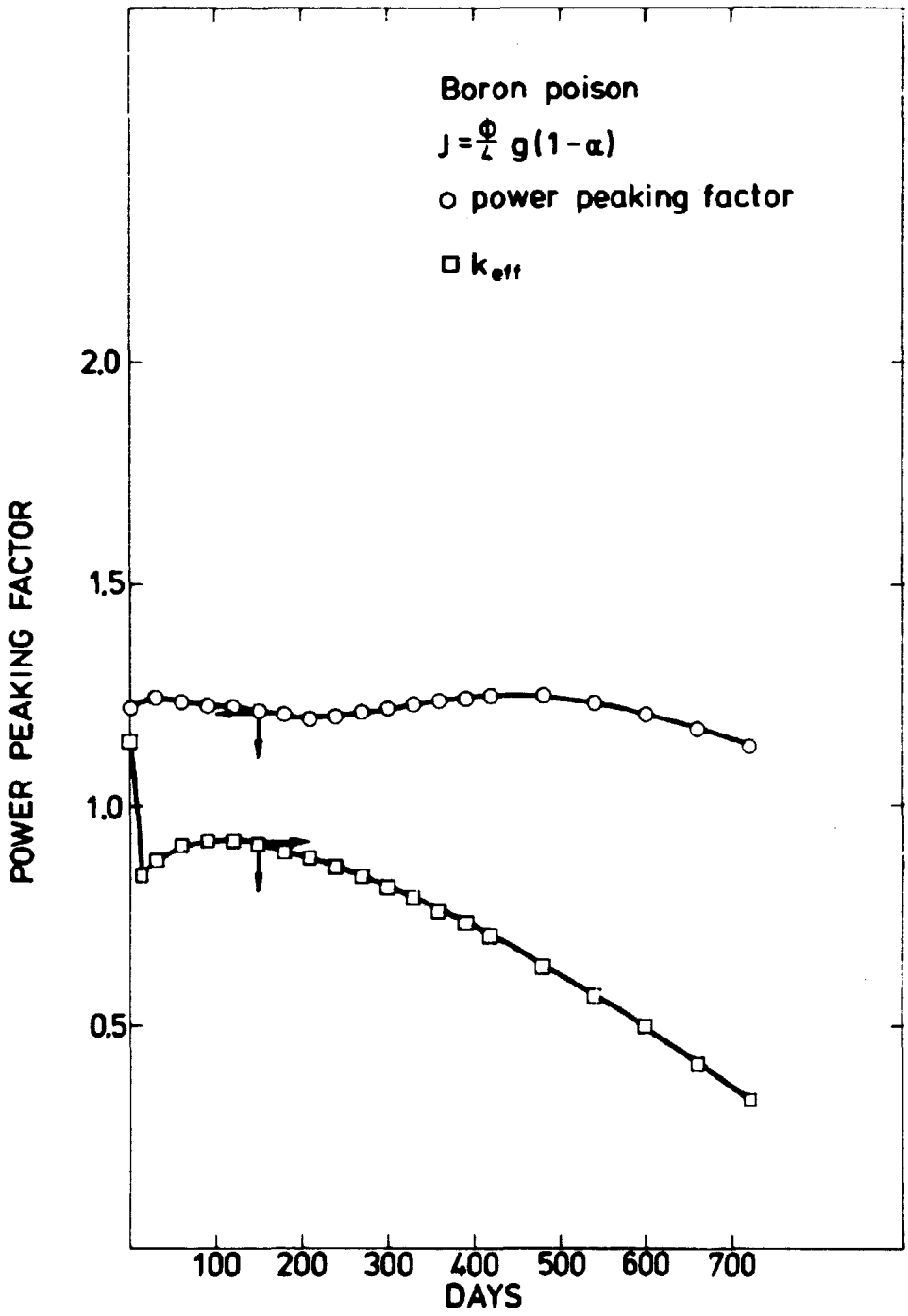

Fig. 20b. Power peaking factor and k_{eff} vs. burn-up using boron as burnable poison calculated with DBU.

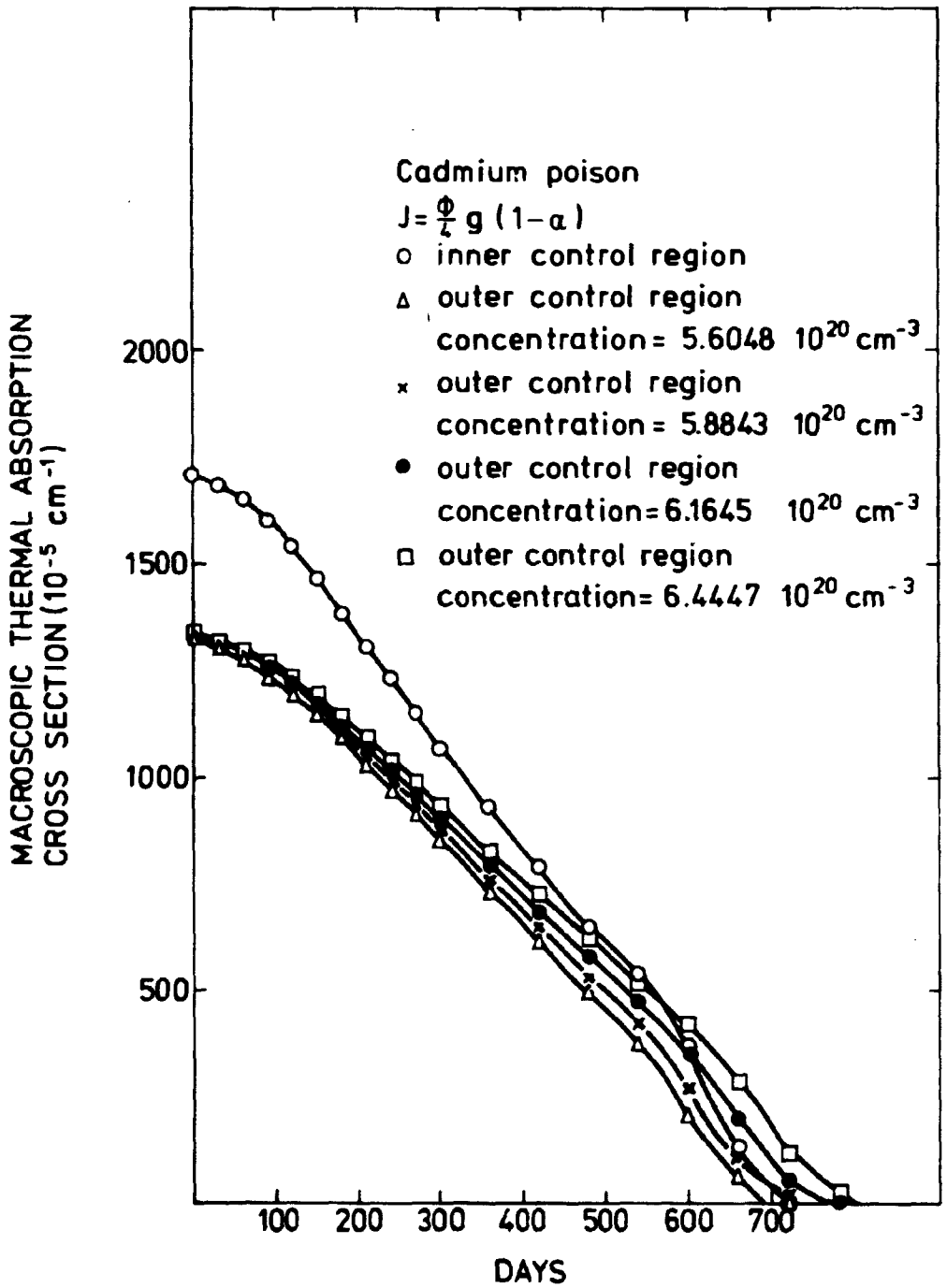

Fig. 21a. Cadmium burn-up calculated with CDB.

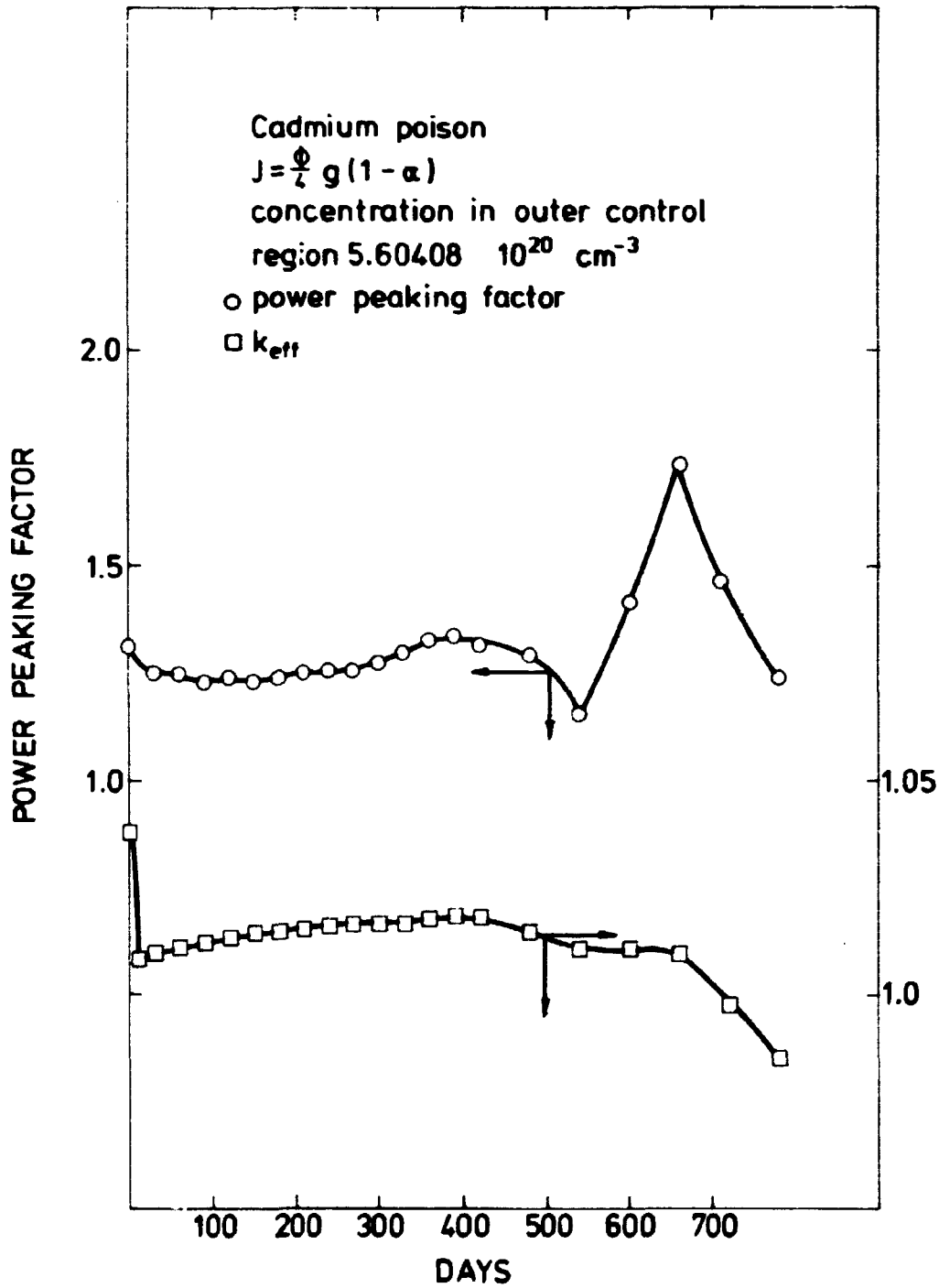

Fig. 21b. Power peaking factor and k_{eff} vs. burn-up using cadmium as burnable poison calculated with DBU.

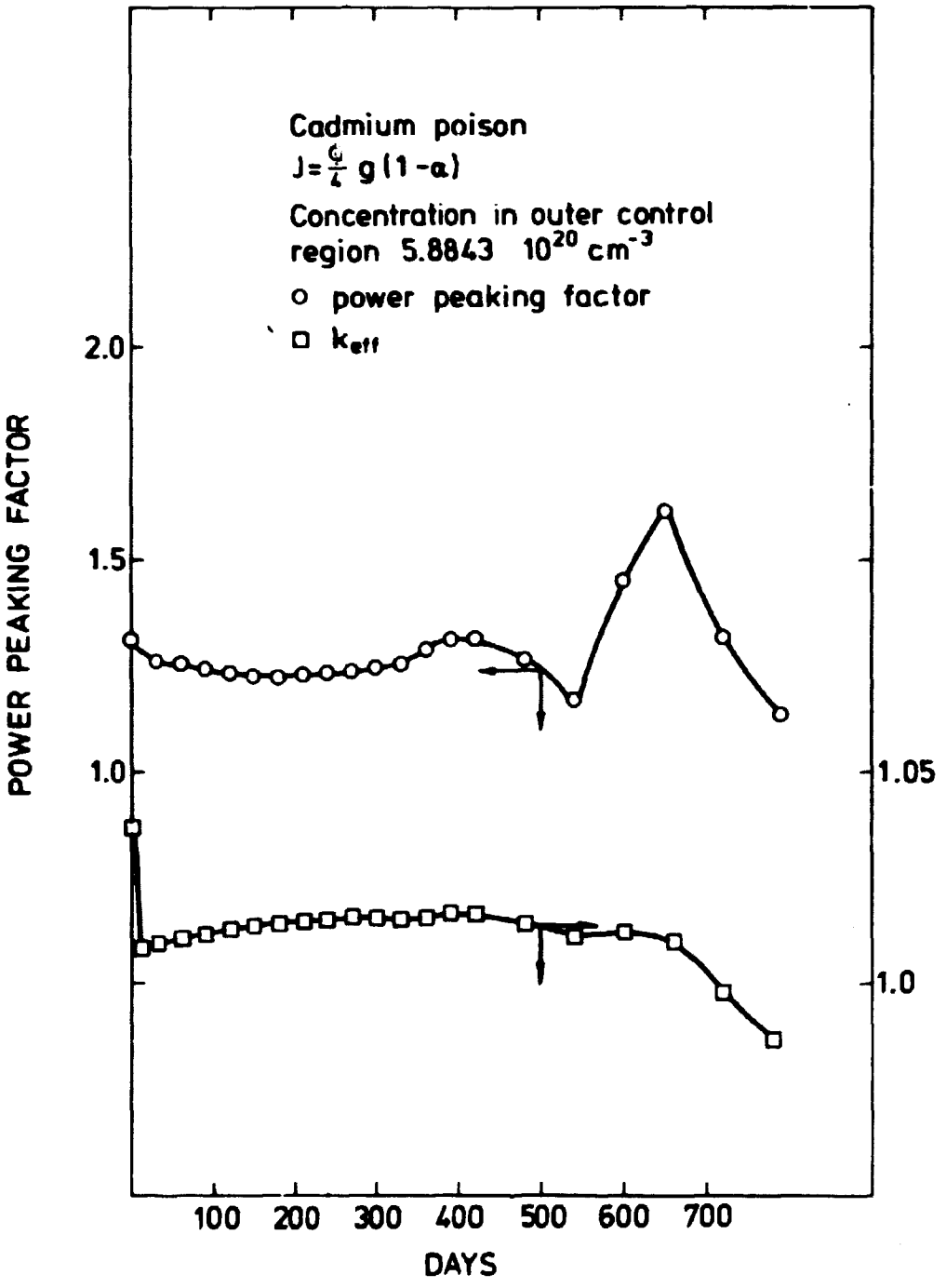

Fig. 21c. Power peaking factor and k_{eff} vs. burn-up using cadmium as burnable poison calculated with DBU.

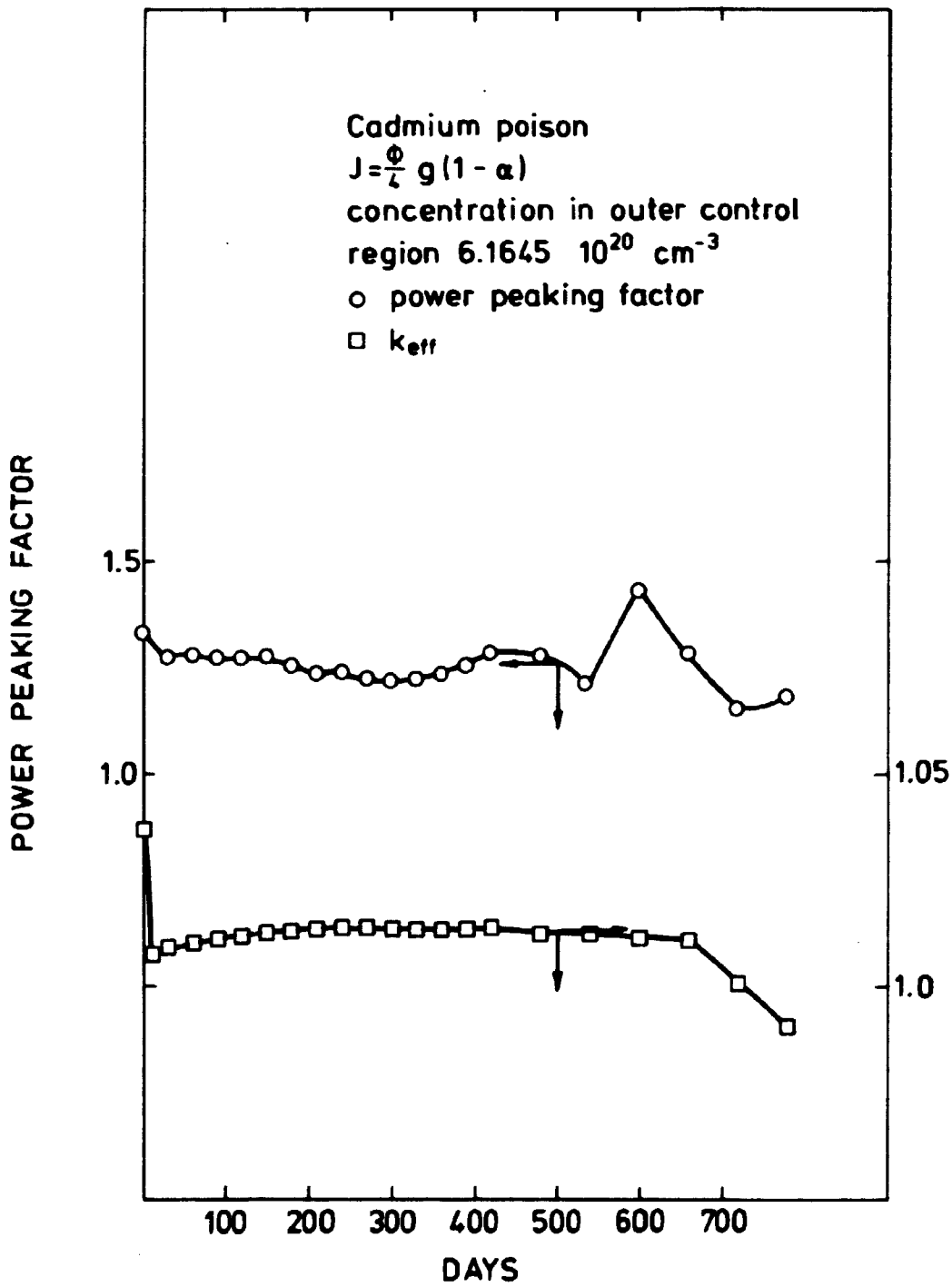

Fig. 21d. Power peaking factor and k_{eff} vs. burn-up using cadmium as burnable poison calculated with DBU.

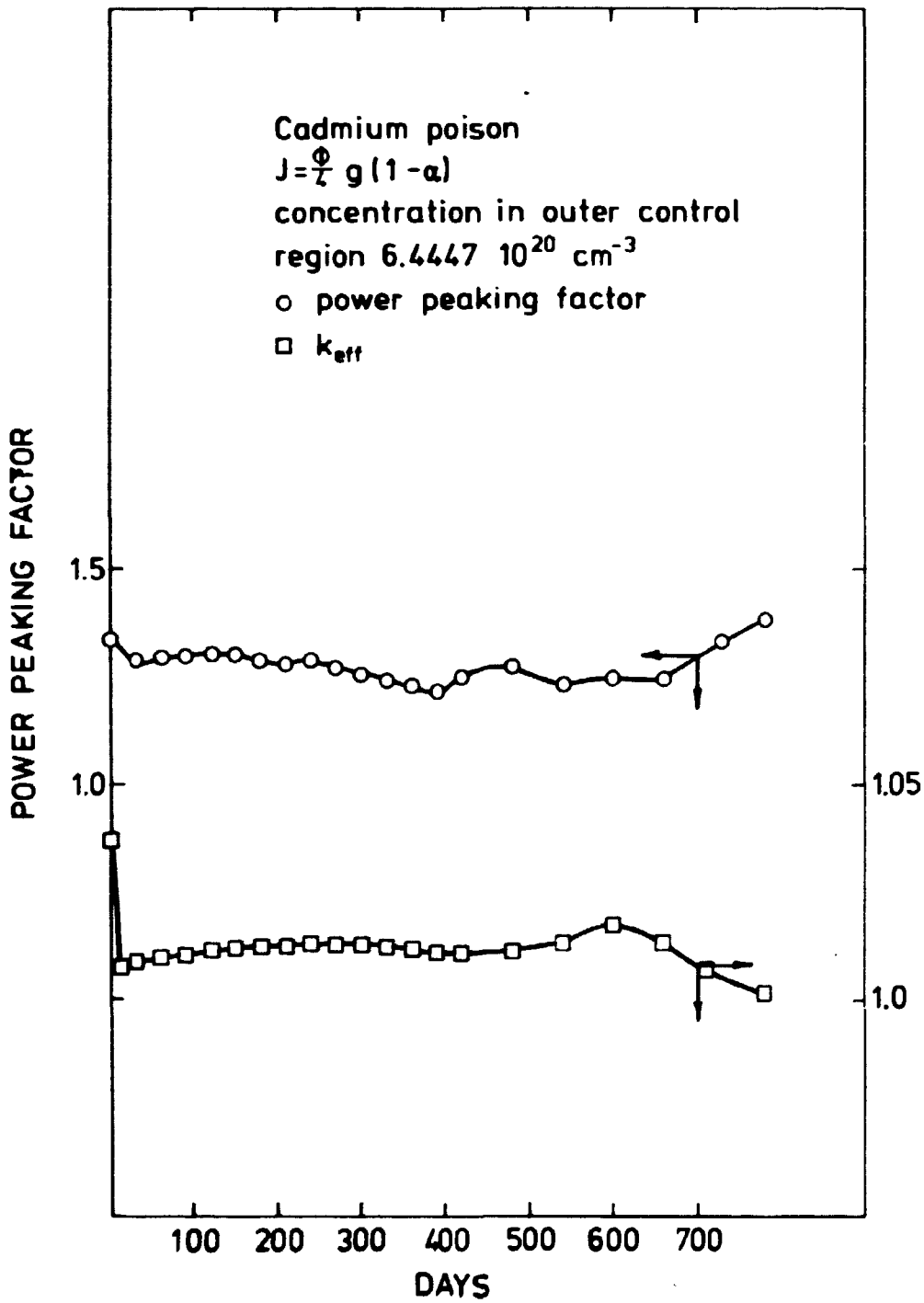

Fig. 21e. Power peaking factor and k_{eff} vs. burn-up using cadmium as burnable poison calculated with DBU.

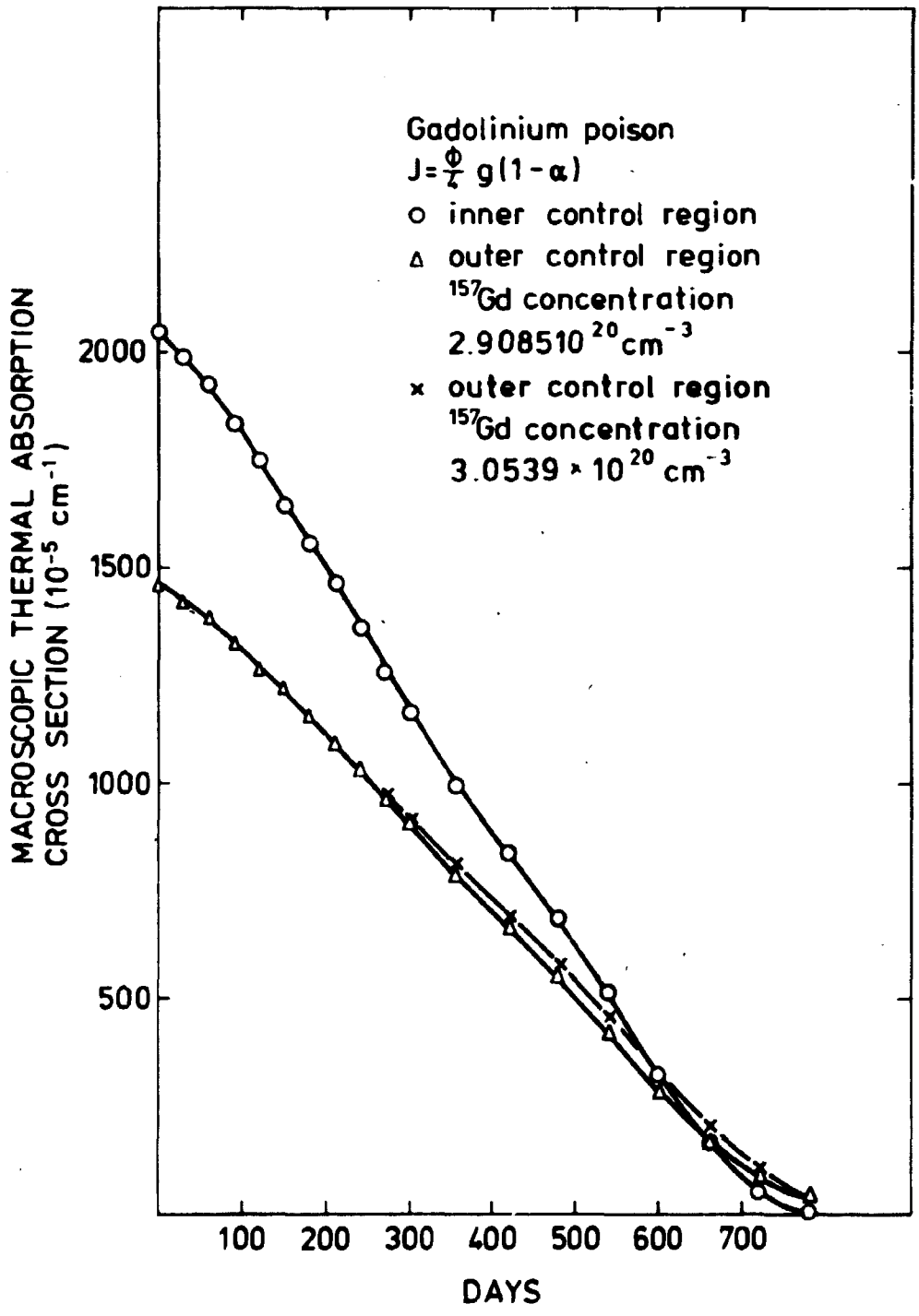

Fig. 22a. Gadolinium burn-up calculated with CDB.

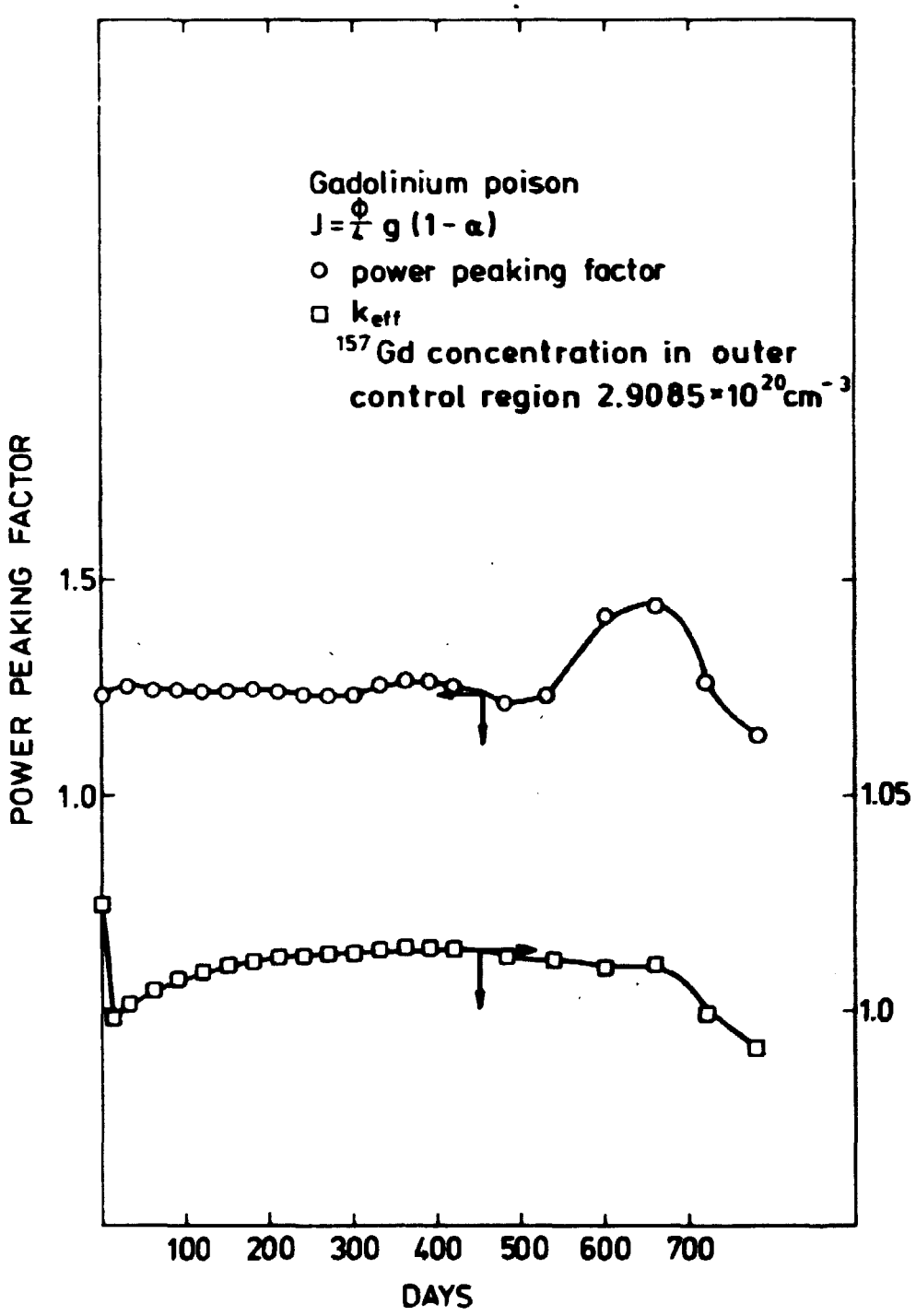

Fig. 22b. Power peaking factor and k_{eff} vs. burn-up using gadolinium as burnable poison calculated with DBU.

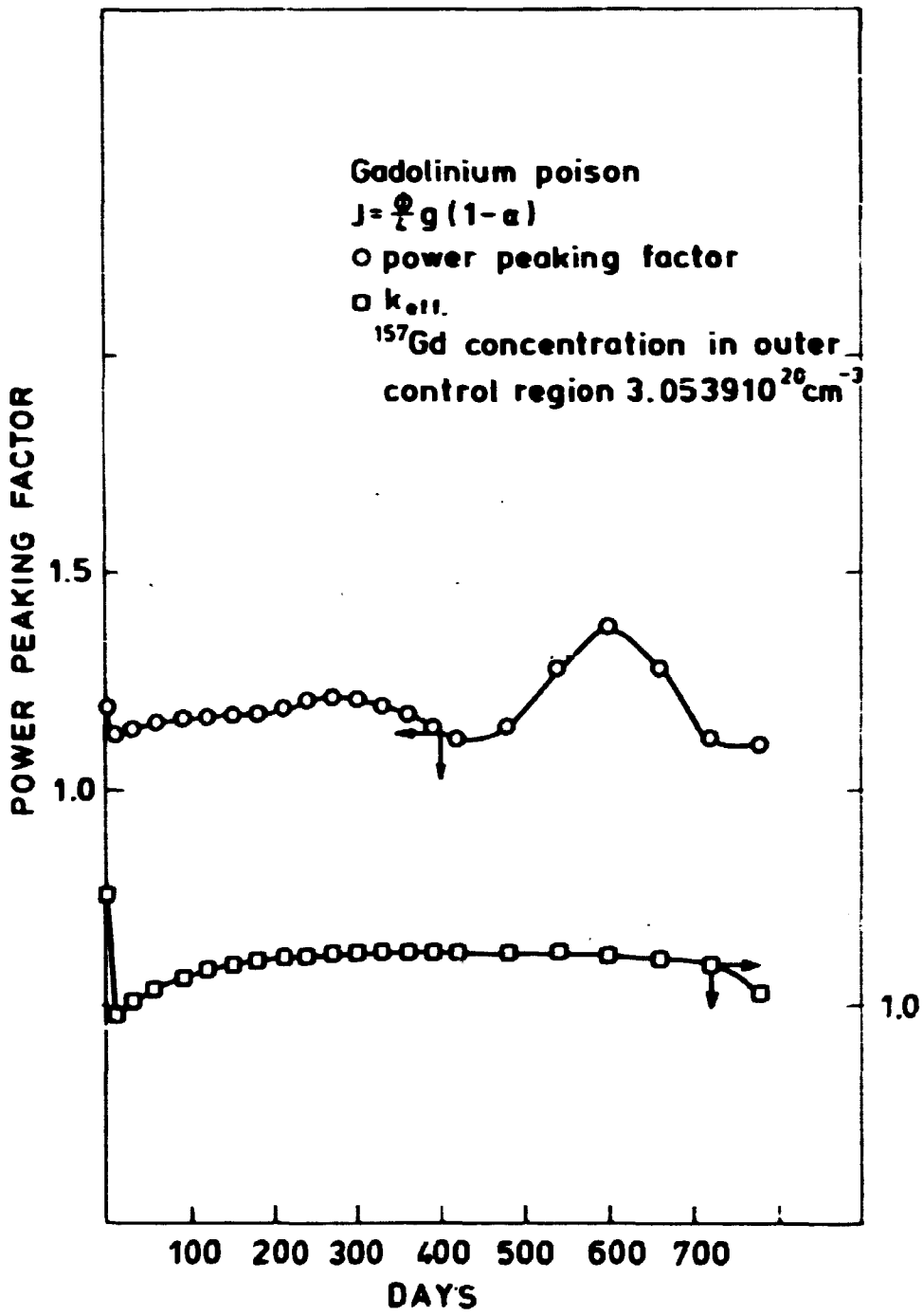

Fig. 22c. Power peaking factor and k_{eff} vs. burn-up using gadolinium as burnable poison calculated with DBU.

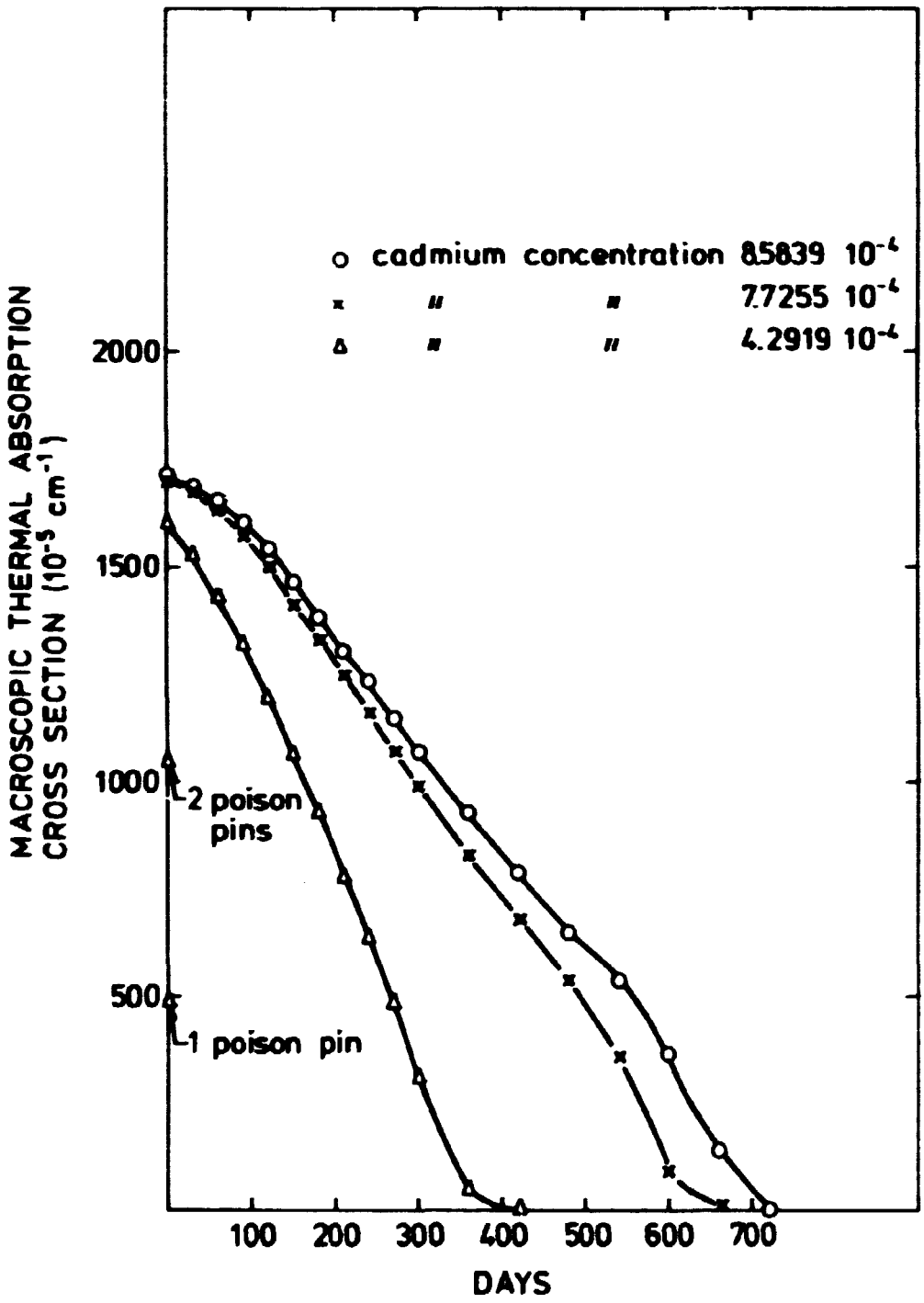

Fig. 23. Cadmium burn-up calculated with CDB.

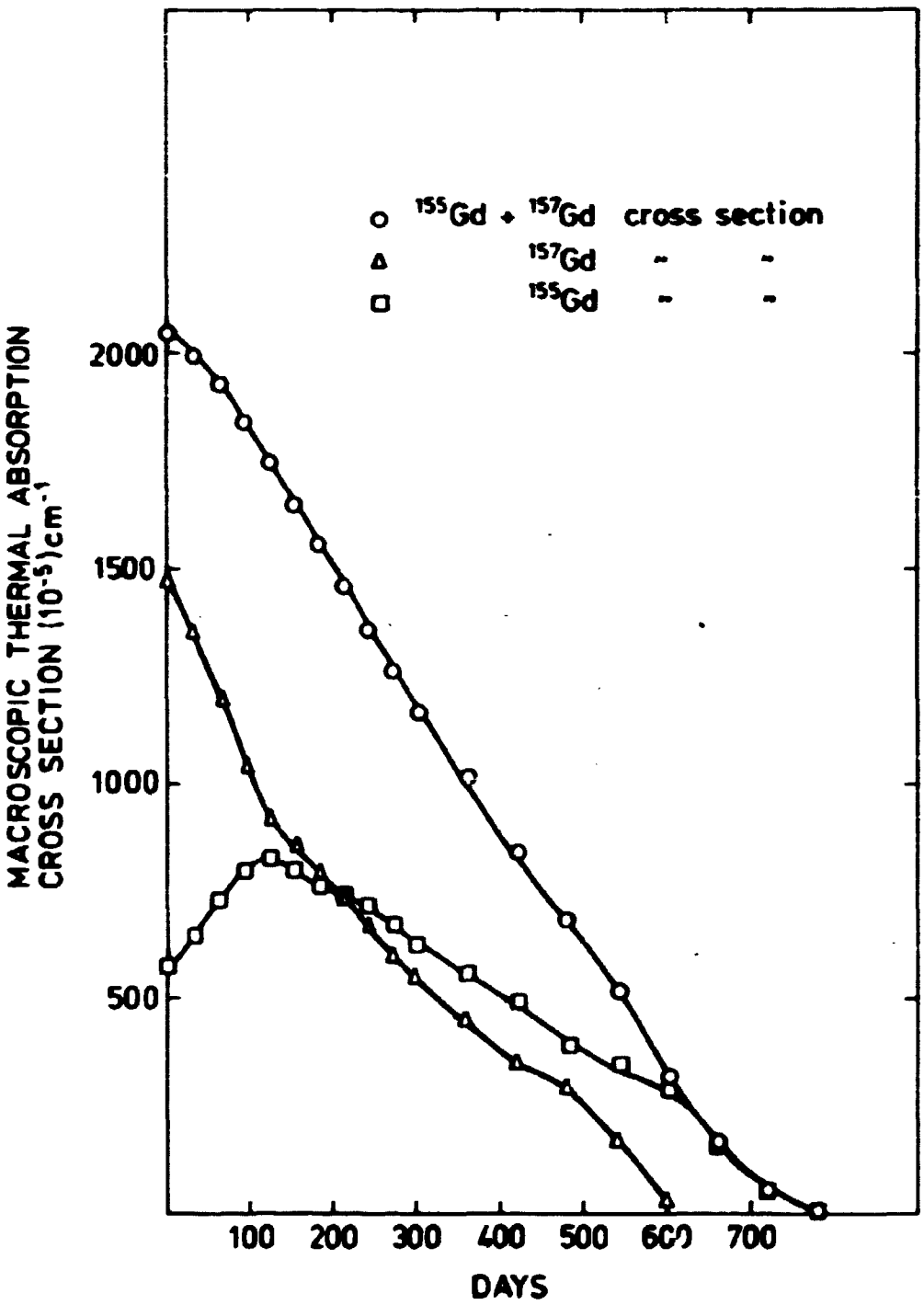

Fig. 24a. Gadolinium burn-up calculated with CBB.

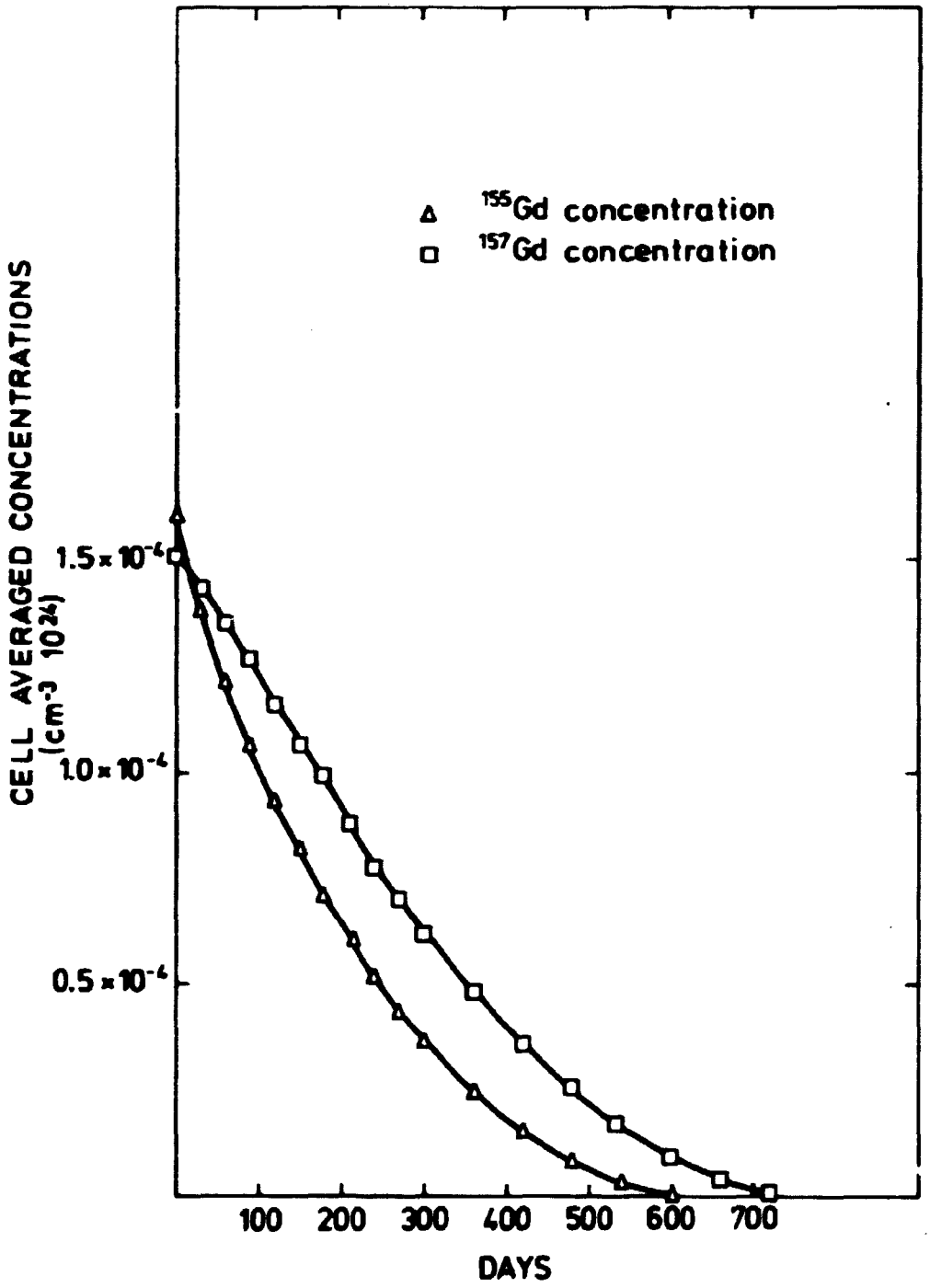

Fig. 24b. Concentration of the gadolinium isotopes vs. burn-up calculated with CDB.

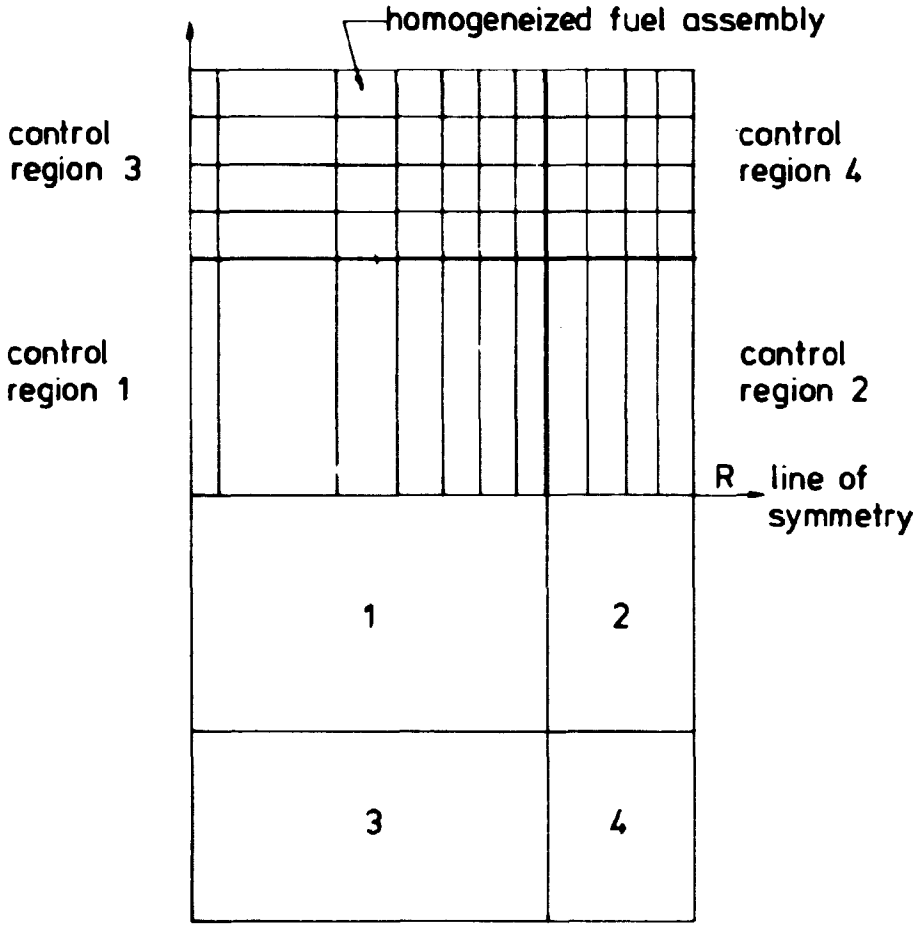

Fig. 25. Control regions used in the RZ calculations.

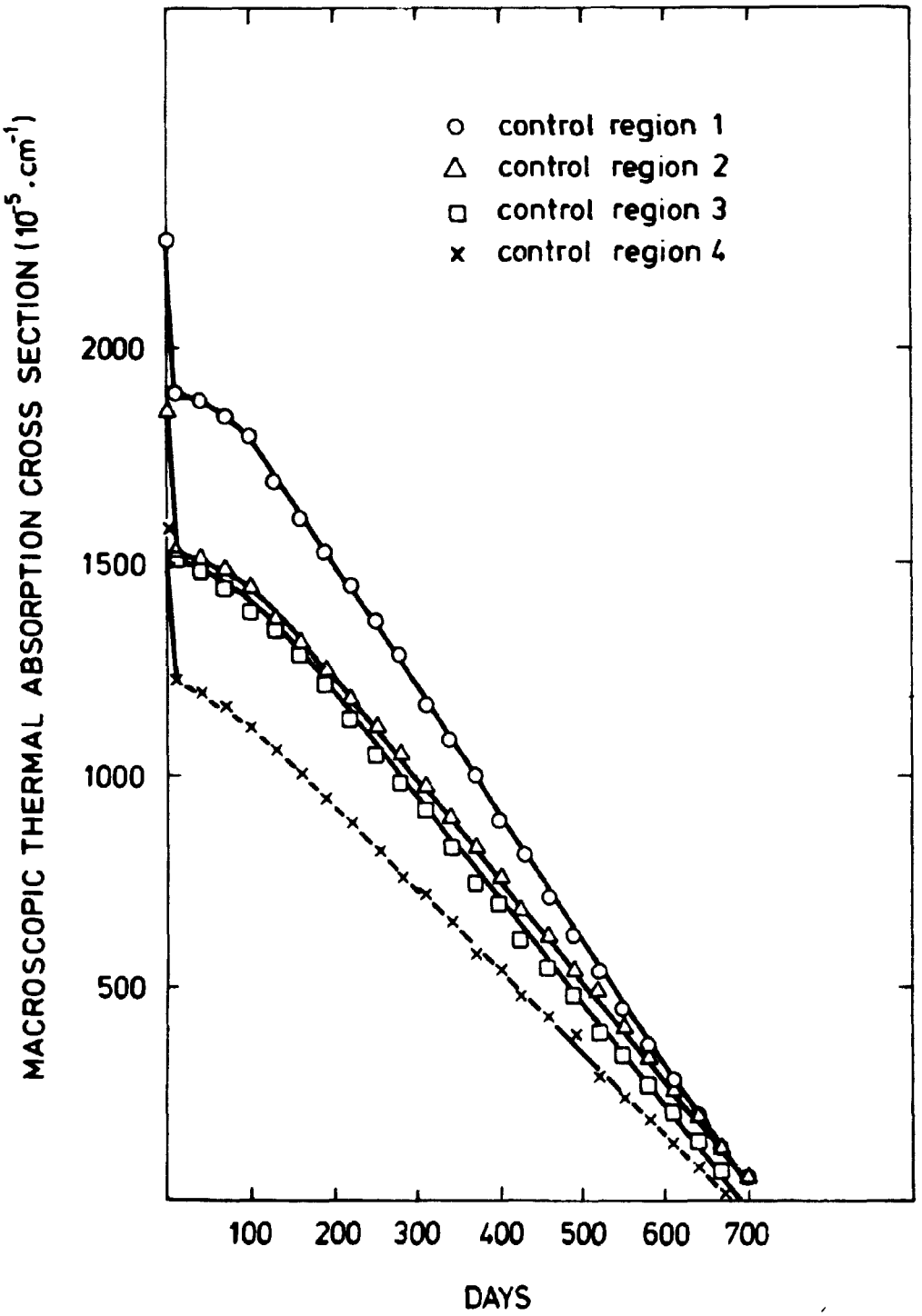

Fig. 26. Macroscopic thermal absorption cross sections for the four control regions used in the RZ calculation for Haddam Neck. Calculated with SELMA2.

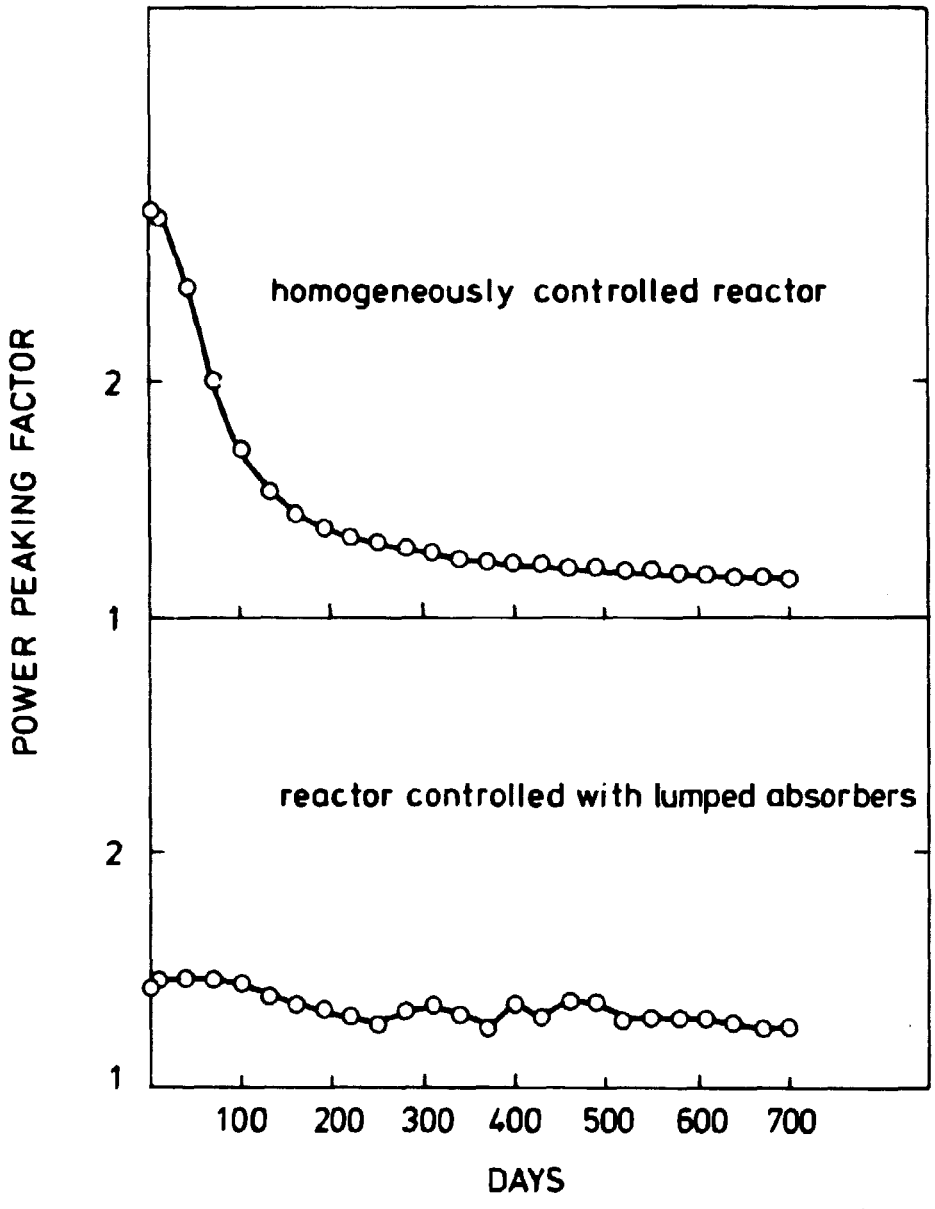

Fig. 27. **Three-dimensional calculation for Haddam Neck. Calculated with SELMA2.**

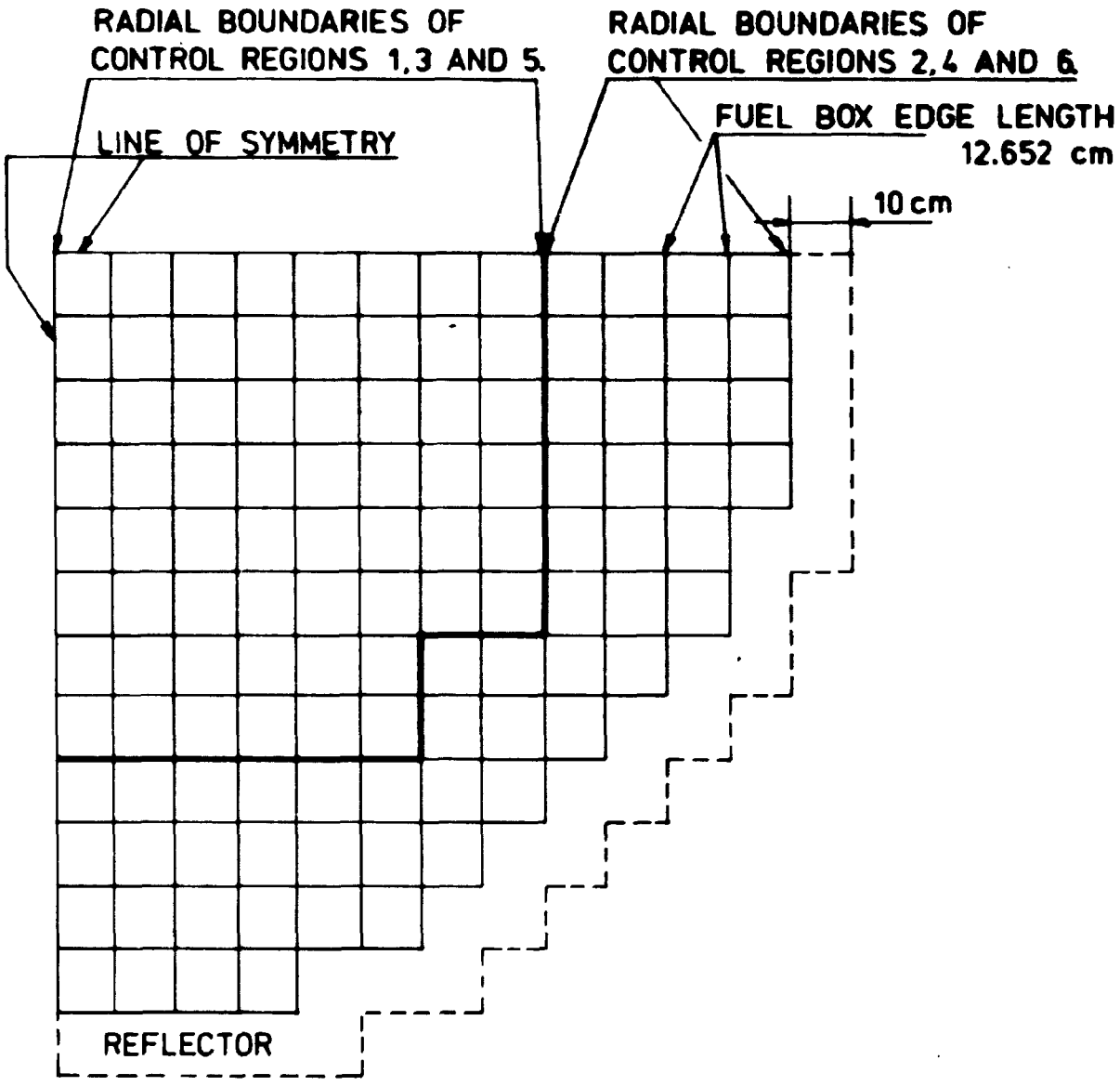

Fig. 28. DRESDEN 1 quarter core with dimensions and radial control region division.

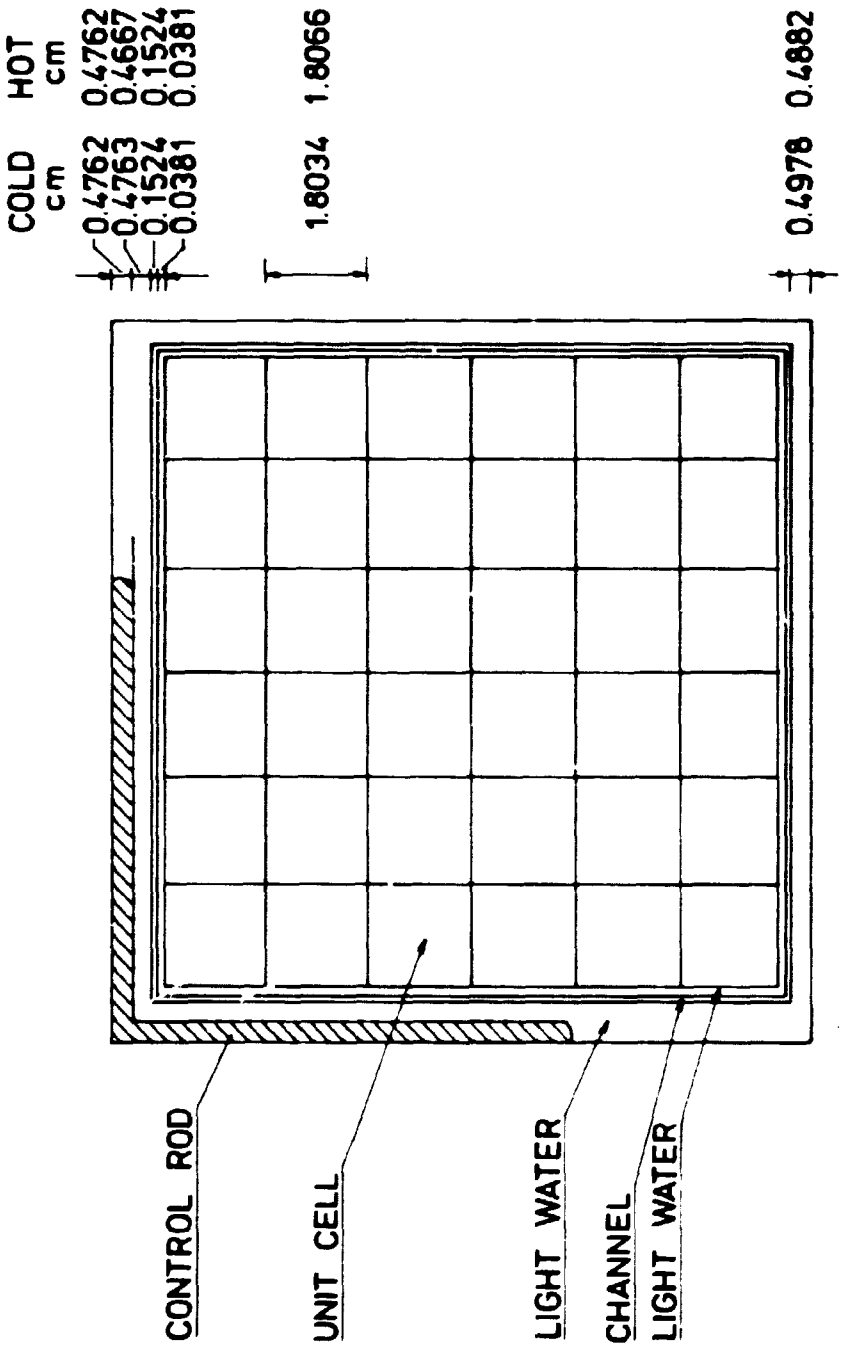

Fig. 29. DRESDEN 1 assembly.

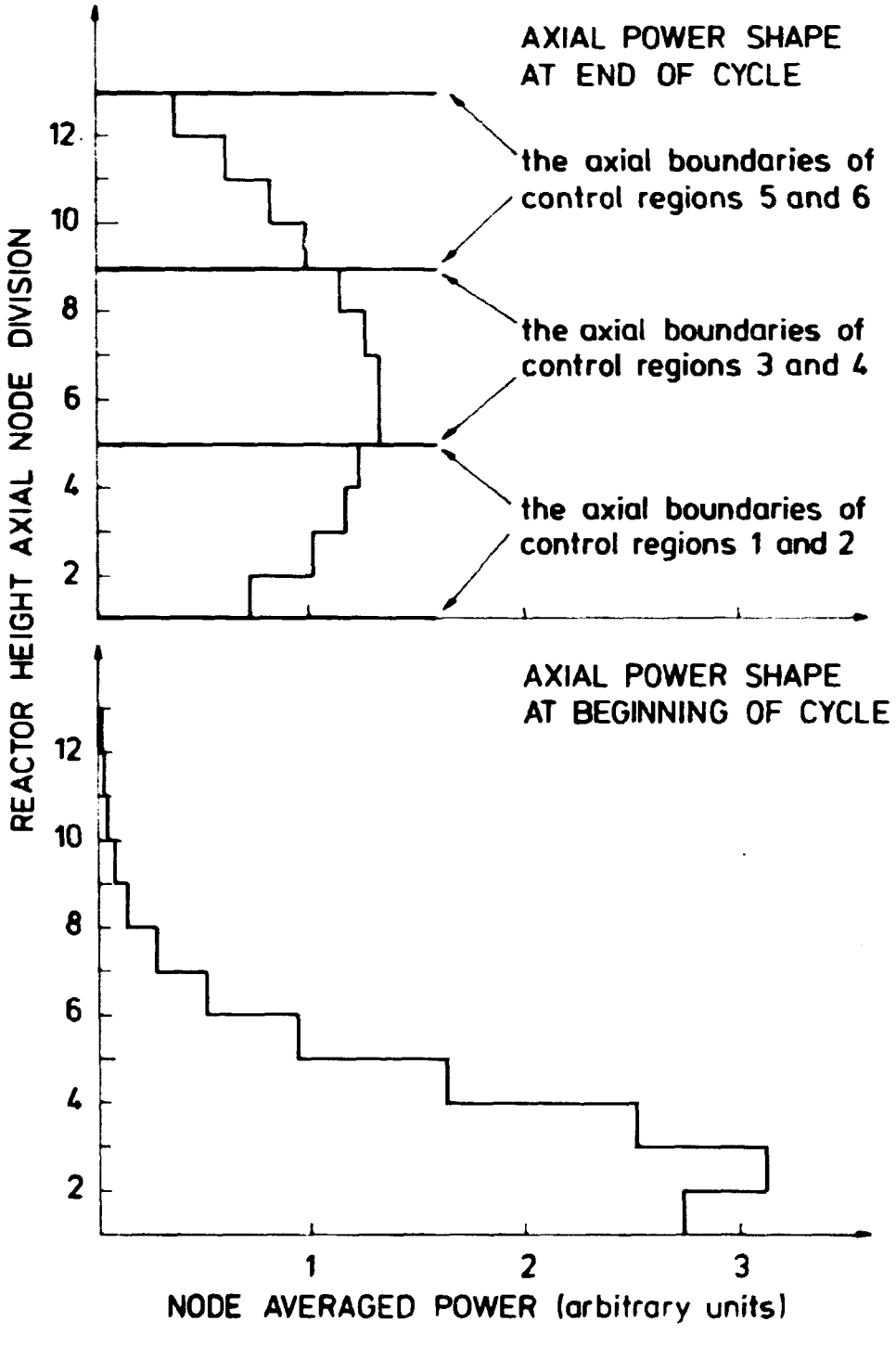

Fig. 30. Axial power shape for DRESDEN 1 calculated with NOTAM.